UNIVERSITY OF CALIFORNIA, SAN DIEGO

Charge Transport and Chemical Sensing Properties of Organic Thin-films

A dissertation submitted in partial satisfaction of the requirements for the degree of

Doctor of Philosophy

in

Materials Science and Engineering

by

Dengliang Yang

Committee in charge:

Professor Andrew C. Kummel, Chair
Professor Sungho Jin, Co-Chair
Professor Yu-Hwa Lo
Professor William C. Trogler
Professor Edward T. Yu

2007

The dissertation of Dengliang Yang is approved, and it is acceptable in quality and form for publication on microfilm:

_____

_____

_____

_____

Co-Chair

_____

Chair

University of California, San Diego

2007

To my parents and wife

Table of Contents

List of Figures and Tables

List of Abbreviations and Symbols

OTFT	Organic thin-film transistor
ChemFET	Chemically sensitive field-effect transistors
SCLC	Space charge limited conduction
SKPM	Scanning Kelvin probe microscopy
AFM	Atomic force microscopy
XRD	X-ray diffraction
BSE	Bias stress effect
MPc	Metal phthalocyanine
CuPc	Copper phthalocyanine
CoPc	Cobalt phthalocyanine
H_2Pc	Metal-free phthalocyanine
DIMP	Diisopropyl methylphosphonate
NB	Nitrobenzene

Acknowledgement

I am in great debt to my advisor, Andy Kummel for his generous support during my Ph.D. study. He has provided me the best research project in the group and is always available for discussion. Andy got me started with the sensing project at my first day in UCSD. Since then, he has been very involved with progress I made in my research. This thesis is the product of many hours of intense and critical discussion with Andy.

Chapter 2, in part, has been published in *Appl. Phys. Lett.* 88 (2006) 074104, by Richard Yang, Bernd Fruhberger, Jeongwon Park, and Andrew Kummel. Chapter 3, in part, has been published in *J. Phys. Chem. B*, 110 (2006) 361, by Karla Miller, Richard Yang, Michael Hale, Jeongwon Park, Bernd Fruhberger, Corneliu Colesniuc, Ivan Schuller, Andrew Kummel, and William Trogler. Chapter 6, in part, has been published in *Appl. Phys. Lett.* 90 (2007) 263506, by Richard Yang, Thoms Gredig, Jeongwon Park, Corneliu Colesniuc, Ivan Schuller, William Trogler, and Andrew Kummel.

I appreciate all the helps from my collaborators. Jeongwon Park, Thomas Gredig, Xiaotian Zhou and Cornel Colesniuc were invaluable collaborators, and I must also thank Forest Bohrer, Amos Sharoni, Bernd Fruhberger and Karla Miller, with whom I worked together on the MURI project. Jeongwon has been my partner from the beginning and throughout my study. We have shared the frustration and joy together solving countless fabrication and device problems in the past three years.

I enjoy the companies of undergraduate students worked with me in the portable probe station and hand-held chemical sensor package projects. They are Thuan Nguyen, Tamara Stuart, Casey Ta, Kate Wagstaff, Jordan Tanabe, Vince So, and Byron Ho.

My thanks are due to many professors and staffs at UCSD. Professor Bill Trogler has provided many critical inputs in my research. Professors Ed Yu, Yuan Taur and Peter Asbeck got me interested in semiconductor device physics. I greatly benefit from the rigorous courses they offered and many helpful discussions about my research problems with them. I wish to thank my other committee members: Dr. Sungho Jin and Prof. Yu-Hwa Lo, for their time and warm encouragement during my thesis work. I also wish to thank ITL staffs: Larry Grissom and Ryan Anderson. They are always ready to help with the fabrication process.

Special thanks go to Charlotte Lauve and Jackie Johnson for taking care of the administrative burdens for me.

Finally, I must thank my parents and my wife. My parents have been very supportive during my 21 years of study in school. Their loving encouragement and commitment to my education is a constant source of motivation. Thanks to my wife Chunmei, for she has made her best effort to assist me to complete the degree.

Richard Yang

La Jolla, June 2007

Vita

1978	Born in Wenzhou, Zhejiang Province, China
2000	B.S., Chemical Engineering, Zhejiang University, Hangzhou, China
2001	M.S., Advanced Materials, Program of Singapore-MIT Alliance National University of Singapore, Singapore
2004	M.S., Chemistry, Texas A&M University, College Station, Texas
2007	Ph.D., Materials Science and Engineering, University of California, San Diego, California

Publications

(1). **R. D. Yang**, S. Tripathy, F. E. H. Tay, L. M. Gan, and S. J. Chua, "Photoluminescence and micro-Raman Scattering in Mn-doped ZnS Nanocrystalline Semiconductors", *J.Vac.Sci.Technol. B* 21 (2003) 984-988

(2). **R. D. Yang**, Y. Li, H.-J. Sue, "Growth of Zinc Oxide Nanorods in Alcohol Solution", *Mat.Res.Soc.Symp.Proc.* Vol. 775, P9.43.1, 2003

(3). M. C. Gurau, E. T. Castellana, F. Albertorio, S. Kataoka, S. Lim, **R. D. Yang**, and P. S. Cremer, "Thermodynamics of Phase Transitions in Langmuir Monolayers Observed by Vibrational Sum Frequency Spectroscopy", *J. Am. Chem. Soc.* 125 (2003) 11166-11167

(4). S. Jung, S. Lim, F. Albertorio, G. Kim, M. C. Gurau, **R. D. Yang**, M. A. Holden, and P. S. Cremer, "The Vroman Effect: A Molecular Level Description of Fibrinogen Displacement", *J. Am. Chem. Soc.* 125 (2003) 12782-12786

(5). S. Kataoka, M. C. Gurau, F. Albertorio, M. A. Holden, S. Lim, **R. D. Yang**, and P. S. Cremer, "Investigation of Water Structure at the TiO_2/Aqueous Interface", *Langmuir* 20 (2004) 1662-1666

(6). Y. Li, **R. D. Yang**, S.Tripathy, H.-J. Sue, N. Miyatake, and R. Nishimura, "Preparation of Ultraviolet Light Emitting ZnO Nanoparticles Via a Novel Synthesis Route", *Mat.Res.Soc.Symp.Proc.* Vol. 829, B4.4.1, 2005

(7). **R. D. Yang**, S. Tripathy, Y. Li, and H.-J. Sue, "Photoluminescence and Micro-Raman Scattering in ZnO Nanoparticles: the Influence of Acetate Adsorption", *Chem. Phys. Lett*. 411 (2005) 150-154

(8). **R. D. Yang**, B. Fruhberger, J. Park, and A. C. Kummel, "Chemical Identification Using an Impedance Sensor Based on Dispersive Charge Transport", *Appl. Phys. Lett.* 88 (2006) 074104-074106

(9). K. A. Miller, **R. D. Yang**, M. J. Hale, J. Park, B. Fruhberger, C. N. Colesniuc, I. K. Schuller, A. C. Kummel, and W. C. Trogler, "Electrode Independent Chemoresistive Response for Cobalt Phthalocyanine in the Space Charge Limited Conductivity Regime", *J. Phys. Chem. B*, 110 (2006) 361-366

(10). **R. D. Yang**, T. Gredig, J. Park, C. N. Colesniuc, I. K. Schuller, W. C. Trogler, and A. C. Kummel, "Ultrathin Organic Transistor for Chemical Sensing", *Appl. Phys. Lett.*, 90 (2007) 263506-263508

(11). **R. D. Yang**, J. Park, C. N. Colesniuc, I. K. Schuller, W. C. Trogler, and A. C. Kummel, "Ultra-low Drift in Organic Thin-film Transistor Chemical Sensors", accepted by *J. Appl. Phys.*, 2007

(12). **R. D. Yang**, J. Park, C. N. Colesniuc, I. K. Schuller, W. C. Trogler, and A. C. Kummel, "Analyte Chemisorption and Sensing on n- and p- Channel Copper Phthalocyanine Thin-film Transistors", to be submitted to *J. Chem. Phys.*

ABSTRACT OF THE DISSERTATION

Charge Transport and Chemical Sensing Properties of Organic Thin-films

by

Dengliang Yang

Doctor of Philosophy in Materials Science and Engineering

University of California, San Diego, 2007

Professor Andrew C. Kummel, Chair

Professor Sungho Jin, Co-chair

Organic semiconducting materials have attracted intense attentions for electronic and chemical sensing applications. The fundamental understanding of charge transport properties of organic thin-films is critical for both applications. This thesis investigates the charge transport properties of phthalocyanine thin-film devices and couples these properties with chemical sensor developments.

In chapter 1, the basic charge transport processes in the two- and three- terminal devices are reviewed. In chapter 2 & 3, we have investigated the AC and DC charge transport properties of the CoPc two-terminal devices. The frequency dispersive charge

transport property in CoPc thin-films has been characterized and applied for analyte identification. The Ohmic conduction and Space-charge-limited conduction (SCLC) processes have been characterized by both macroscopic and microscopic measurements. A practical sensing technique has been developed based on the fundamental understanding of the charge transport process: operating in the SCLC region to enhance the device to device repeatability. In chapter 4, the bias-induced charge trapping is identified as the major source of electrical instability of OTFT sensors. A pulsed gating method has been developed to obtain ultra-low drift even for low vapor pressure analytes, such as organophosphonate nerve agent simulants. In chapter 5, the chemical sensing properties of phthalocyanine thin-film transistors have been investigated using n-type and p-type devices. The effects of surface pre-adsorbed oxygen in channel conductivity and chemical responses have been investigated. In chapter 6, ultrathin organic transistors have been reported for chemical sensing by maximizing the charge trapping effect in chemical sensor responses, thereby, greatly enhance the chemical sensitivity.

1. INTRODUCTION

1.1. Organic Semiconductor Thin-films and Electronic Devices

1.1.1. Charge Transport in Organic Semiconductor Thin-films

Organic semiconductors have found a wide range of technological applications in electronic devices such as organic light-emitting diodes (OLEDs)[1,2], organic photovoltaics cells (OPVs)[3,4], and organic thin-film transistors (OTFTs)[5-7]. These devices utilize organic materials as the electrically or optically active layers and therefore enable low temperature processing of materials and devices. Organic materials have immensely tunable electrical and optical properties due to the versatile chemical structure modifications. The combined advantages in low processing cost and superior materials properties enable the OLEDs technology to reach the commercialization markets such as flat panel displays. However, the OPVs and OTFTs technologies have not grown out of research laboratories yet, which are limited by the charge transport properties of organic thin-films. The weak intermolecular forces between organic molecules limit the charge transport mobility to below 10 cm^2/V s, due to the existence of large density of trap states.[8] Therefore, it is a fundamentally and practically important topic to investigate the charge trapping properties of organic thin-films.

Organic materials are also sensitive to the chemical environment and have demonstrated tunable chemical sensitivity and selectivity.[9] Therefore, organic semiconductor materials are natural candidates for chemical sensors. Commercialized

chemical sensors are typically made of inorganic semiconductor materials such as Si, SnO_2, and ZnO.[10] These devices are typically required to be operated at elevated temperature (>100 ^oC) and typically consume over 0.5 W of power. These inorganic materials also have poor chemical selectivity. Chemical sensors made of organic materials in the configuration of chemiresistor or chemically sensitivity field-effect transistors (ChemFETs) have been reported.[7] The operating principles of these organic chemical sensors strongly depend on the fundamental understanding of charge transport properties of organic thin-films. This thesis work is to couple the fundamental study of charge transport properties with chemical sensing applications of organic thin-films.

Organic semiconductor materials are delocalized pi-electron systems. Materials with different functional groups are selected to cater various device applications. Typical materials used in OLEDs, OPV, OTFTs, and ChemFETs are surveyed in Figure 1.1. Aluminum tris(8-hydroxyquinoline) (Alq_3) is the electron transport material and *N*,*N*′-Di-[(1-naphthyl)-*N*,*N*′-diphenyl]-1,1'-biphenyl)-4,4'-diamine (NPD) is the hole transport material in OLEDs. [6,6]-Phenyl-C_{61} butyric acid methyl ester (PCBM) and Poly[2-methoxy-5-(2-ethylhexyloxy)-1,4-phenylenevinylene] (MEH-PPV) are typically used in OPVs, although MEH-PPV is also used in polymer OLEDs. Pentacene and polythiophene are the most popular materials used in OTFTs. For ChemFETs, phthalocyanine and thiophene derivatives such as didodecyl α-sexithiophene (DDα6T) are used.

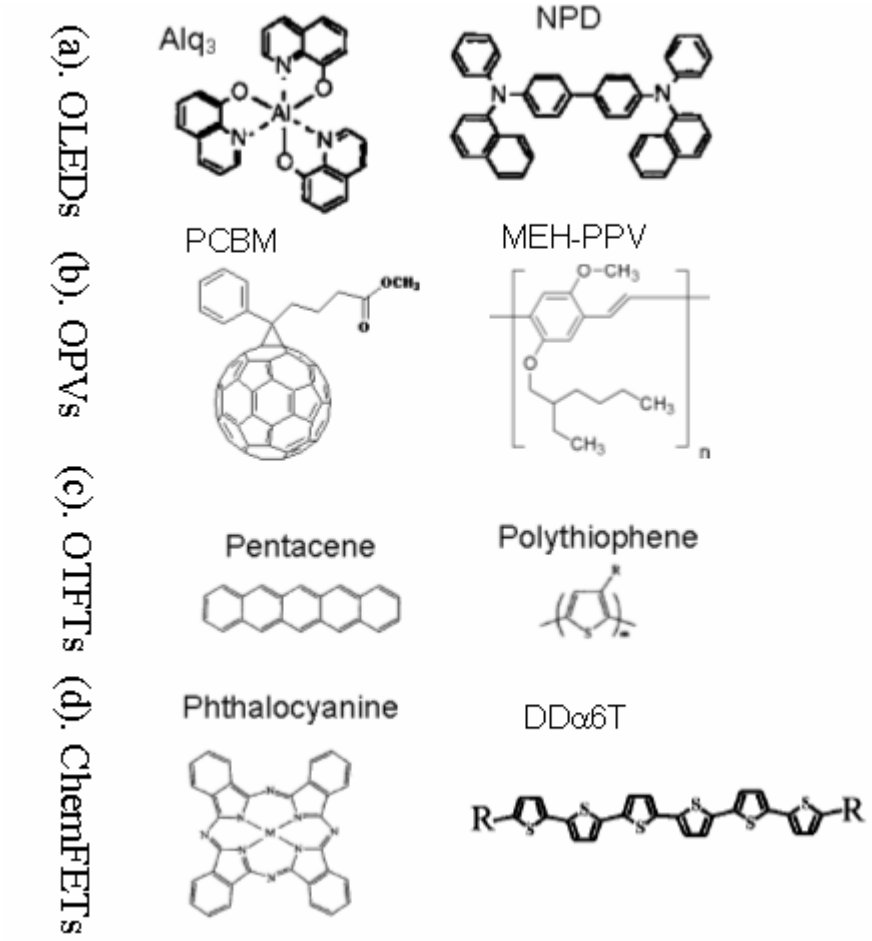

Figure 1.1. Molecular structures of organic semiconductors utilized in organic electronic devices: (a). OLEDs, (b). OPVs, (c). OTFTs, and (d). ChemFETs.

Organic thin-films are held together by weak intermolecular forces such as van der Waals force. Therefore, organic thin-films contain a high density of trap states originated from either structural defects or impurities. Traps strongly affect charge transport properties since the trapped carriers do not contribute to drift or diffusion currents. Furthermore, the columbic force of the trapped charge will affect the electrical field distribution in a device and thereby the charge transport.[11] Using the conventions in inorganic semiconductors, the charge trapping processing can be illustrated in a

schematic diagram shown in Figure 1.2. Taking a p-type material as an example, there are shallow hole trap states located above the valence band. These trap states reduce the drift current in an operating device by trapping the mobile charges.

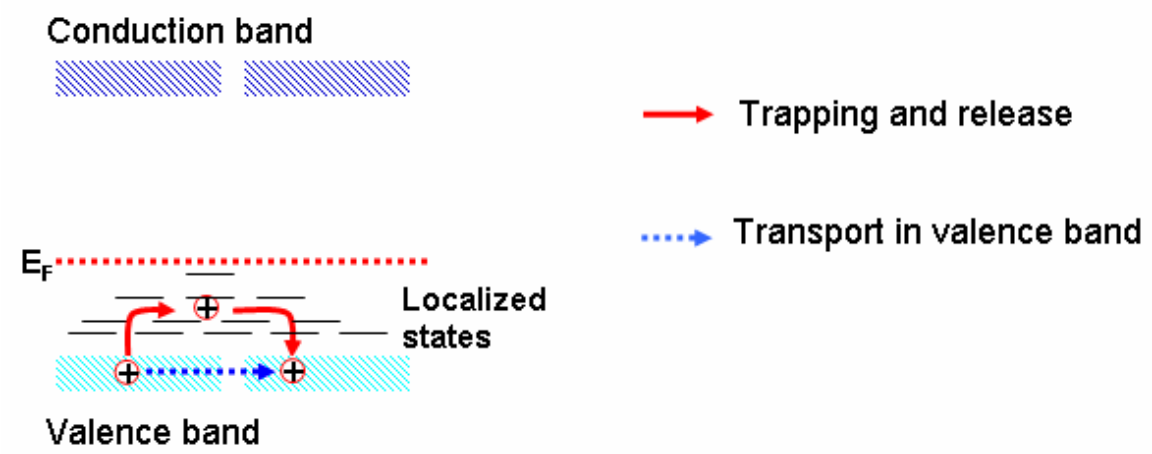

Figure 1.2. Electron energy band diagram of charge trapping processes for a p-type material. The dash lines above the valence band represent hole trap states.

In the two-terminal organic devices, the charge transport properties of organic thin-films have been well studied. Given an Ohmic contact between electrodes and organic thin-films, there are two processes occurring depending on the electrical field.[12] At the low electrical field, charge transport by thermal carrier dominates. The injected carriers are compensated by dielectric relaxation process and no net charges build up in the film. At the high electrical field, however, the injected carrier density exceeds the thermal carrier density. The injected carriers form space charges to limit the current flow. Therefore, the conduction mechanism is called space-charge-limited conduction (SCLC). The current – voltage relationship in the two-terminal devices can be derived with analytical terms. The $J - V$ characteristic follows Ohm's law in the Ohmic conduction region as

$$J = qp_o\mu_p \frac{V}{d} \qquad (1.1)$$

where J is the current density, q is the elementary charge, p_o is the thermal carrier density, μ_p is the hole mobility and d is the electrode spacing. The $J - V$ characteristics in SCLC region can be modeled by solving the Poisson's equation with boundary condition. The electrical field is related to charge density by Poisson's equation

$$\frac{dF(x)}{dx} = \frac{q\left[p(x) + p_t(x)\right]}{\varepsilon} = \frac{\rho}{\varepsilon} \qquad (1.2)$$

where $F(x)$ is the electrical field, $p(x)$ and $p_t(x)$ are the densities of injected free and trapped charge density, ε is the material dielectric constant. The current density can be written as

$$J = q\mu_p p(x) F(x), \qquad (1.3)$$

neglecting the diffusion current, since the diffusion current is very low in organic thin-films. The density of trapped charge is given as

$$p_t(x) = \int_{E_t}^{E_V} h(E,x)\, f_p(E)\, dx \qquad (1.4)$$

where $h(E,x)$ is the distribution function for trap states, $f_p(E)$ is the Fermi Dirac distribution function, E_V and E_t are the valence band and trap state energies respectively.

We are going to derive the $J - V$ characteristics in two simple trap distribution cases. In the first case, the thin-film is assumed to be trap free ($p_t(x) = 0$). Multiply both sides of equation 1.2 with *2F(x)* and substitute *p(x)* with equation 1.3, we obtain

$$2F(x)\frac{dF(x)}{dx} = \frac{d\left[F(x)\right]^2}{dx} = \frac{2J}{\varepsilon\mu_p} \qquad (1.5).$$

Integrate equation 1.5 and use the boundary condition

$$V = \int_0^d F(x)\,dx, \qquad (1.6)$$

yields

$$J = \frac{9}{8}\varepsilon\mu_p \frac{V^3}{d^2}. \qquad (1.7)$$

Equation 1.7 is the well-known Mott and Gurney equation for the space-charge limited current in insulators. The equation accurately predicts the cubic dependence of current density on the applied voltage and square dependence on the electrode spacing.[13] However, the actual current densities in these solids are found to be much lower than the predicated values. The effect is attributed to reduced free carrier density by trap states. The *J* - *V* characteristics in SCLC region depend on the trap energy distribution.

In the second case, we assume trap states are confined in a single energy level - E_t. Using the same procedure as above, the *J* - *V* characteristic is derived as following

$$J = \frac{9}{8}\varepsilon\mu_p\theta_t \frac{V^3}{d^2} \qquad (1.8).$$

Equation 1.8 is a simple modification of equation 1.7 with the ratio of free to total charge density

$$\theta_t = \frac{p}{p + p_t} = \frac{g_p N_v}{H_a}\exp\left(-\frac{E_t}{k_b T}\right) \qquad (1.9)$$

where g_p is the degeneracy factor, N_v is the density of state at valence band, H_a is the density of traps, k_b is the Boltzmann constant and T is the temperature. For other more complicated trap energy distribution functions such as exponential or Gaussian distributions, the *J* - *V* characteristics have been derived by Kao and Huang.[12]

1.1.2. Device Physics of Organic Thin-film Transistors

The predominant three-terminal organic device structure is thin-film transistor (TFT), which has at least four different configurations, regarding to the location of gate, source, and drain electrodes. Bottom-gate structure is the dominate configuration in literature reports, which has top contact (TC) and bottom contact (BC) structures as shown in Figure 1.3.[6] A thin insulator layer separates gate electrode from the organic semiconductor layer. Charge carriers are accumulated by the gate capacitor and flow between the source and drain electrodes. Typical organic materials used in OTFTs are listed in Figure 1.1c &1.1d. The bottom-gate TC structure generally shows better performance than those with BC structure. However, the TC structure on Si wafer substrates is difficult to fabricate using photolithography process and therefore, is limited to long channel devices. The bottom-gate BC structure is more suitable for device scaling and chemical sensing studies.

Figure 1.3. Bottom-gate OTFT device structures. (a) Top contact electrode configuration, (b) bottom contact electrode configuration.

The charge transport properties of OTFTs are reported to be confined in a few monolayers above the gate dielectrics.[14] Therefore, the chemical and physical properties of the gate dielectric/organic interface is of tremendous importance. It is found that the surface treatment of SiO_2 with self-assembly monolayers (SAMs) can change the

mobility values of pentacene thin-film transistors by an order of magnitude.[15] Surface functionalization with SAMs can also change the threshold voltages of OTFTs due to the built-in dipole moment of SAMs or charge transfer between SAMs and SiO_2.[16]

There are two existing analytical models describing the field-effect mobility in OTFTs: one is the variable range hopping (VRH) model by Vissenberg et al.[17] and the other is the multiple trapping and release (MTR) model by Horowitz et al.[18] According to the VRH model, the charge transport is by hopping of carriers between localized states. This model predicts a thermally activated mobility, as hopping is a phonon assisted process. Experimental results on conducting polymers and some polycrystalline thin-films agree with this prediction.[17] According to the MTR model, the majority of the carriers are immobilized in the localized trap states. Carriers are thermally released to the delocalized band to enable carrier transport between trapping events, which also predicts temperature dependent mobility. The field-effect mobility dependence on gate voltage and temperature in pentacene and polythienylene vinylene (PTV) transistors is shown in Figure 1.4.[17,19]

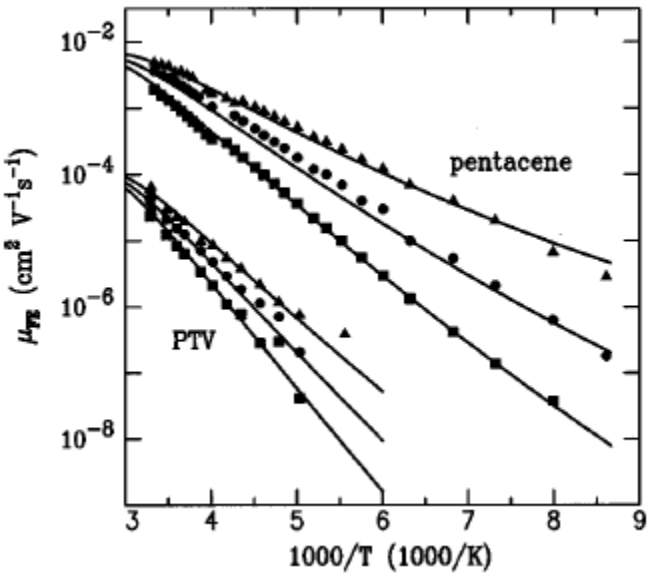

Figure 1.4. Gate voltage and temperature dependent properties of field-effect mobility (μ_{FE}). The gate voltages are -20 V (triangles), -10 V (circles), and -5 V (squares).

The theoretic derivation of the field-effect mobility in VRH model is summarized, followed by a brief description of the results in the MTR model. In the VRH model[17], an exponential density of (localized) states (DOS) is assumed:

$$g(E) = \frac{N_t}{k_b T_0} \exp\left(\frac{E}{k_b T_0}\right) \quad (-\infty < E \le 0) \qquad (1.10)$$

where N_t is the number of states per unit volume and T_0 is a parameter that indicates the width of the exponential distribution. The VRH model assumes the transport of carriers is governed by the hopping of carrier between localized states. The conductance can be written as $G_{ij} = G_0 e^{-s_{i,j}}$ between site i and j, where

$$s_{ij} = 2\alpha R_{ij} + \frac{\left|E_i - E_f\right| + \left|E_j - E_f\right| + \left|E_i - E_j\right|}{2k_b T}. \qquad (1.11)$$

Here, the first term on the right-hand side (RHS) describes the tunneling process. The second term in RHS takes into account the activation energy for a hop upwards in energy and the occupational probability of sites i and j. According to the percolation theory, the conductivity of the system is given by $\sigma = \sigma_0 e^{-s_c}$, where σ_0 is the prefactor and s_c is the exponent of $G_{ij} = G_0 e^{-s_{i,j}}$. Expression for the conductivity as a function of occupation δ and the temperature T is obtained as

$$\sigma(\delta, T) = \sigma_0 \left(\frac{\pi N_t \delta (T_0 / T)^3}{(2\alpha)^3 B_c \Gamma(1 - T/T_0) \Gamma(1 + T/T_0)} \right) \qquad (1.12)$$

where B_c is the percolation criterion factor.

For a transistor in the linear region, the current is given as

$$I = \frac{WV_d}{L} \int_0^t dx \sigma \left[\delta(x), T \right] \qquad (1.13)$$

where W, L, and t are the width, length, and thickness of the channel, respectively, and V_d is the drain voltage. The field-effect mobility can be derived from

$$\mu_{FE} \equiv \frac{L}{C_i W V_d} \frac{\partial I}{\partial V_g} \qquad (1.14)$$

where C_i is the gate capacitance. Therefore, the field-effect mobility is obtained as following

$$\mu_{FE} = \frac{\sigma_0}{e} \left(\frac{\pi (T_0 / T)^3}{(2\alpha)^3 B_c \Gamma(1 - T/T_0) \Gamma(1 + T/T_0)} \right)^{T_0/T} \left[\frac{(C_i V_g)^2}{2 k_b T_0 \varepsilon} \right]^{T_0/T - 1} . \qquad (1.15)$$

In the MTR model,[18] a similar exponential trap distribution function as in equation 1.10 is assumed. The model splits the surface charge into trapped charge and free charge. At the end of derivation, the field-effect mobility is obtained as

$$\mu_{FE} = \mu_0 \frac{N_V}{N_{to}} \left(\frac{C_i V_g}{q N_{to}} \right)^{T_C / T - 1} \qquad (1.16)$$

where μ_0 is the mobility at band edge, N_{t0} is the total surface density of traps and T_c is a characteristic temperature that accounts for the width of trap energy distribution.

Both models claim to fit well the temperature and gate voltage dependent results shown in Figure 1.4. However, the above two models have not taken into account the inhomogeneous distribution of trap states at the interface of gate dielectric/organic film and the bulk of organic films. Therefore, these two models can only be applied for qualitative description of a real device.

1.1.3. Chemical Sensing Properties of Organic Thin-films

Organic thin-films are natural candidates for chemical sensing as their charge transport properties are highly sensitive to chemical environments. In comparison to commercial metal oxides chemical sensors, organic thin-films sensors have the advantages of low temperature operation and tunable selectivity with great choices of organic materials. Both small organic molecules and conducting polymers have been applied for chemical sensors, including metal phthalocyanines (MPc) and thiophene derivatives shown in Figure 1.1d.

Both two-terminal chemiresistors and three-terminal ChemFETs have been utilized in chemical sensing. In the simplest form of a chemiresistor, small organic molecules or conducting polymers are deposited between a pair of electrodes on an insulating substrate. The gaseous species act as either electron donor or electron acceptor and therefore change the device conductivity. Schottky diodes have also been used for chemical sensing. In the three-terminal ChemFET configuration, either TFT or insulated gate field-effect transistor (IGFET) may be used. In the TFT configuration, the gas species change the channel conductivity of the transistor. In the IGFET configuration, the gas species change the work-function of the organic thin-film, and therefore the current of the device. Both device configurations using conducting polymer as an example are shown in Figure 1.5.[20] In this thesis, we refer TFT chemical sensors as the ChemFETs.

In practical applications, chemical sensor arrays are typically constructed to collect a pattern response of devices to gas analytes. Such system is denoted as electronic noses (e-noses), which carries a high price tag and thus limits their practical application. OTFT arrays are printable by ink-jet or screen printing techniques.[9] The low cost and integratable fabrication technique can greatly reduce the cost of electronic nose systems. The desirable properties of individual chemical sensor element are high sensitivity, high selectivity and high stability. For organic electronic sensors, these sensor properties are related by the charge transport properties of organic films. However, there is no existing analytical model accounting for the chemical sensing properties of organic devices.

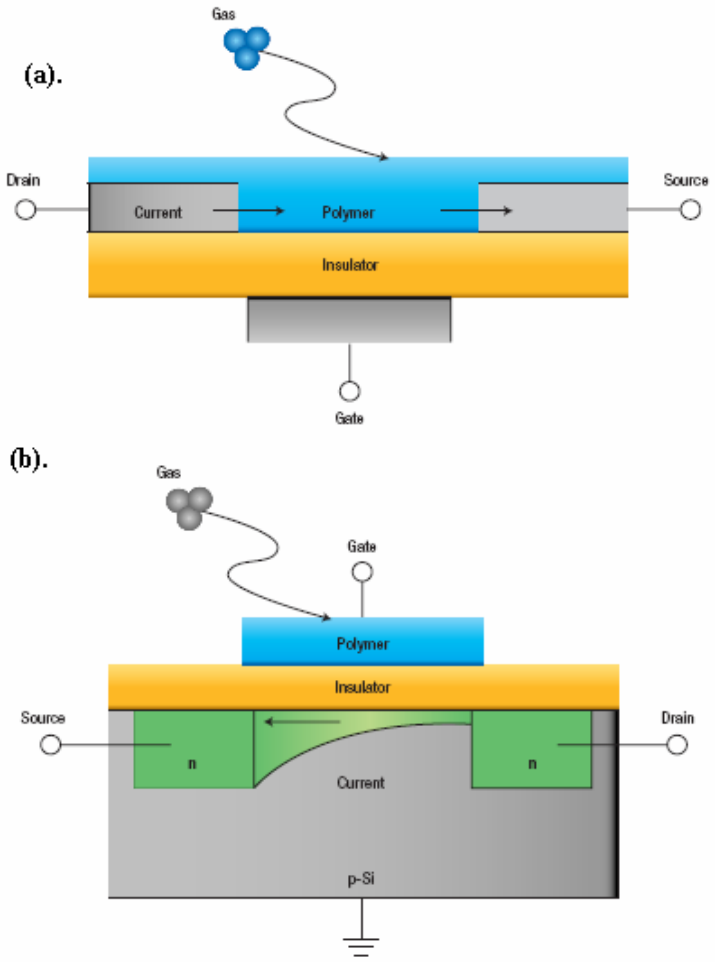

Figure 1.5. Device configuration of three-terminal organic chemical sensors. (a). Chemical sensor in the thin-film transistor (TFT) configuration; (b). chemical sensor in the insulating gate field-effect transistor (IGFET) configuration.

1.2. Thesis Outline

This thesis aims to couple the charge transport study of organic thin-films with the advanced chemical sensor development. We have investigated the charge transport properties of MPc thin-films in both two-terminal and three-terminal devices. In the two-terminal devices, Ohmic and SCLC charge transport properties of CoPc thin-films have been studied by current-voltage characterization, scanning Kelvin probe microscopy and impedance spectroscopy. The frequency dependent AC properties are utilized to identify

gas analytes. We have developed a practical device operation technique to obtain good device to device repeatability by operating the two-terminal device in SCLC region. In the three-terminal FET devices, the charge transport properties are found to be dominated by charge trapping process. We have studied the baseline stability of ChemFETs in detail. An ultra-low drift technique has been developed by pulsed gating. The roles of pre-adsorbed oxygen in channel conductivity and chemical responses in ChemFETs have been investigated with n- and p- type CuPc materials. Ultrathin organic transistors have been designed to enhance the chemical sensitivity and stability. In this thesis work, we have addressed the selectivity, sensitivity and stability of organic chemical sensors from both fundamental investigation and practical application perspectives.

The following papers have been included in the thesis:

1. R. D. Yang, B. Fruhberger, J. Park, and A. C. Kummel, "Chemical Identification Using an Impedance Sensor Based on Dispersive Charge Transport", *Appl. Phys. Lett.* 88 (2006) 074104-074106

2. K. A. Miller, R. D. Yang, M. J. Hale, J. Park, B. Fruhberger, C. N. Colesniuc, I. K. Schuller, A. C. Kummel, and W. C. Trogler, "Electrode Independent Chemoresistive Response for Cobalt Phthalocyanine in the Space Charge Limited Conductivity Regime", *J. Phys. Chem. B*, 110 (2006) 361-366

3. R. D. Yang, T. Gredig, J. Park, C. N. Colesniuc, I. K. Schuller, W. C. Trogler, and A. C. Kummel, "Ultrathin Organic Transistor for Chemical Sensing", accepted by *Appl. Phys. Lett.,* 2007.

2. FREQUENCY DISPERSIVE CHARGE TRANSPORT AND IMPEDANCE SPECTROSCOPY TECHNIQUE FOR ANALYTE IDENTIFICATION

2.1. Introduction

Organic semiconducting materials have been successfully used to fabricate electronic devices such as light-emitting diodes and thin-film transistors. The electrical properties of these materials are sensitive to gaseous species which makes them appealing for chemical sensing.[20-23] Chemical sensors based on metallophthalocyanine (MPc) thin films have been developed in the forms of chemiresistors and surface acoustic wave (SAW) devices since the 1980s.[24] MPcs are thermally and chemically stable; therefore, high quality thin films can be deposited by molecular beam epitaxy in vacuum. Furthermore, the chemical sensitivity of MPc materials can be tuned by varying metal centers or peripheral organic substituents. However, most thin film gas sensors mentioned above monitor the response at a single frequency, which is either the DC resistance or capacitance at a specific frequency.[25] Therefore, the selectivity of the chemical response is limited. In this chapter, we will investigate the frequency dispersive charge transport properties of MPc thin-films. An impedance technique will be described for the application of chemical analytes identification.

For disordered organic thin-films, the conduction mechanism involves charge transport between localized sites, with a rate depending on the temperature and the

applied electrical field. Carrier mobility μ, the proportional factor between drift velocity and electrical field, is a microscopic parameter describing charge transport in solids. The time-of-flight (TOF) measurements of carrier mobility in organic films gave clear evidence for dispersive charge transport in organic films,[26,27] although nondispersive behavior under certain preparation conditions has also been reported.[28] The transient experiments like TOFT provide information about the distribution of transient time.

Impedance spectroscopy measures the frequency dispersive charge transport properties of thin solid films over a wide frequency range.[29] In the Impedance spectroscopy, the complex impedance or admittance of the device can be measured as functions of the modulation frequency and the applied dc voltage. The technique has been applied in both conducting polymers such as poly(*p*-phenylene vinylene) [30] and small organic molecule such as Alq_3 and NPD[31,32] and confirms the dispersive nature of charge transport in organic thin-films.

Changes in the impedance characteristics of thin-films exposed to gaseous analytes provide rich information about charge, dielectric and dipolar relaxation behavior of a material, and have been applied for chemical sensing.[33-35] In this chapter, the changes in AC conductance induced by gas analytes are measured over the frequency range in which the charge carriers can respond to the AC modulation. Due to the disordered nature of organic materials, there is a distribution of transit times for the injected carriers. The responses of all these carriers to chemical analytes can be acquired in one spectrum. We have analyzed impedance spectra of cobalt phthalocyanine (CoPc) thin films exposed to a

variety of solvent vapors. It is demonstrated that analytes can be identified based on the unique frequency response pattern using a single film.

2.2. Samples and Experiment Setup

2.2.1. Sample Preparation

A 6500 Å SiO_2 layer was thermally grown on Si(100) substrates. Interdigitated electrodes (IDEs) with 50 pairs of 10 μm wide, 5 μm spaced fingers were prepared via photolithography in a clean room. The length of the fingers is 4 mm. A 50 Å Ti adhesion layer was deposited on SiO_2 before depositing 450 Å thick Au electrodes using an electron-beam evaporator. CoPc was purchased from Aldrich and purified by zone sublimation at 400 ºC and 10^{-3} to 10^{-4} torr. Films of 500 Å thickness were evaporated from a differentially-pumped hot-lip evaporation cell in an organic molecular beam epitaxy (OMBE) chamber. The OMBE chamber had a base pressure of $< 5x10^{-10}$ torr and a fast introduction loadlock. The substrate temperature was kept at 300 K during deposition. The growth rate was monitored using a water-cooled quartz crystal microbalance (QCM), which was calibrated with X-ray diffraction (XRD) and atomic force microscopy (AFM) measurements. During deposition, the chamber background pressure was around $8x10^{-9}$ torr. Three duplicate sets of devices were fabricated with resistance between 2.8 – 3.8 MΩ in air.

2.2.2. Impedance Spectroscopy

The impedance spectroscopy studies were performed with a Solartron 1260 impedance analyzer interfaced to the sample through a Solartron 1296 dielectric

interface. A small amplitude AC voltage (100 mV) was applied in the frequency range of 0.1 Hz – 10 MHz. The impedance spectra were acquired with the Solartron SMaRT v2.8.0 program (Solartron Analytical, Hampshire, UK) and processed by ZView v2.0 program (Scribner Associates, Inc., North Carolina). Measurements at different AC voltages (v_{ac} = 20 -200 mV) showed no dependence of response on v_{ac}. The DC bias during the measurement was held at 0 V.

A schematic diagram of the device under measurement is shown in Figure 2.1. Electrical contacts were made by using a spring load edge connector.

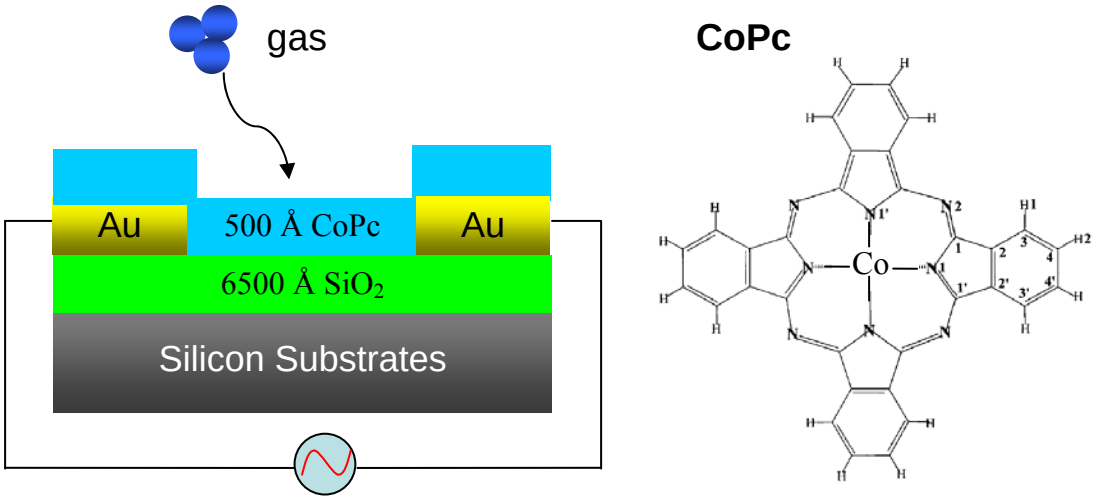

Figure 2.1. The schematic diagram of a CoPc device under impedance measurement. The electrode spacing is 5 μm.

2.2.3. Flow System Setup

Chemical sensing experiments were carried out in the same flow chamber used for the impedance measurements. The internal volume of the chamber was 45 cm^3. The temperature in the chamber was kept at 25 ^oC using a Haake constant temperature bath to

circulate coolant through the chamber walls. Ultra-high purity N_2 was used as both the purge and the carrier gas. A constant total flow of 500 sccm was employed for the dosing measurements. A four-way valve was used to minimize the dead time between introduction of each analyte. Bubblers filled with liquid analyte were kept in a water bath chilled to 15 ^{o}C. Mass flow controllers were used to dilute and introduce vaporized analytes at a known concentration into a manifold to premix with the carrier gas before introduction into the test chamber. Solenoid valves before and after the analyte bubblers were used to prevent cross-contamination between analytes. A diagram of the flow system is shown in Figure 2.2. The gas flow rates and temperatures were controlled by a Labview program.

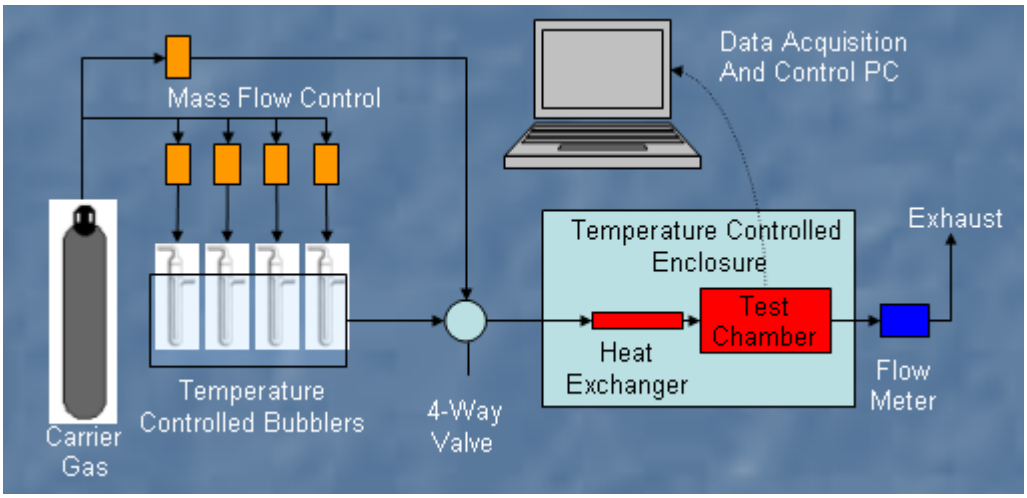

Figure 2.2. A schematic diagram of the gas flow system for chemical sensing measurements.

2.3. Frequency Dispersive AC Conductivity of CoPc Thin-films

The complex admittance $Y = i_{ac} / v_{ac}$ of the CoPc thin-films was measured as a frequency and DC bias voltage at room temperature. The ac conductance $G = \mathrm{Re}(Y)$ is shown in Figure 2.3. The AC conductance demonstrates clear frequency dependent behavior: a relative frequency independent conductance below 100 Hz, a strong frequency dependent conductance above 100 kHz and bumps in the intermediate frequency region between 100 Hz to 100 kHz. The AC conductance is relatively DC bias independent at frequency higher than 100 kHz. The results are consistent with the frequency dependent properties observed on parallel plate devices.[30-32]

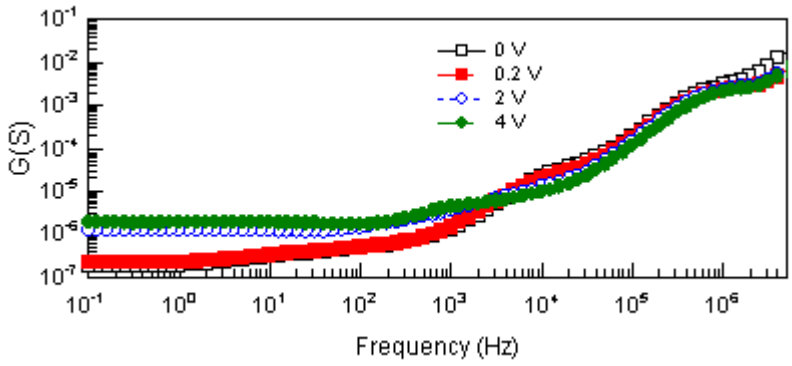

Figure 2.3. The DC bias and frequency dependent AC conductivity of a 50 nm CoPc thin-film.

2.4. Differential AC Conductivity at the Presence of Analytes

2.4.1. Frequency Dependent AC Conductance to Alcohols

The impedance spectra were recorded at 25 ^{o}C to monitor the chemical response of the devices sealed in a temperature controlled stainless steel flow chamber. Various concentrations of methanol, ethanol or isopropanol were introduced into the chamber with a dry N_2 carrier gas using a custom designed flow system. Each impedance spectrum

was recorded after the sensor had been equilibrated with each dose for one hour. The impedance (Z) measurement allows determination of admittance (Y), conductance and capacitance, which are related as shown in equation 2.1,

$$Y(\omega)=1/Z(\omega)=G(\omega)+i\omega C(\omega), i=\sqrt{-1} \qquad (2.1)$$

where G and C are the conductance and capacitance of the device and $\omega = 2\pi f$ is the angular frequency. Figure 2.4a shows differential AC conductance results for methanol in the concentration range of 190 ppm (parts per million) to 95000 ppm (the current limits of our flow system). The analyte induced AC conductance between 5 kHz – 40 kHz saturates above 950 ppm, while it continues to decrease with increasing methanol concentration below 1 kHz. The relative conductance changes at 0.5 Hz and 31 kHz are plotted in Figure 2.4b. In the concentration range of 950 ppm – 19000 ppm, the conductance change at 31 kHz is 2.10 ± 0.18%. For a 20 fold concentration variation, the AC conductance change varies by less than 10%. Conversely, the AC conductance changes at 0.5 Hz increased monotonically with concentration. This result is important for selective chemical sensing because the change in conductance at the high frequency conductance peak can be used to identify analytes. Furthermore, the concentration dependent low frequency change in conductance can be calibrated to determine analyte concentrations using the same sensing film.

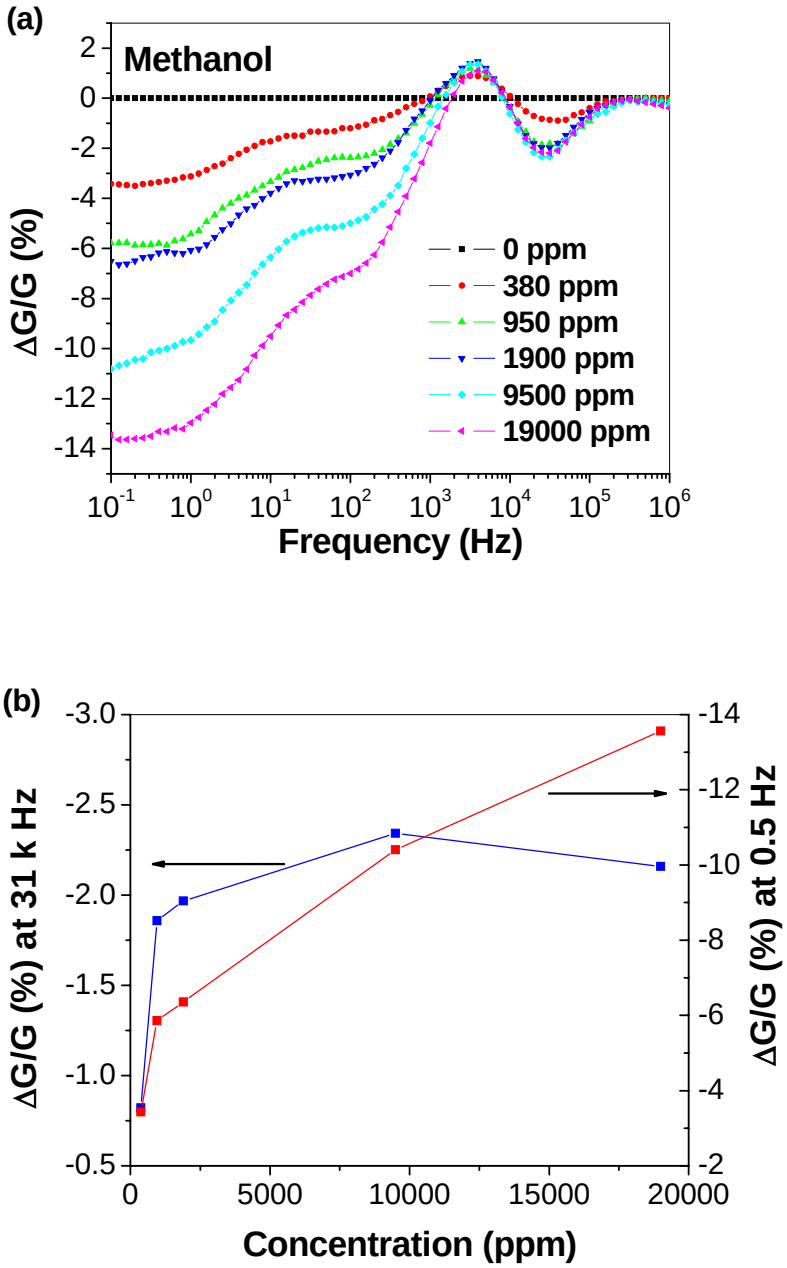

Figure 2.4. (a) AC conductance shift with methanol vapor on 50 nm CoPc thin-film; (b) Conductance shift with concentration at 31 kHz and 0.5 Hz.

To explore the potential of analyte identification with the high frequency differential conductance peak, the impedance spectra of a single film exposed to ethanol and isopropanol vapors have also been recorded. This is a stringent test of the technique

because these analytes have identical functional groups and similar dipole moments. The frequency dependence of the analyte induced changes in conductivity for ethanol and isopropanol are similar to that of methanol, as shown in Figure 2.5 a & b; this is expected for molecules with identical functional groups. However, at the high frequency points (2.5 kHz and 31 kHz), the magnitude of the analyte induced conductivity for each is unique above the saturation concentration. The data are tabulated in Table 2.1. The magnitude of the analyte induced conductivity changes is unique for each alcohol above the saturation concentration. With this finding, the phenomena can be employed to identify analytes using data measured at a few frequency values.

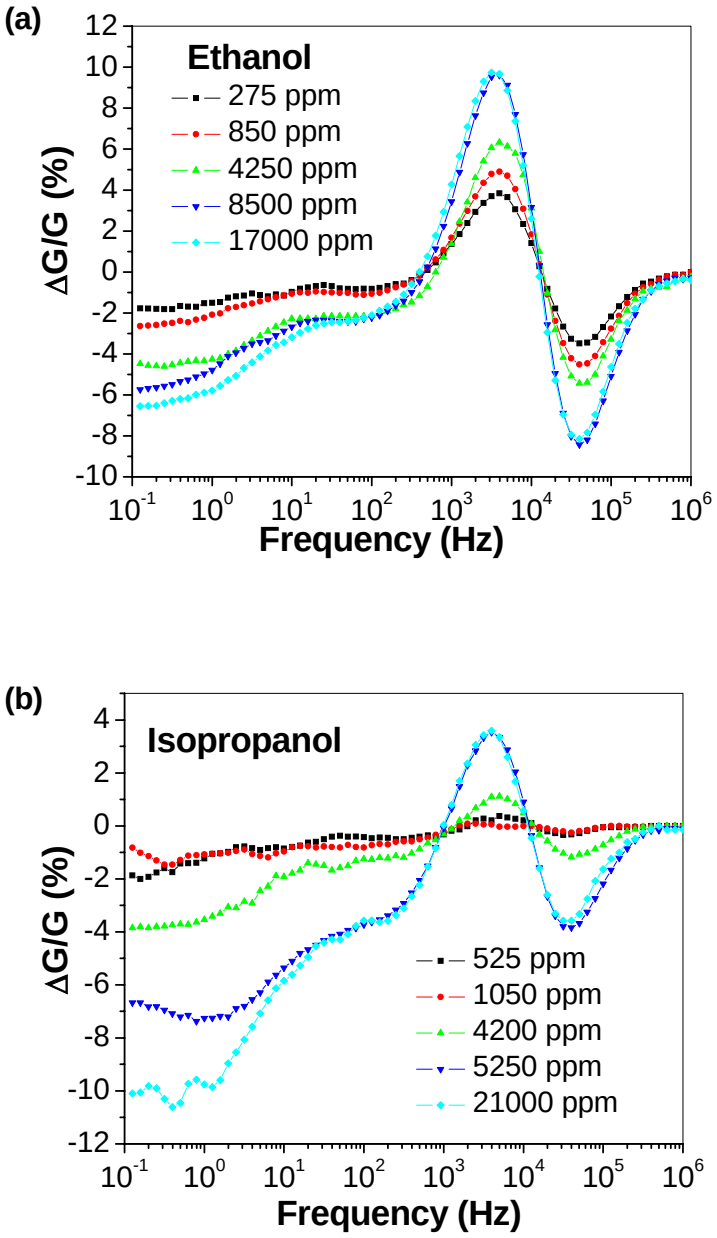

Figure 2.5. AC conductance shift with ethanol (a) and isopropanol (b) vapors on 50 nm CoPc thin film.

2.4.2. Concentration Independent AC Conductance

The saturation behavior in the analyte induced conductivity could be due to microcapillary condensation of analyte at grain boundaries in the polycrystalline CoPc thin films. The analytes responses are also concentration independent above a threshold partial pressure (P*) and lack chemical specificity. The signature of microcapillary concentration is that P* increases with the saturated vapor pressure of the analyte (P_o). Our experiments show that the data are inconsistent with simple microcapilliary condensation because P* does not scale with P_o (Table 2.1.). We speculate that the films have two different types of analyte binding sites. The high frequency feature is associated with tight binding sites which are saturated at much lower concentration than the low frequency ones which are associated with weak binding sites.

Table 2.1. Saturation concentrations of three alcohols and the percentage shift in AC conductivity at 31 kHz. The source temperature is kept at 15 ^{0}C. P_0 is the saturated vapor pressure at 15 ^{0}C. P^* is the threshold partial vapor pressure.

Alcohol	P_0 (mbar)	Saturation Concentration	$P^*/P_0 \times 10^3$	$\Delta G/G$ at 31 kHz
Methanol	127.05	760 ppm	4.6	- 2.3 %
Ethanol	59.02	8500 ppm	109.0	- 5.8 %
Isopropanol	42.74	4200 ppm	75.0	- 3.5 %

To determine the electrical origin of the response in the two frequency regimes, DC bias was applied to probe the charge induced changes in AC conductivity as a function of frequency. In Figure 2.6, the bias induced conductivity change is plotted between 0.1 Hz – 1 MHz for a DC bias of 0.2 V. The differential plots (conductivity w/o

DC bias) should reveal the relaxation properties of injected charges. The DC bias is known to alter charge relaxation times in organic thin films.[36] As shown in Figure 2.6, the DC induced charge injection creates three distinct peaks in the differential AC conductance spectrum. The maximum peak at 2.5 kHz and the minimum one at 31 kHz are similar to the features found in Figure 2.4a, Figure 2.5 a & b. The results suggest that exposure to the analytes and charge injection by DC bias has a similar effect on the charge transport of CoPc thin films. In both cases, the charge relaxation times have been changed.

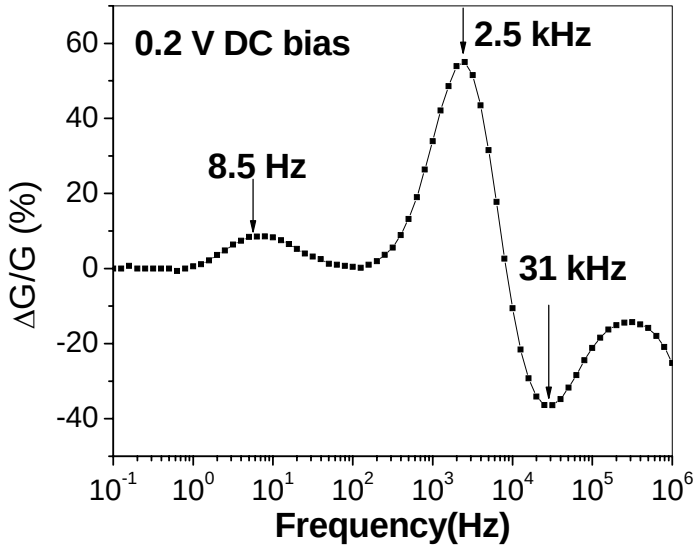

Figure 2.6. AC conductance change with 0.2 V DC bias on 50 nm CoPc thin film.

AC conductance in a semiconducting film can be expressed as shown in equation 2.2[37]

$$G(\omega) = \sigma_0 + C_{HF}\omega^2 \frac{n_1\tau_1}{1+(\omega\tau_1)^2} \qquad (2.2)$$

where σ_0 = DC conductance, C_{HF} = high frequency capacitance, τ_1 = bulk charge relaxation time, n_1= correction factor for the trap distribution. The carrier transit time between electrodes can be determined from the peak in the differential plot of the imaginary part of admittance.[36] The carrier transit time τ between electrodes is defined in equation 2.3,

$$\tau = \frac{L^2}{\mu V} \qquad (2.3)$$

where L is the electrode spacing, μ is the carrier mobility and V is the applied potential. τ determined from transient measurement is one form of charge relaxation time τ_1, which was used in fitting. The transit time in the 50 nm CoPc film on the 5 micron spaced interdigitated electrodes was determined to be 34 μs. This value corresponds to relaxation frequency of 29 kHz, which is very close to the feature at 31 kHz shown in Figure 2.6. The high frequency capacitance of the device was measured to be 2.1 nF above 20 kHz. By fitting the conductance data under exposure to 950 ppm of methanol in nitrogen, we can deduce that methanol increases the bulk charge relaxation time to 37 μs (or 10%). We assumed $n_1 = 0.1$ (n_1 is the correction factor for the ratio of interface to bulk traps) in the fitting, which gives a consistent value for the estimated charge relaxation time.

The carrier relaxation time is known to be dependent on the carrier concentration in organic semiconducting films.[38] One possible mechanism by which the alcohols in our study increased the carrier relaxation time is by decreasing the hole concentration in the MPc thin film. It has been suggested that –OH functional groups could reduce the hole concentration in CoPc thin films.[39] All the alcohols we tested increased the carrier

relaxation time, consistent with the fact that all contain electron donating –OH groups which reduce the hole concentration. The carrier relaxation time is also dependent on the material properties. The resonance frequency is found to appear at higher frequency on films deposited at high temperature.

2.5. Analyte Identification in Frequency Domain

We have converted the magnitude of impedance changes into frequency shifts in a resonant circuit using dissipation spectroscopy. The dissipation factor (DF) is defined as the ratio of the real to imaginary part of the impedance, as shown in equation 2.4. When the imaginary part of the impedance goes to zero, a sharp resonance peak is induced in the DF spectrum.

$$DF = \frac{\mathrm{Re}\, Z(\omega)}{\mathrm{Im}\, Z(\omega)}, \text{when } \mathrm{Im}\, Z(\omega) \to 0, DF \to \infty \qquad (2.4)$$

Dissipation spectroscopy has been used before to detect volatile organic vapors (VOC) with conducting polymers.[40] This technique is a resonance detection method; therefore it has higher resolution than conductivity magnitude measurements. Furthermore, a simple circuit can be employed to detect the change in the dissipation resonance instead of a spectrum analyzer. Instead of using the device self-resonance, in our experiments, an inductor was added in series to the chemical sensor films to tune the resonance frequency to the range where the saturation phenomena occur. The method is briefly explained in equation 2.5, and a detailed report will appear elsewhere.

$$Z(\omega) = R(\omega) - i\frac{1}{C\omega} + iL\omega, DF = \frac{R(\omega)}{\frac{1}{C\omega} - L\omega}, DF = 0 \text{ when } \omega = \sqrt{\mathrm{LC}} \qquad (2.5)$$

where R is the film resistance, C is the device capacitance and L is the inductance. Conceptually, the imaginary part of the impedance goes to zero at the frequency at which the film capacitance is in resonance with the circuit inductance. The external inductor allows lowering this frequency to the kilohertz range where the analytes induce maximum changes in capacitance. Thus the external inductor allows us to use dissipation spectroscopy to detect analyte in MPc films even though the device's self-resonance occurs at higher frequencies.

The respective spectra for the sensor exposed to the three alcohols at their saturation concentrations in nitrogen carrier gas are shown in Figure 2.7. Methanol, isopropanol and ethanol were found to increase the resonance frequency from the background value in nitrogen carrier gas by 50 Hz, 60 Hz and 116 Hz respectively in the saturation range. The frequency resolution of our data easily allows identification of the 3 analytes. Similar results were obtained with dry air as the carrier gas.

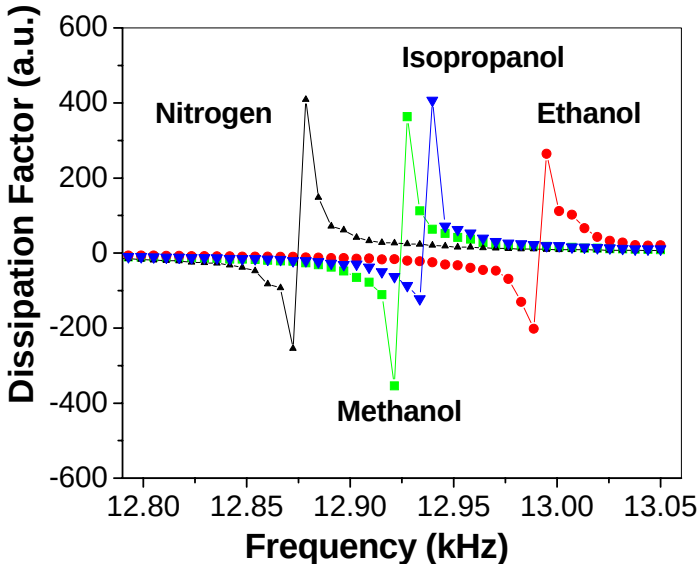

Figure 2.7. Resonance dissipation spectra for methanol (760 ppm), isopropanol (4200 ppm), and ethanol (8500 ppm) in nitrogen carrier gas on 50 nm CoPc thin film.

The dissipation spectroscopy method is well-suited to identify analytes in the frequency domain because each analyte induces a different change in the dissipation frequency relative to the carrier gas peak (air or nitrogen). Drift in chemical sensors is always a challenge. In the dissipation spectrum, the resonant frequency of the carrier gas peak drifts due to film aging or contact changes. However, the dissipation frequency shift (260 Hz ± 8 Hz) by methanol relative to the dry air carrier gas peak was found to be constant on multiple trials. Therefore, the dissipation technique can be calibrated using the background air resonance in practical applications.

2.6.Conclusion

In conclusion, Impedance spectroscopy has been used to demonstrate analyte identification in semiconducting metallophthalocyanine thin films. Above a critical concentration, the magnitudes of the conductivity changes at high frequency are invariant

with concentration and can be used to identify the chemical analyte. The analyte induced AC conductivity changes above 5 kHz have been converted to frequency shifts of 50 Hz to 116 Hz in a sharp circuit resonance and used to differentiate methanol, ethanol, and isopropanol vapors in a nitrogen (and air) carrier gas. The analyte induced changes in the conductivity as a function of frequency have similar response pattern with charge injection by DC bias, suggesting that the analyte induced conductance changes may be due to charge relaxation time changes. The chemical response based on dispersive features of charge transport in organic semiconducting films holds great promise for identification and quantification of analytes using a single sensing film.

This chapter, in part, has been published as "Chemical Identification Using an Impedance Sensor Based on Dispersive Charge Transport", by R. D. Yang, B. Fruhberger, J. Park, and A. C. Kummel, *Appl. Phys. Lett.* 88 (2006) 074104-074106.

3. ELECTRODE INDEPENDENT CHEMICAL SENSITIVITY IN THE SPACE-CHARGE-LIMITED CONDUCTION REGION

3.1. Introduction

Charge transport mechanism in organic films is an important topic for both fundamental study of organic semiconductors and practical applications of organic electronic devices. This chapter first investigates the charge transport properties of organic two-terminal devices at the macroscopic and microscopic levels. Impedance spectroscopy is then used to understand the interface properties of the metal/organic contacts. Finally, a chemical sensing technique is proposed and tested with the basic understanding of charge transport processes in the two-terminal MPc devices.

MPC materials such as CuPc have been used as model systems for charge transport study of organic materials because they are chemically stable and can be readily deposited in vacuum.[41,42] MPc have several technological applications,[43] such as charge transport layers in OLED[44] and thin film transistors.[45] Electrical conductivity measurements have been systematically performed on MPc thin-films for thicknesses between 0.1-20 μm[46-53] It has been found that the conductivity is dominated either by thermally-generated or electrode-injected carriers.[49] At low field, the primary conduction behavior is Ohmic, as thermally generated carriers and carriers created by oxidation from atmospheric oxygen[54,55] exceed those of electrode injected carriers. At high field, space-

charge-limited conduction (SCLC) dominates as electrode-injected carriers exceed the thermally generated ones in the film. Previous studies of undoped ZnPc films 20 nm thick on Au electrodes showed Ohmic conduction in the 1-5 V region.[56] Studies of GaClPc suggest that electrode surface impurities can lead to Ohmic instead of SCLC behavior. If charge transport is determined by carrier-injection from the electrode, it raises the question as to whether the chemical sensing properties might also depend on the electrode materials and conduction mechanism. This is an important issue for chemosensing devices based on MPc materials.

Most of the research studies on charge transport properties of MPcs have been done on micron thick films sandwiched between two parallel metal plate electrodes.[46-53,57-60] Planar electrodes are more practical for chemical sensing applications, because they have larger areas exposed for analytes adsorption. However, there are only a few studies about MPc charge transport properties in a planar electrode configuration[50,55,61] In this chapter, we report studies employing interdigitated electrodes fabricated using photolithography with an electrode spacing of 5 microns. Nanoscale films have been deposited by OMBE under ultra high vacuum (UHV) and results show that the MPc-electrode interface plays a significant role in charge transport, especially at low applied voltages. The MPc-electrode interfacial region traps injected charge carriers and increases the bulk resistance. To probe the influence of the MPc-electrode interface on the transitional voltage between Ohmic and SCLC, MPc thin films were deposited by OMBE on several metal electrodes.

We have also compared chemical sensitivity of MPc thin film devices on different electrode materials in both Ohmic and SCLC regimes to determine if the source of the

charge carriers influences the chemical sensitivity of the films. A key question is whether analyte-induced changes at the MPc-electrode junction influence the sensor response. Maintaining a constant resistance from device to device is difficult to control, but this issue is crucial for obtaining reproducible chemical sensor responses. In particular, we investigated whether the operational conditions of the device can be manipulated to obtain consistent chemosensor responses. Most previous studies on MPc films have focused on chemical sensing of strong hole generating oxidants, such as nitrogen dioxide and ozone at high device operating temperatures (> 100 ^{o}C) ,[24,50,62-70] whereas few have examined less reactive vapor analytes, such as dimethylmethylphosphonate (DMMP).[66,71] In the present study, the exposure of 50 nm CoPc thin films at 25 ^{o}C to water and to nonreactive volatile organic vapors, such as methanol, toluene, and a nerve gas stimulant, DMMP are examined. The results demonstrate sensitive responses from the above non-reactive vapors at ambient temperature. The chemical sensing results correlate well with the charge transport studies. A practical operation strategy is proposed to minimize sensor drift and maintain uniform chemosensitivity among different devices. By operating devices under SCLC conditions, the chemosensor response becomes independent of the analyte absorption at the MPc-electrode interface causing the response to become uniform and reliable.

3.2.Experimental Techniques

3.2.1. Sample Preparation

The sample preparation is similar to the procedures described in Chapter 2. Briefly, CoPc was purchased from Aldrich and purified by zone sublimation at 450 ºC and 50 mtorr. A 6500 Å SiO_2 layer was thermally grown on silicon substrates.

Interdigitated electrodes (IDE) (5 μm spacing, 50 pair fingers, 50 nm Au, Pd or Pt) were prepared by photolithography process. Films of 500 Å were deposited in an OMBE chamber at the base pressure of 1.2 $x10^{-7}$ Torr. The substrate temperature was held at room temperature (25 ^{o}C).

3.2.2. Electrical Characterization and Chemical Sensing Setups

Current-Voltage (I-V) curves were measured between 5 ^{o}C and 70 ^{o}C using a Keithley 6517/6521 electrometer interfaced to a computer. The IDE devices were allowed to equilibrate at each temperature, and the voltage was scanned through +10 V to –10 V in 0.1 V increments at each temperature. Several samples were tested for hysteresis and none was observed.

The impedance spectroscopic studies were performed using a Solartron 1260 impedance analyzer interfaced to the sample through a Solartron 1296 dielectric interface. A small amplitude AC voltage (100 mV) was applied in the frequency range of 0.1 Hz – 10 MHz.

Chemical sensing experiments were carried out in a similar flow chamber described in chapter 2. The internal volume of the chamber was 15 cm^3. The analytes employed were DMMP ($C_3H_9O_3P$) (a simulant for sarin), water, methanol (CH_3OH), and toluene ($C_6H_5CH_3$)).

3.2.3. Scanning Kelvin Probe Microscopy (SKPM)

The local surface potential profiles of CoPc devices were measured using the Nanoscope IIIa SKPM module. SKPM measures the spatial distribution of surface

potential in an operating device and provides valuable information about the electrical field and charge distribution. The technique has been successfully applied to characterize charge transport properties in OFET by several groups.[72,73] SKPM is based on traditional Kelvin probe measurement, which uses a vibrating capacitor device to measure the work function or surface potential of the material. Figure 3.1a shows a schematic diagram of the SKPM apparatus. DC and AC voltages are simultaneously applied between the tip and sample, which creates an oscillating electrostatic force

$$F = \frac{dC}{2dz}(V_{dc} + V_{ac}\sin(\omega t) - \phi(x)) \qquad (3.1)$$

where $\phi(x)$ is the surface potential. When $V_{dc} = \phi(x)$, the cantilever feels no electrostatic force. Therefore, the surface potential can be recorded as the tip DC voltage.

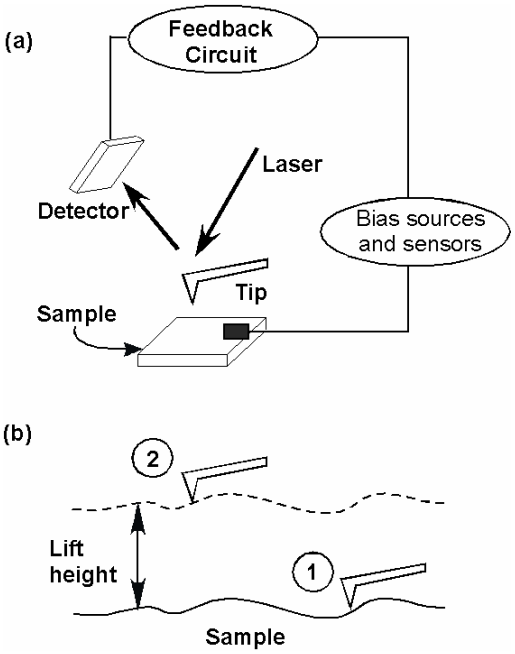

Figure 3.8. Schematic diagram of (a) scanning Kelvin probe microscopy setup and (b) two-pass scan used in the SKPM measurement.

In order to minimize the influence of the topography on the SKPM results, the measurement adopts a two-pass scan method, as illustrated in Figure 3.1b. In the first scan, the topography of the sample is recorded; while in the second scan, the tip is raised to a certain height (10-100nm) above the sample, retraces the topography and the SKPM measurement is performed. Topography-induced scanning artifacts are dramatically reduced by this two-pass scan method.

3.3. Results and Discussion

3.3.1. Microscopic View of Charge Transport in CoPc Thin-films

The charge transport mechanism in an organic film can be inferred macroscopically from the current-voltage curves. Two different behaviors have been observed in the I-V curve plotted in double logarithmic scale, shown in Figure 3.2. In the low voltage region (<1 V), the slope of $log\ I - log\ V$ is 1. In the high voltage region (>=1 V), the slope of $log\ I - log\ V$ >= 2. The slope at voltage > 4 V levels off, which may be ascribed to trap-filling-limited SCLC.[13] It is consistent with literature reports that there is a transition from Ohmic to SCLC behavior in organic films, from low to high applied voltage.[13] In the Ohmic region, all the injected carriers are relaxed by the thermal carriers. Therefore, no net charge builds up in the film. While at higher voltage, the injecting carriers exceed the thermal carrier density, and an opposite electrical field to the applied field is built up that limits the current. The SCLC behavior has been observed in low thermal carrier materials including conducting polymers[74] and small organic molecules.[75]

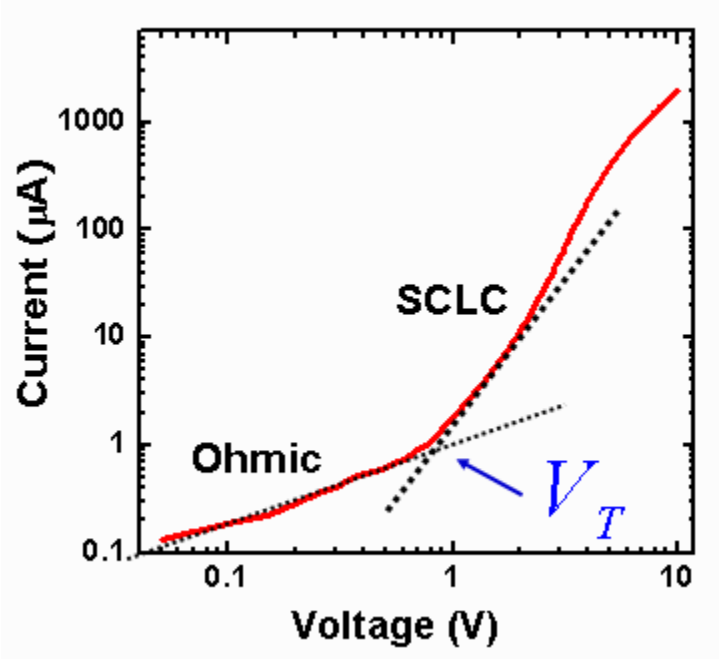

Figure 3.9. Current-voltage curves of a 50 nm CoPc film with 5 micron wide gold contacts. The device shows Ohmic behavior at low voltage region (<1 V) and SCLC behavior at high voltage region (>=1 V).

The surface potential profiles of the above device were measured with SKPM. The device was wired bonded to gold contact pads. The voltage was applied though an external power supply. The surface potential profiles between two electrodes have been recorded between 0 to -15 V at -0.5 V/step shown in Figure 3.3a. It has been observed that the potential profiles are linear between the two electrodes (< 1.5 V). While at higher voltage, the potential profiles are parabolic (>= 1.5 V). We have noted the difference between the applied and measured potentials at both injecting and extracting electrodes. Since there are 50 nm CoPc film coverage on the metal electrodes, charge buildup in these organic films will cause the potential drop over the film. Additionally, these organic films are typically doped by atmosphere molecules such as O_2 and H_2O. These surface dopants will also cause the potential drop. The electrical field profiles were derived from

the surface potential profile and shown in Figure 3.3b. At low bias, the electrical field is constant in the channel, corresponding to zero charge buildup. At higher bias, the electrical field varies with space, clearly proving the space charge buildup in the film. The results are consistent with the EFM study of NPD molecules dispersed in polystyrene matrix.[76] Large electrical field magnitude has been observed near the gold electrode contacts. It reflects a large driving force for charge injection, although the electric field may be influenced by the large topography variation near the electrodes.

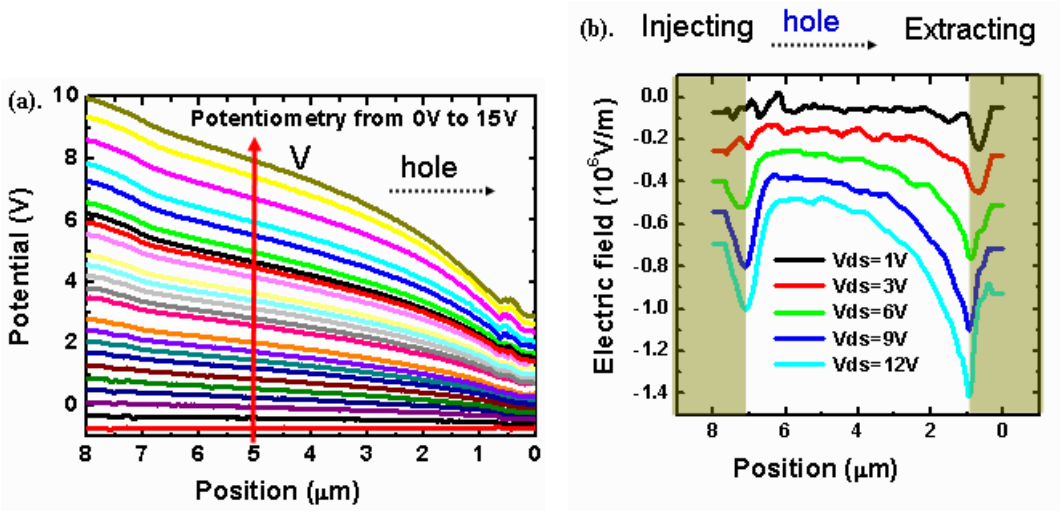

Figure 3.3. The SKPM characterization of a 50 nm CoPc film. (a). Surface potential profiles measured between 0 to -15 V at -0.5 V/step; (b). The electrical field derived from the surface potential shown in (a). The electrodes are shadowed in (b).

The contact resistance between metal electrodes and organic films limits the carrier injection in organic devices. SKPM is a direct technique to image the potential drop between metal electrodes and organic films. In the CoPc thin-films, we found the potential drop is determined by the growth temperature of CoPc films. Shown in Figure 3.4 are the AFM images and the SKPM profiles for the CoPc films grown at room temperature and 200 ^{o}C. Using the same electrode material, the potential drop at injecting

electrode is 2 V larger for the sample grown at 200 °C. The increased potential drop may be ascribed to two effects. Firstly, the grain size of the CoPc film increases with growth temperature, therefore, the bulk resistance is reduced. Secondly, de-wetting between organic material and electrode material has been reported to occur at higher temperature.[77] Therefore, the contact resistance becomes more significant for the sample grown at higher temperature. For the 200 °C sample, the resistance of the CoPc planar electrode device is dominated by the contact resistance.

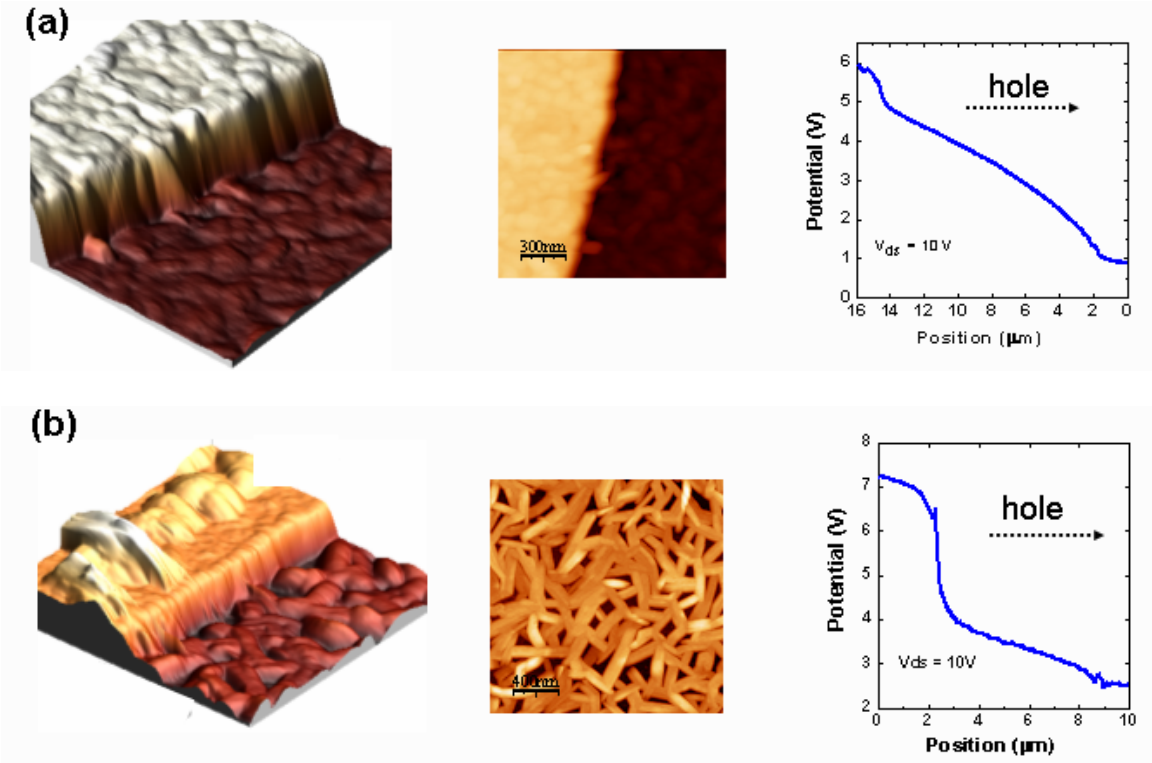

Figure 3.4. Morphology and surface potential profiles between gold and CoPc films grown at room temperature (a) and 200 °C (b).

3.3.2. Impedance Measurement of CoPc/electrode Interface Properties

Impedance spectroscopy uses variable frequency AC signals to simultaneously measure the frequency dependent resistance and capacitance. The studies have revealed the co-existence of low and high frequency traps in the CoPc thin films, which may result from interfacial vs. bulk charge traps.

The impedance of a device can be expressed as in equation 3.2:

$$Z(\omega)=Z'(\omega)+jZ''(\omega)=R(\omega)-j\frac{1}{\omega C(\omega)},\ j=i=\sqrt{-1} \qquad (3.2)$$

where Z' and Z'' are the real and imaginary parts of impedance, which represent resistive and capacitance components in the device, and $\omega = 2\pi f$ is the angular frequency. Shown in Figure 3.5 are the impedance spectra of CoPc/Au, CoPc/Pd and CoPc/Pt devices plotted in the complex plane. The frequency increases from right to left, from 0.1 Hz to 1 MHz. For a circuit with an ideal resistor and capacitor in parallel, one perfect semicircle should be observed in the complex plane. The RC relaxation time τ can be determined when the magnitudes of real and imaginary parts are equal.

$$Z'=-Z''$$
$$\tau=\frac{1}{\omega}=R*C \qquad (3.3)$$

In real organic devices, the semicircles are often distorted due to a relaxation time distribution. If the relaxation times differ by more than two orders of magnitude, then two semicircles can be observed instead of one.[78-82] For example, two semicircles are clearly resolved in the CoPc/Au device shown in Figure 3.5a. The low frequency semicircle is attributed to interfacial traps because such traps typically have longer relaxation

lifetimes.[83] The high frequency semicircle is attributed to bulk traps - because bulk materials are typically more ordered than the interface, and thus have faster charge relaxation. In the CoPc/Pt device, only one semicircle is found, which suggests that charge transport is dominated by the bulk material. This is also consistent with DC conductivity measurements, which show that SCLC behavior is dominant for the Pt electrode device. In the CoPc/Pd device, an intermediate behavior was found, and there are two semicircles in the impedance spectrum of Figure 3.5b. Since the relaxation time constants do not differ by at least two orders of magnitudes, only distorted semicircles are observed.

The co-existence of interface and bulk traps is further documented by DC voltage dependence impedance experiments. At the interface between organic semiconductors and metals, localized electronic states may trap significant amounts of charge, which act as potential barriers for carrier transport. With an applied DC bias, the interface traps are turned into fixed charges and do not follow the AC signals impedance measurements.[84] As shown in Figure 3.5a, the low frequency semicircle diminishes with increasing bias. Therefore, for organic films with high density of interface trap states, operating the device at higher voltage can mitigate the contribution from the interface traps.

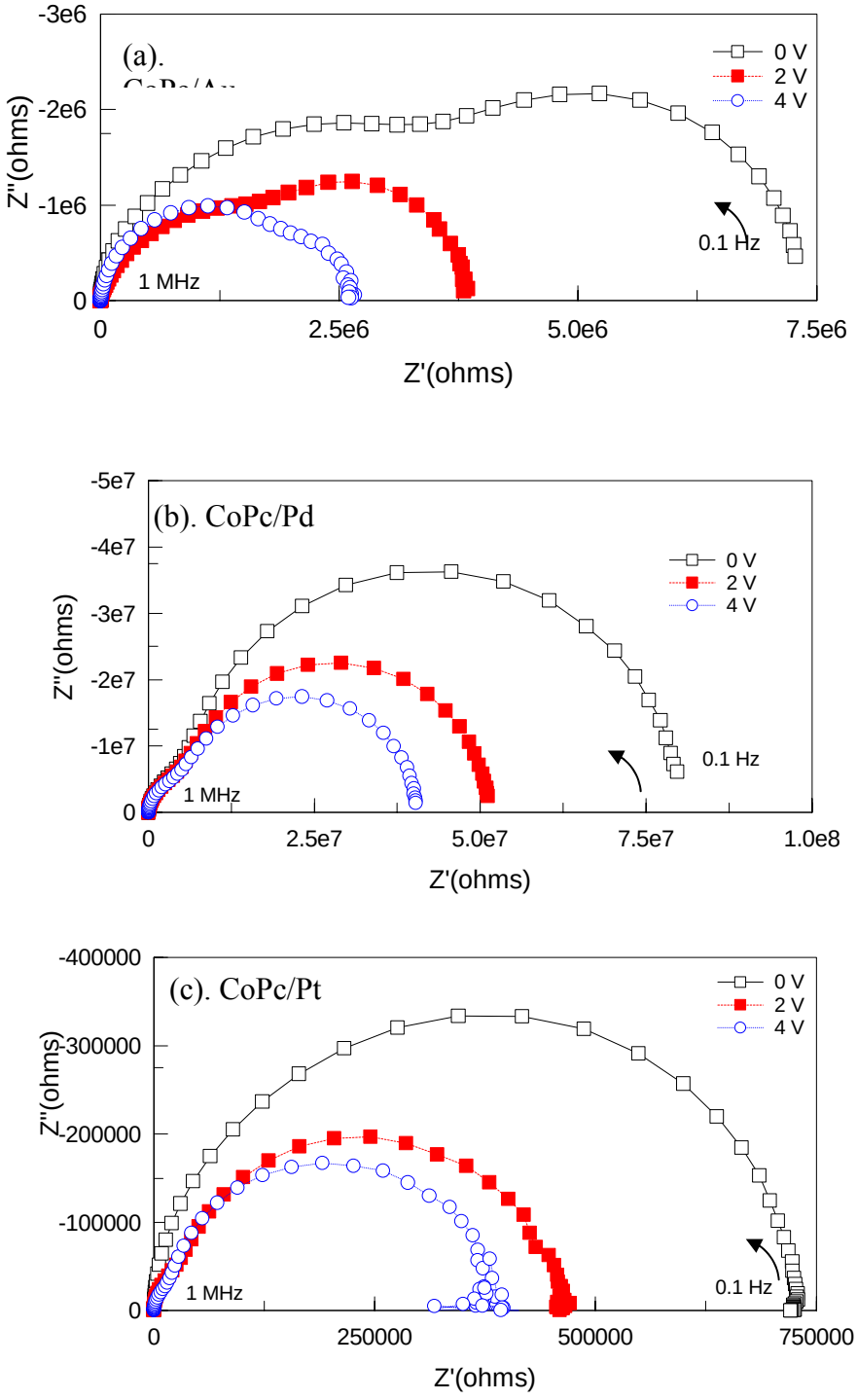

Figure 3.5. Plots of the complex impedance plane responses of (a) CoPc/Au, (b) CoPc/Pd, and (c) CoPc/Pt 5 μm IDE devices.

3.3.3. Electrode Independent Chemical Sensitivity in SCLC Region

The same devices used in the conductivity studies were tested as chemosensors at room temperature and exposed to four different analytes. The use of 50 nm thick CoPc sensor films provides reasonable current response and reversibility to analyte exposure in minutes at room temperature as shown at Figure 3.6. While the initially prepared sensors show significant baseline drift, several annealing cycles at 50 ^{o}C produce sensors that show good baseline stability (Figure 3.6).

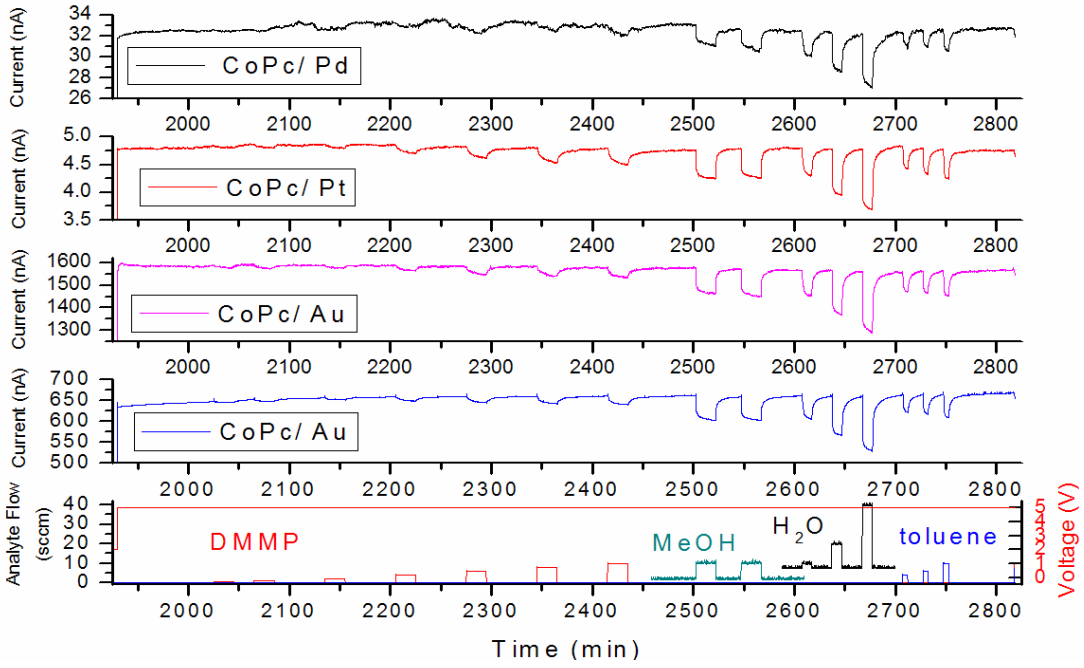

Figure 3.6. Chemical response of CoPc devices for DMMP, methanol, water and toluene for 5 V applied across the electrodes. The bottom panel shows the dosing sequence, the other panels show the device chemical response.

Varying the electrode material results in over a 300x difference in conductivity for the different devices. However, at 5 V, where SCLC behavior dominates, the devices all show (Table 3.1) the same relative response (within 5 %) toward analytes, such as

DMMP, water, methanol, and toluene. Such independence, regardless of the overall conductivity, suggests that the analyte and MPc film interact by the same mechanism, independent of differences in the electrode-MPc or growth front interfaces. Since most of the MPc film lies between the metal electrodes, it seems reasonable that this large adsorbing region of MPc dominates the chemical sensor response. The relative response toward analytes does not depend on the CoPc-metal interface at high voltage where SCLC dominates, which suggests that the interfacial traps effect is mitigated.

Table 3.2. Relative sensitivities ($I_{analyte}/I_{H2O}$) in the SCLC regime (5 V) normalized to that of a 5% relative humidity (RH) change for devices tested.

5 V	DMMP (100 ppm)	MeOH (1900 ppm)	H_2O (5 % Δ RH)	Toluene (400 ppm)
CoPc/Pd	1.19	1.15	1	1.13
CoPc/Pt	1.22	1.15	1	1.15
CoPc/Au	1.19	1.13	1	1.13
CoPc/Au	1.20	1.13	1	1.14

From device to device, MPc-metal electrode interfacial layers may have larger variation than the bulk film and a greater tendency to change over time as the electrode corrodes, or as the interfacial strain between the dissimilar materials relaxes. To test the above hypothesis, similar experiments were carried out in the Ohmic regime for the three devices. The relative chemical sensitivity data is tabulated in Table 3.2. It has been found that the variation in chemical sensor response among devices can be as high as 26% in the case of DMMP, which is 10 times higher than the variation observed when the device

is operated in the SCLC regime. This finding suggests that resistive MPc chemical sensors should be operated in the SCLC regime to minimize the influence of interfacial variations on the device's chemosensor response.

Table 3.3. Relative sensitivities ($I_{analyte}/I_{H2O}$) in the Ohmic regime (a V) normalized to that of a 5% relative humidity (RH) change for devices tested.

1 V	DMMP (100 ppm)	MeOH (1900 ppm)	H_2O (6 % Δ RH)	Toluene (400 ppm)
CoPc/Pd	1.17	1.13	1	1.11
CoPc/Pt	1.48	1.29	1	1.23
CoPc/Au	1.28	1.18	1	1.18
CoPc/Au	1.36	1.24	1	1.19

3.4.Conclusion

The DC conductivity of CoPc thin-film on different metal electrodes exhibits Ohmic conduction at low applied potentials and space-charge limited conduction at higher applied potentials. The Ohmic to SCLC transition has been proved by microscopic SKPM measurements. Over a 300x variation in bulk conductivity has been observed in CoPc film deposited on different metal electrodes. The results indicate that the transition voltage between Ohmic and SCLC, as well as the net conductivity of a device depends strongly on the interface between MPc and metal electrodes. The interface trapping effect can be mitigated by operating the device at higher voltage.

In spite of these large CoPc-electrode interfacial effects on device conductivity, the chemical sensor response ($\Delta I/I_{baseline}$) toward various analytes in the SCLC region is not affected by the metal electrode employed. It is concluded that the bulk film is responsible for chemical sensing when the device is operated within the SCLC regime. Because the low frequency interfacial traps are filled in the SCLC region, the sensor response becomes independent of the influence of the analyte absorption at the MPc-electrode interface and the analyte response is independent of electrode material.

This chapter, in part, has been published in "Electrode Independent Chemoresistive Response for Cobalt Phthalocyanine in the Space Charge Limited Conductivity Regime", *J. Phys. Chem. B*, 110 (2006) 361-366, by K. A. Miller, **R. D. Yang**, M. J. Hale, J. Park, B. Fruhberger, C. N. Colesniuc, I. K. Schuller, A. C. Kummel, and W. C. Trogler.

4. ULTRA-LOW DRIFT IN ORGANIC THIN-FILM TRANSISTOR CHEMICAL SENSORS BY PULSED GATING

4.1. Introduction

Organic thin-film transistors (OTFTs) have been investigated for chemical vapor sensing since 2000;[85] these devices are one of the new types of chemically sensitive field-effect transistors, in this report, we refer to these devices as ChemFETs. ChemFETs composed of small organic molecules[21-23,85,86] or conducting polymers[9,87] show high sensitivity and selectivity to a range of gas vapors. It has been demonstrated that ChemFETs reach part per billion (ppb) level sensitivity to volatile organic vapors[86], ozone[88] and explosive agent simulants[89]. The ChemFET response has also been demonstrated to be tunable by changing the functional groups of organic materials, therefore, making these sensors appealing for electronic nose application.[9,87] In an e-nose, chemical responses acquired from an array of chemical sensors are used for pattern recognition.[90] E-noses can identify complex odors, but are especially sensitive to baseline drift and have to be frequently recalibrated.[91] While reference sensors or complicated drift compensation algorithms are often used to reduce the drift effect,[90] e-nose systems can be greatly enhanced by using low drift sensing techniques. Despite many studies of the chemical sensitivity of OTFT sensors, the baseline stability of these sensors is still an issue.[92,93]

The sources of baseline instability of a ChemFET include electrical, thermal and analyte induced instabilities. For OTFTs, the electrical instability is usually the major cause of the baseline drift. Under static bias condition, even encapsulated OTFTs exhibit a large bias stress effect (BSE).[94] Such bias instability has been observed on OTFTs fabricated with a wide range of active materials, i.e. pentacene[94] and thiophene derivatives[95] and is associated with charge trapping in the organic film. The thermal instability of OTFT is related to the thermally activated charge transport properties of organic thin-films,[18,96,97] which can be circumvented by stabilizing the temperature of the device. The analyte induced drift of ChemFETs has been found to depend on film thickness which can be minimized by employing ultrathin channel materials.[98]

The electrical instability of organic materials impairs sensing applications of OTFTs, including chemical[98] and thermal sensing[99]. In the report by Jung, Ji and Vardan, a time delay over 300 s between consecutive current measurements was applied to circumvent the BSE problem in thermal sensing.[99] A number of groups have investigated the BSE in OTFTs and shown that BSE is reversible after either long relaxation, reverse gate biasing or photo illumination[100], suggesting that BSE is an electronic phenomenon rather than physical degradation of devices.[101] Organic thin-films are known to contain a high density of trap states due to either structural or electrical defects.[11] Charge trapping at these states occurs at a large time scale, ranging from second to hour. The kinetics of trapping depends on film structure[95], electrical field[94] and gate dielectric surface treatments[102]. Therefore, the baseline drift of ChemFETs related to BSE can not be solved by applying a simple baseline compensation method.

In this chapter, a pulsed gating method has been demonstrated to greatly reduce the charge trapping effect in OTFTs. The method is proven to effectively eliminate the baseline drift in ChemFETs of three different channel materials and channel thicknesses over 20 hours period. Upon exposure to volatile organic vapor pulses, the chemical response under pulsed gating is completely reversible with a flat baseline. It is suggested that the intrinsic trap states rather than chemically induced traps are the major sources of baseline instability in ChemFETs when the analyte has a reversible absorption.

4.2. Experiment

The organic channel materials used in this work were metal phthalocyanine with copper or cobalt metal centers (CuPc or CoPc) and metal free phthalocyanine (H_2Pc).The phthalocyanine materials are known to have high chemical sensitivity and selectivity to organic vapors.[70] The thicknesses of the organic thin films were between 4 – 50 monolayers (MLs). CuPc, CoPc and H_2Pc materials were purchased from Aldrich and purified three times by zone sublimation. Bottom-contact devices were fabricated on n^+ silicon wafers with 100 nm of thermally grown SiO_2. Gold was evaporated onto the back of the silicon wafers to form the gate electrode. The channel length and width of the devices were 10 μm and 2 mm respectively, defined by a photolithography process. Interdigitated electrodes with 25 pair fingers were used to increase the current. A schematic cross-section of a ChemFET and the molecular structure of the sensing materials are shown in Figure 4.1.

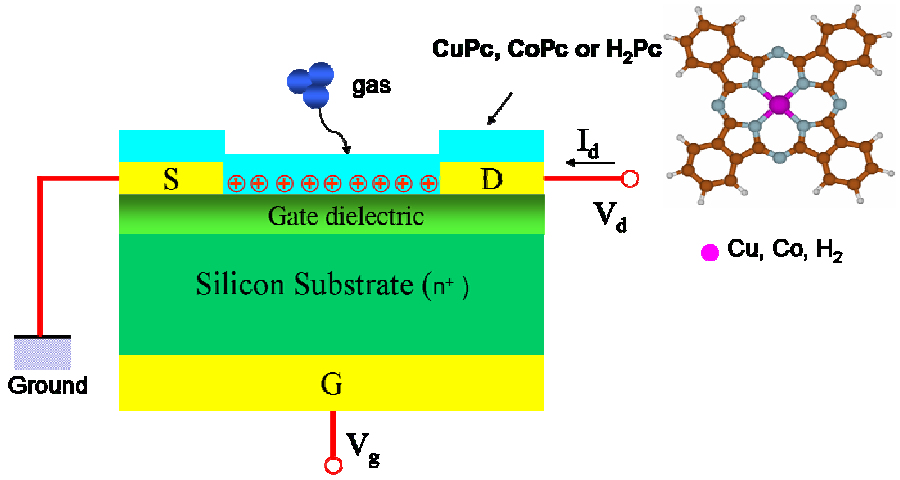

Figure 4.1. Cross section of a ChemFET. A 5 nm Ti adhesion layer and 45 nm thick gold source (S) and drain (D) pads are e-beam evaporated onto the 100 nm SiO_2 gate dielectric. Back gate is 100 nm thick gold evaporated at the back of n+ silicon substrate.

CuPc, CoPc and H_2Pc films were deposited by organic molecular beam epitaxy at 80 ^oC. The films were 20 ML CuPc, 4 ML CoPc, 50 ML CoPc, and 25 ML H_2Pc. The film thicknesses were measured by quartz crystal microbalance and calibrated by atomic force microscopy and x-ray diffraction. The d-spacing is 13.3 Å in accordance with previous measurements that show the molecular planes of phthalocyanine are oriented perpendicular to the substrate surface.[98,103] Six duplicate sets were deposited for each device under investigation. The six devices had only 5% variation in electrical conductivity and chemical sensing response. The fabrication process has been optimized to operate the device at low voltage range (0 to -10 V). A typical output and transfer characteristics of OTFT sensors is shown in Figure 4.2. All the devices were p-channel transistors and had threshold voltage between -0.38 V to + 0.38 V. The mobility values extracted in linear regions are between 2.0 x 10^{-5} cm^2/Vs and 2.6 x 10^{-4} cm^2/Vs.

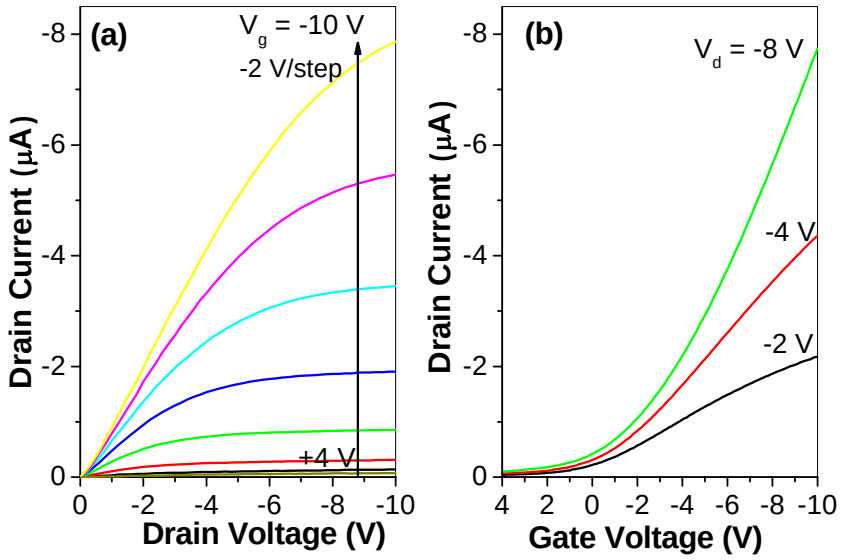

Figure 4.2. Output (a) and transfer (b) characteristics of a typical ChemFET (50 ML CoPc).

The electrical properties of the devices were measured using a Keithley 6385 picoammeters and programmable Agilent E3631A power supply. The electrical measurement system was calibrated with a HP 4156B precision semiconductor parameter analyzer. For the pulsed measurement at different frequencies, a home built transient spectroscopy system has been developed utilizing National Instrument 6040E DAQPad and a FEMTO DLPCA-200 variable gain low-noise current amplifier. The transient spectroscopy system was also calibrated with the HP 4156B parameters analyzer.

The chemical sensing experiments were carried out inside a custom built flow system controlled by a computer. The devices were loaded inside the optically isolated chamber under dry air flow for 2 days before testing to eliminate photocurrent and doping by H_2O, O_3, and other ambient reactive trace gasses. The temperature in the chamber was kept at 27 $\pm$ 0.2 ^oC using a Haake constant temperature bath. Bubblers filled with liquid

analyte were kept in a water bath chilled to 15 ^{o}C. Mass flow controllers were used to dilute and introduce vaporized analytes at a known concentration into a manifold to premix with the carrier gas before introduction into the test chamber. Solenoid valves before and after the analyte bubblers were used to prevent cross-contamination between analytes. A four-way valve was used to minimize the dead time between introductions of analyte at each pulse. The analyte employed were methanol, diisopropyl methylphosphonate (DIMP) and dimethyl methylphosphonate (DMMP) at a constant flow rate 500 sccm in dry air. All the devices have been found to have stable output characteristics for one year after fabrication. However, the electrical noise of all the ChemFET devices increased after of one month of intense testing. The increase in noise was more severe for the ultrathin devices but was consistently between all the ultra-thin devices. Replacing the cables or resoldering the lead to the contact pads does not reduce the noise. We hypothesize that the electrical noise is due to the aging of contacts between organic films and metal electrodes, and we are investing this phenomena.

4.3. Results and Discussion

In the first part of the chapter, we refined the gate pulsing technique to eliminate baseline drift in the CuPc ChemFETs without chemical analytes. Using relatively short test periods (2 hours), the gate duty cycle effect on the baseline stability was measured as a function of gate duty cycle and frequency to find an optimized operating condition. Subsequently, the optimal pulse cycle was applied in a testing period of 20 h to measure the long term baseline stability. We have tested the pulsed gating in the absence of

analyte on ChemFETs made of two other phthalocyanine materials to demonstrate the pulsed gating method is general for ChemFETs.

In the second part of the chapter, the impacts of BSE on CuPc ChemFET baseline stability and chemical response were quantified by comparing responses to methanol vapor pulses under static versus pulsed gating.

In the third part of this chapter, the pulsing method was applied for ChemFET detection of low vapor pressure organophosphonate nerve gas simulants. Large baseline drift was found on DIMP even under the optimal pulsing condition. The analyte pulse duty cycle has been varied to separate analyte induced baseline drift from electrically induced drift and to reduce the analyte induced drift to negligible levels.

4.3.1. Optimal Gate Pulse Selection

To better understand and control the electrical stability of ChemFETs, we first measured the evolution of drain current over 2 h in the absence of analytes. The CuPc ChemFET devices were loaded in the chamber for two days and fully relaxed from bias stress. Gate pulse trains of 0.1 Hz were applied at the gate electrode between duty cycles 1% - 100%. The “on” gate voltage was fixed at –8V while the “off” gate voltage was fixed at 0 V. Shown in Figure 5.3a are the drain currents normalized to the initial current in each measurement. We found that under static gate bias (100% gate duty cycle), the baseline drifted 25% after 2 h. The baseline drift with 1% gate duty cycle was less than 0.1% over 2 h, which is 250 times less than that of the static gate bias. During the tests, the drain voltage was held at constant (-4 V). We didn’t observe baseline drift at low gate

duty cycle. Therefore, bias stress due to static drain bias can be excluded as a cause of BSE in these devices..

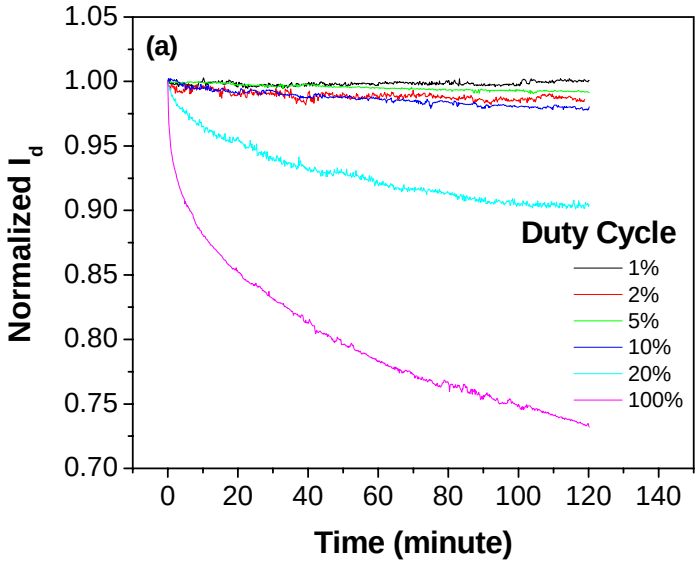

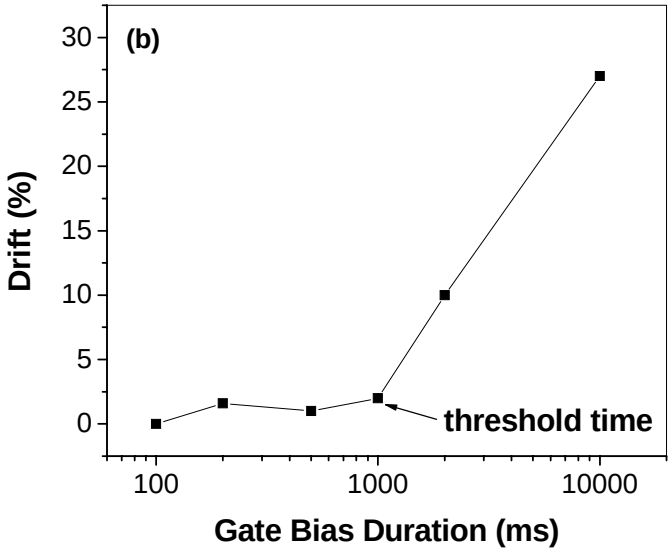

Figure 4.3. ChemFET baseline study in the absence of analytes (20 ML CuPc). (a). Normalized drain current for 0.1 Hz gate pulses with duty cycles between 1 % - 100 %. The drain voltage is held constant at -4 V; (b). The baseline drift vs pulse duration for 0.1 Hz gate pulses.

From data in Figure 4.1a, the percentage baseline drift as a function of the pulse duration is shown in Figure 5. 3b in order to understand the mechanism of BSE. For 0.1 Hz gate pulses, the baseline drift over 2 h rose above 1% only for pulse durations greater than 1 sec. We have also measured baseline drift at constant pulse duration (100 ms) while varying the frequency of the pulses between 0.05 Hz and 5 Hz. We found the baseline drift in 2 h rose above 1% for pulse frequency above 1 Hz. Further reducing the pulse duration to keep the duty cycle constant increases the noise. Therefore, in all the following measurement, the pulse frequency was held at 0.1 Hz.

To test the feasibility of the pulsed gating method for continuous operation of ChemFETs, we compared the baseline stability of the devices over a period of 20 h. The drain current has been measured a with -8V 0.1 Hz 1% duty cycle gate bias, -8 V static gate, and -4 V static gate biases. The baseline drift was found to be less than 1% over 20 h with pulsed gating as shown in Figure 4.4. Conversely, the baseline drift was 55% over 20 h for a static gate bias at -8 V. The BSE is reported to depend on gate bias in amorphous silicon TFTs.[104] Reducing the static gate bias by half to -4V only reduced the drift with the static gate from 55% to 38% over 20 h. The results indicate that the baseline drift can only be effectively solved by the pulsed gating method.

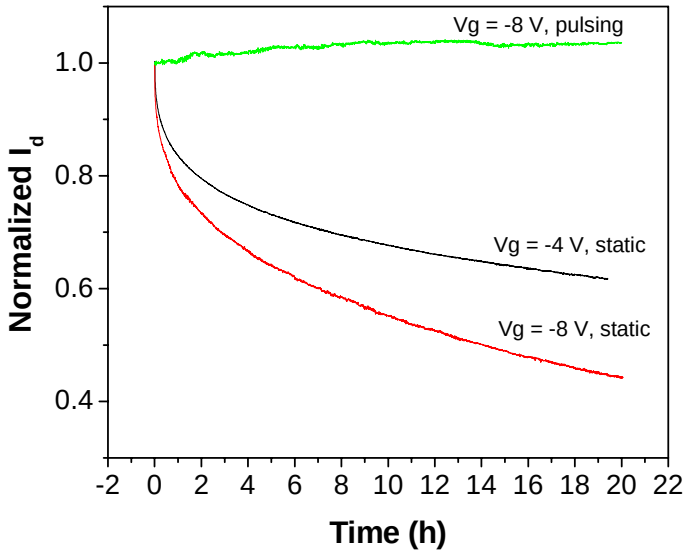

Figure 4.4. The baseline stability for ChemFETs (20 ML CuPc) over 20 h for 0.1 Hz 1% duty cycle (V_g = -8 V) vs static gate bias at -4 V and -8 V. Gate voltage was varied to show no dramatic decrease in drift under static bias condition.

To prove that the pulsed gating method is of general utility for ChemFETs and not exclusive to CuPc devices, the pulsed gate operation was tested on CoPc and H_2Pc ChemFETs. The baselines measured over 20 h using the 0.1 Hz gate pulses are shown in Figure 4.5. The same gate pulse train (0.1 Hz, 1% duty cycle, -8 V) employed for the 20 ML CuPc ChemFET was applied in the measurements. For channels of all three materials and for all channel thicknesses tested (4 ML to 50ML), the pulsed gating operation reduced the baseline drift to 0.05 %/hr. In all the above measurements, the rest gate voltage was set at 0 V, which is within 0.5 V of the threshold voltages for all of the above devices. The threshold voltages of the 50ML and 4 ML CoPc ChemFETs are -0.38 V and +0.38 V respectively. The 0 V rest voltage causes a positive drift in the 50 ML CoPc ChemFET while a negative drift in the 4 ML CoPc ChemFET (see Figure 4.5). For

devices with nonzero threshold voltage, we found the rest gate voltage needs to be set close to the threshold voltage to minimize the bias stress at rest gate bias.

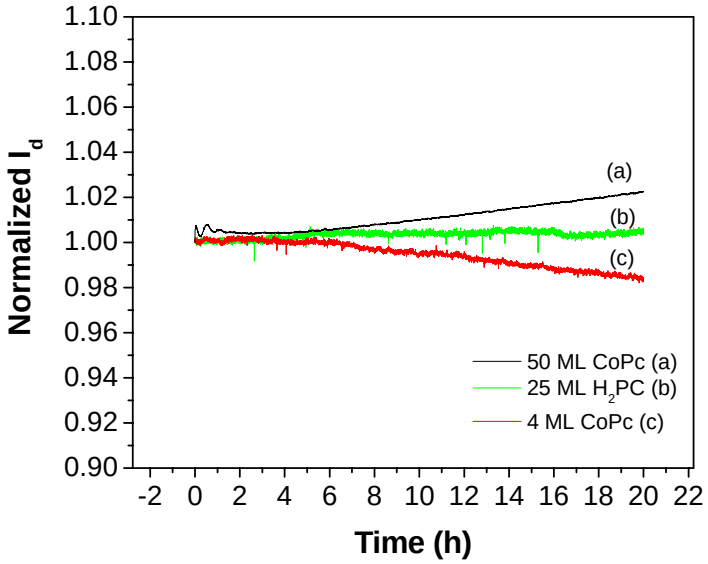

Figure 4.5. Pulsed gating operation (0.1 Hz, 1% duty cycle, -8V) of ChemFETs with three different channel materials/thicknesses over 20 hrs. (a) 50 ML CoPc, (b) 25 ML H_2Pc, and (c) 4ML CoPc.

The baseline drift under static gate bias in OTFTs has been attributed to the threshold voltage shift over time induced by a slow charge trapping process.[94] Trap states are distributed both near the gate dielectrics and in the bulk films in OTFTs. Trapping and de-trapping processes occur simultaneously in OTFTs. The device response to gate pulses can be qualitatively explained by an energy band diagram model shown in Figure 4.4. At 0 V gate bias, the device is assumed to rest in flat band condition. There is no charge accumulation in the channel at this bias condition. The flat band voltage depends on the threshold voltage of the devices, which is 0 V for the device in Fig 4.. Conversely, at -8 V, hole carriers are accumulated in the channel by the gate capacitor. Carriers are

trapped in states within the band gap at different rates depending on the capture cross-section of trap states.[105] For gate bias pulses between 0 V and -8 V, the above device goes between flat band and accumulation conditions. There is a finite charge trapping time τ_t for the trap states to capture holes. We hypothesized that if the gate stress time t is less than τ_t, the charge trapping effect can be greatly reduced. The phenomenon was observed on all devices under test. The results shown in Figure 5.3b indicate a charge trapping time between 1 and 2 s in the 20 ML CuPc ChemFETs.

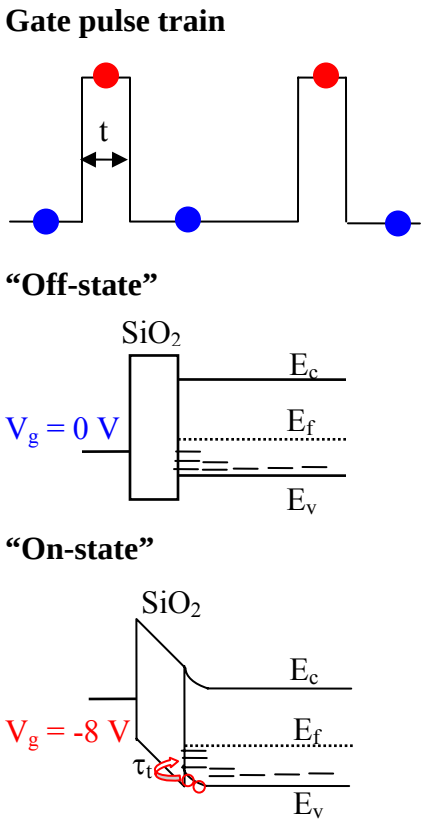

Figure 4.6. Energy band diagrams of OTFT response to gate pulses. The band diagrams of the "off" and "on" states of OTFTs are shown at different voltages. Broken lines represent trap states located near SiO_2 interface and in the bulk.

The time dependence of electrical instability in amorphous silicon and organic thin-film transistors have been investigated in detail.[104] The kinetics of BSE is usually

modeled from the time dependent threshold voltage shift. The evolution of threshold voltage in the 20 ML CuPc ChemFET can be calculated from time dependent drain current shown in Figure 5. 5. In the linear region, the drain current of OTFT is

$$I_d = \frac{W}{L} C_i \mu \left(V_g - V_t \right) V_d \qquad (4.1)$$

where C_i is the gate capacitor, W and L is the transistor width and length and μ is the effective field-effect mobility. The mobility has been found to be constant during the bias stress experiments.[100] Based on the above assumption, the threshold voltage shift can be deduced from the drain current as following,

$$V_t(t) = V_{to} - (I_d(t) - I_{do}) / (\frac{W}{L} C_i \mu V_d) \qquad (4.2)$$

where V_{t0} and I_{d0} are the initial threshold voltage and drain current. The kinetics of BSE at V_g = -8 V has been fitted with a power law dependent function,

$$\Delta V_t = -0.333(t)^{0.32}, \text{ with } R^2 = 0.9999. \qquad (4.3)$$

Similarly, the BSE at V_g = -4 V can be well fitted by the power law with a power coefficient 0.27. On amorphous silicon TFTs, it has been experimentally found that charge trapping in the gate dielectrics follows logarithmetic kinetics while charge trapping in the a-Si channel follows the power law kinetics.[104] Our bias stress has a power law dependence and a time scale consistent with the charge trapping effect in the organic channel.

4.3.2. Baseline Drift with High Volatility Analyte

The baseline stability of the 20 ML CuPc ChemFETs in the presence of high volatility analytes has been investigated. Highly volatile analytes were employed to insure that the chemically induced drift is negligible and all drift is due to electrical instability. Shown in Figure 4.7 is a comparison between static and pulsed gating operation of the ChemFETs exposed to 15 methanol chemical pulses. Each chemical pulse is 20 minutes long followed by 1 h recovery. With 1% duty cycle, 0.1 Hz gate pulsing at -8V, the chemical response was found to be fully reversible. The mean baseline drift value is calculated by measuring the accumulated drift each of the 15 pulses referring to the same starting point. The baseline drift was 0.09 $\pm$ 0.016 %/h within the 20 h test duration, which is comparable within a factor of two to the rate of drift observed in the absence of analyte. Similar ultra-low baseline drift to methanol pulses has been found with the CoPc and H_2Pc ChemFETs shown in Figure 4.6. Conversely, with a static gate bias, the baseline drifted over 60% during the 20 h of methanol pulsing.

The electrical instability under static gate bias also impairs the accuracy of chemical sensitivity measurement. For the 1% duty cycle, 0.1 Hz pulsed gating, the chemical sensitivity to methanol is 4.05 +/- 0.03 x 10^{-3}%/ppm. For static gate operation, the chemical sensitivity is 4.33 +/- 0.34 x 10^{-3}%/ppm without correcting for baseline drift. A control experiment of baseline drift due to bias stress at the absence of analyte is also shown in Figure 4.7 b. At a macroscopic level, the chemical response of OTFTs can be attributed to changes in threshold voltage and mobility values. Bias stress increased the uncertainty in chemical sensitivity measurement by a factor of 10. The increased

chemical sensitivity uncertainty with static gate bias is due to the nonlinear behavior of bias stress effect discussed. Even though the baseline of ChemFETs in the absence of analytes is highly repeatable and can be well fitted with the power law, the exposure to analyte changes the kinetics, which cannot be accurately modeled.

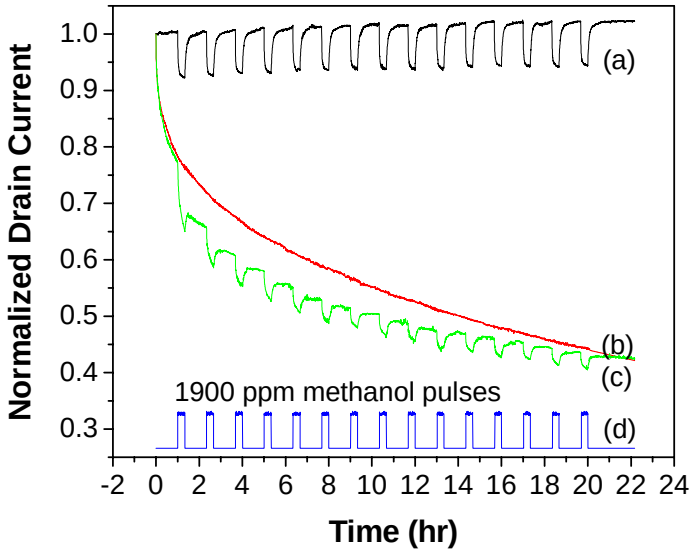

Figure 4.7. ChemFET baseline study in the presence of methanol in dry air (20 ML CuPc). (a) 1% 0.1 Hz duty cycle gate bias with methanol exposure; (b) static bias with methanol exposure; (c) static bias without methanol exposure; (d) 1900 ppm methanol pulses.

4.3.3. Baseline Drift with Low Volatility Analytes

For low volatility analytes, such as nerve gas simulants, it is important to separate the electrical and chemical sources of baseline drift. The 20 ML CuPc ChemFET was employed for nerve gas simulants detection using the 1% duty cycle, 0.1 Hz at -8v gate pulsing. The chemical responses to fifteen pulses of 19 ppm DIMP (simulant for Soman) and 32 ppm DMMP (simulant for Sarin) are shown in Figure 4.8. The chemical sensitivity to DIMP is 327.5 +/- 11.79 x 10^{-3}%/ppm with a drift of 1.15 +/- 0.73 %/h. The

chemical sensitivity to DMMP is 178.7 +/- 4.9 x 10^{-3}%/ppm with a drift 0.45 +/- 0.1 %/h. The drifts for DIMP and DMMP are 12 and 5 times larger in comparison to methanol with the same testing protocol.

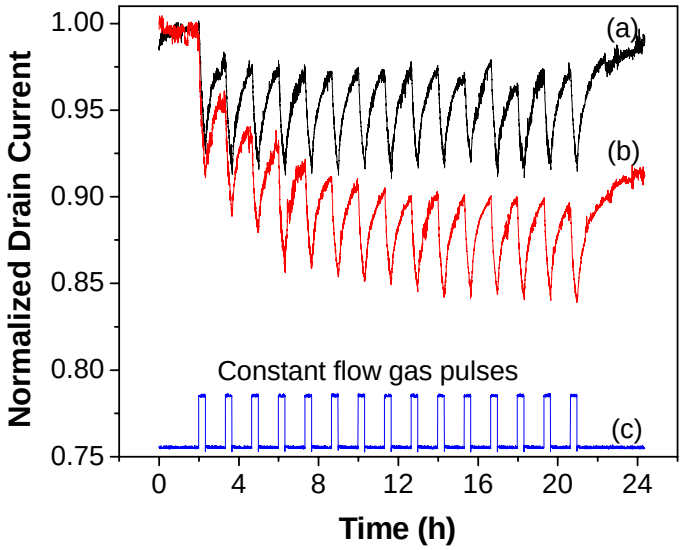

Figure 4.8.ChemFET (20 ML CuPc) responses to nerve gas simulants in dry air (1% duty cycle, 0.1 Hz at -8V gate pulse train). (a) Chemical response to DMMP (32 ppm); (b) Chemical response to DIMP (19 ppm); (c). Analyte gas pulses, 20 minute long followed by 60 minute recovery.

To prove that the increase in drift for DIMP and DMMP is due to purely analyte induced drift, the chemical responses to DIMP pulses were recorded as a function of the recovery time. A longer recovery time allows a low vapor pressure analyte sufficient time to desorb from the ChemFET thereby reducing the analyte induced drift. Shown in Figure 4.9 is the chemical response with the same dosage but different recovery time. It has been found that the drift is reduced by 30 times to 0.036 +/- 0.007 %/h when the recovery time is increased to 3 h. Therefore, these drifts should be ascribed to analyte induced drift. This study show that combining a low duty cycle analyte dose with a low

duty cycle pulsed gating, the baseline drift for low vapor pressure analytes can be reduced to a level similar to those highly volatile analytes.

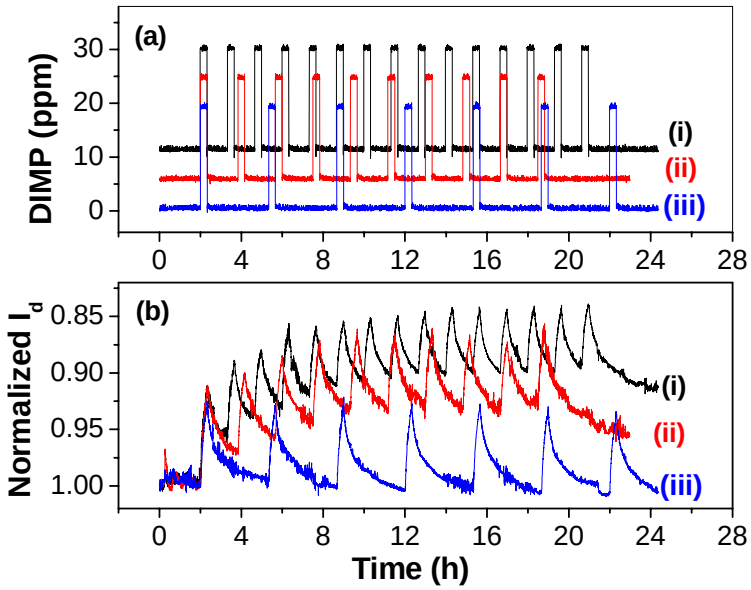

Figure 4.9. ChemFET (20ML CuPc) response to DIMP pulses using different recovery times in dry air with 1% duty cycle, 0.1 Hz at -8V gate pulsing. (a) 20 minute DIMP pulses with 60 minute (i), 90 minute (ii) and 180 minute (iii) recovery time. The concentration has been offset by 10 and 5 ppm for (i) and (ii). (b). Chemical response to the DIMP pulses shown in (a).

4.4. Conclusion

The impacts of the bias stress effect on the baseline stability of ChemFETs have been investigated. Under static gate bias, a nonlinear baseline at an average rate of 2.5%/h has been observed in CuPc ChemFETs exposing to methanol pulses. By pulsing the gate voltage at 0.1 Hz with a 1% duty cycle, the baseline drift has been reduced to 0.09%/h. The pulsed gating method also decreases the uncertainly in chemical sensing by an order of magnitude. The pulsed gating method has been found to be generally

applicable for ChemFETs made of two other materials and for low vapor pressure nerve gas simulants.

5. ANALYTE CHEMISORPTION AND SENSING ON N- AND P- CHANNEL COPPER PHTHALOCYANINE THIN-FILM TRANSISTORS

5.1. Introduction

Organic thin-film transistors (OTFTs) are a new form of chemically sensitive field-effect transistors (ChemFETs).[93] ChemFETs have advantages in multi-parameter readouts[85] and potentially higher chemical sensitivity in comparison to chemiresistors.[106] Three-terminal organic transistors can have higher electrical conductivity as compared to two-terminal organic devices, therefore, very thin monolayer (ML) devices may be utilitized to enhance the chemical sensitivity and baseline stability.[107] Metal phthalocyanine (MPc) based ChemFETs have been investigated for detecting O_3[88], volatile organic vapors (VOC) and explosive agent simulants.[107] Despite intensive study of OTFTs in chemical sensing, the transduction mechanism of ChemFETs is not fully understood.[21,23,108] In this chapter, the chemical sensing mechanism are investigated using n- and p- channel MPc ChemFETs.

MPc ChemFETs have potentially high selectivity for chemical sensing. The chemical interactions between analytes and MPc molecules are tunable by either changing the metal centers or the peripheral ligands of the macrocycle molecular structure. Combinatorial MPc ChemFET arrays (metal centers: Cu, Zn, Ni and Co) were reported for VOC detection by Bora, Schut and Baldo.[109] In this work, the peripheral of copper phthalocyanine (CuPc) has been modified with electron withdrawing fluorine groups to change the charge carriers from holes to electrons. Dimethyl methylphosphonate (DMMP), a simulant for sarin,[110] is investigated as a model tight

binding analyte to MPc molecules and methanol is investigated as a model weak binding analyte to MPc molecules. The roles of oxygen surface doping in the electrical conductivity and chemical response are studied. The electronic effects of analytes adsorption on MPc molecules are compared between n- and p- channel devices in air and nitrogen carrier gases.

5.2 Samples and Experiments

Copper phthalocyanine (CuPc) and copper-hexadecafluorophthalocyanine (F_{16}CuPc) were purchased from Aldrich and purified by zone sublimation. The molecular structures of CuPc and F_{16}CuPc are shown in Figure 5. 1. The CuPc material was readily purified by zone sublimation at 400 ^{o}C after three cycles within 50 h with a yield over 70%. We noted that the F_{16}CuPc material required over 75 h of purification (three cycles at 400 ^{o}C) and the yield after the purification was below 10%. The low yield in F_{16}CuPc material purification has been noted by others.[111] However, good quality thin-films[112,113] and excellent OTFT characteristics have been reported with F_{16}CuPc channels[114-116]. CuPc and F_{16}CuPc films were deposited by organic molecular beam epitaxy at 80 ^{o}C at rates of 0.3 Å/s and 0.5 Å/s. Both films were about 30 nm in thickness. The ChemFET device structure and fabrication processes have been described elsewhere.[107,117] Briefly, the channel length was defined by photolithography to be 5 micron. The gate dielectric was 100 nm thermally grown SiO_2. Interdigitated source and drain electrodes were used to increase the channel width and therefore the drain current. The channel widths were 50 mm and 400 mm for the p- and n- channel devices respectively. The mobility of the CuPc device is typically about 10 times higher than that of the F_{16}CuPc device in literature.[114]

The longer channel width of the F_{16}CuPc device compared to the CuPc device insures that the two devices have comparable drain current at the same magnitudes of drain and gate biases.

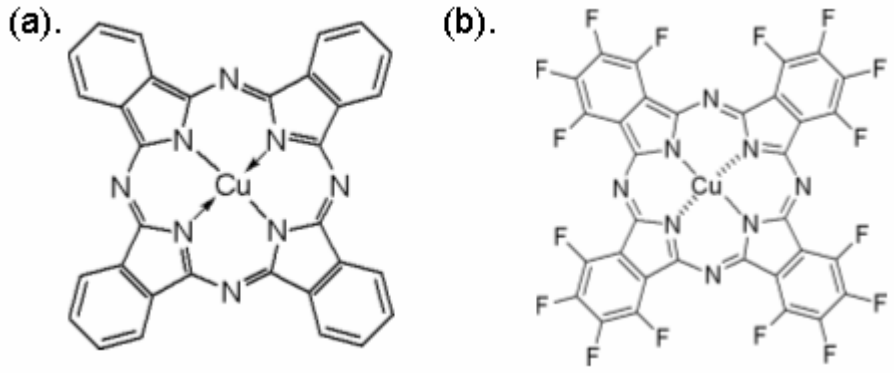

Figure 5. 1. The molecular structures of CuPc (a) and F_{16}CuPc (b) channel materials for ChemFETs.

The electrical properties of the OTFTs were measured using a Keithley 6385 picoammeter and programmable Agilent E3631A power supply. The electrical measurement system was calibrated with a HP 4156B precision semiconductor parameter analyzer. The output characteristics of the CuPc and F_{16}CuPc devices were measured in air before analyte exposure to ensure the proper behavior of the ChemFETs. CuPc has HOMO level (5.3 eV) close to the gold work function (5.0 eV) and is known to be a good hole transport material. The peripheral fluorine groups in F_{16}CuPc withdraw electrons from the CuPc molecule, lowering the LUMO level (4.8 eV) for electron injection from gold electrodes.[84,118] The transistor output curves (see Figure 5.2) show p- and n- channel formation for the CuPc and F_{16}CuPc devices, consistent with literature reports.[45,114,115]

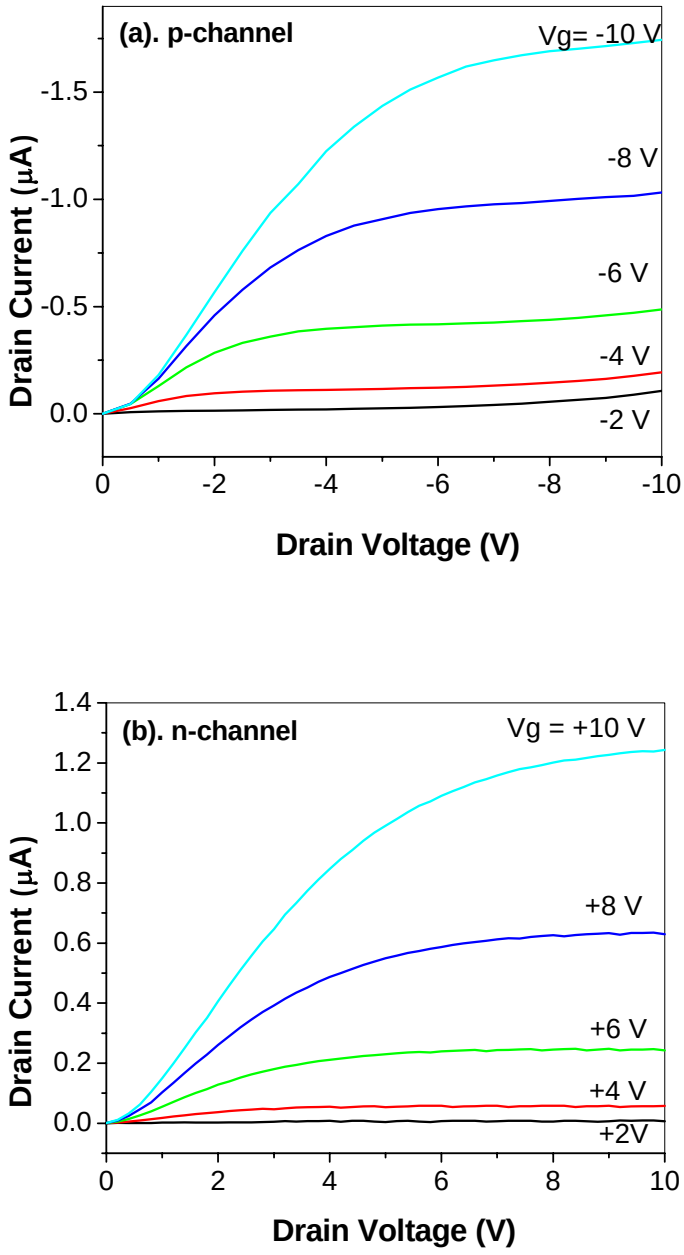

Figure 5.2. Output characteristics CuPc (a) and F_{16}CuPc (b) transistors. The gate oxide is 100 nm SiO_2. The channel length is 5 μm. The channel widths are 50 mm and 400 mm for the p- and n- channel devices respectively.

We investigated the chemical sensing mechanism with the tight binding molecule (DMMP) and a weak binding molecule methanol (MeOH). Other analytes such as

diisopropyl methylphosphonate (DIMP), H_2O, and nitrobenzene, were also tested for comparison of chemical sensitivity. Analytes were delivered by a custom built flow system with a stainless steel chamber. The temperature in the chamber was kept at 25 ^oC using a Haake constant temperature bath to circulate coolant through the chamber walls. Ultra-high purity dry air or dry N_2 was used as both the purge and the carrier gas. Bubblers filled with liquid analytes were kept in a water bath at 25 ^oC. Mass flow controllers were used to dilute and introduce vaporized analytes into a manifold to premix with the carrier gas before introduction into the test chamber. Solenoid valves before and after the analyte bubblers were used to prevent cross-contamination between analytes. The total flow rate of the experiments was 500 sccm.

All the organic thin-films outside of vacuum are doped by atmospheric gases such as O_2, O_3, and H_2O. The organic ChemFETs in this study are not pristine devices. For MPc ChemFETs, stable electrical conductivity and chemical response are only attainable after aging in air for at least 1 month. The devices in this study have been aged in atmosphere conditions for 6 months before testing. The ChemFETs were mounted on a custom designed printed circuit board (PCB). Indium was used as solider to connect source and drain electrodes to the contact pads in PCB. All the devices were annealed at 55 ^oC in dry air for 3 h and stabilized in the optically sealed chamber overnight with dry air flowing over the devices before the chemical sensing measurements. The procedure minimized doping by atmospheric H_2O. The pulsed gating technique[117] (0.1 Hz, 1% duty cycle) was applied in the chemical response measurements to mitigate the bias-stress effect[95] in baseline stability. The chemical responses to DMMP and methanol doses were compared in dry air and N_2 carrier gases. The devices were measured in the saturation

region at the same electrical field strength for n- and p- channel ChemFETs (V_{ds} = 6 V, V_{gs} = 8 V), unless otherwise stated. The bias is positive for the n-channel device and negative for the p-channel device. The chemical sensing measurements were repeated three times on n- and p- channel ChemFETs unless otherwise stated. For each type of ChemFETs, we compared the chemical responses to DMMP and MeOH between two duplicated devices and found good reproducibility.

The devices were intensively tested over two months (continuously biased at drain electrode and exposed to analytes). For the above analytes, the n- and p- channel ChemFETs have good chemical stability and reproducible chemical responses from run to run. We noted that the drain current may decrease up to 50% over 2 months under intensive testing. The decrease in channel conductivity was typically due to the degradation of indium soldering between source and drain electrodes and the contact pads of the PCBs. The problem can be fixed by re-soldering the joints. To minimize the electrical contact degradation, the chemical sensing data for side-by-side comparison were acquired within two weeks, unless otherwise stated.

5.3. Results and Discussion

5.3.1. The Role of Oxygen Surface Doping in Channel Conductivity

Since the channel conductivities of all the MPc ChemFETs change significantly after exposing to atmosphere after the deposition in vacuum, we hypothesize that the MPc films are doped with atmospheric dopants. We focus on the effect of oxygen doping by comparing the channel conductivities and sensing properties of the n- and p- type films in air and N_2. The devices have been stored in dry air over 24 h in dark to minimize

H_2O and photocurrent doping. To understand the role of oxygen doping, the time evolution of the n- and p- channel devices have been monitored after removing the oxygen from the environment and flowing dry N_2 over the devices. Shown in Figure 5. 3 are the drain currents for CuPc and F_{16}CuPc ChemFETs over 50 h in dry N_2. We note occasionally there was a fast initial current change. The time evolution of ChemFET (shown in Figure 5. 3) was recorded 20 min after switching to N_2. The 20 minutes delay removes any transient responses due to temperature or pressure change in the process of switching the carrier gases. The drain current increased 34% for the n-channel device and decreased 26% for the p-channel devices within 50 h. We note we have only performed these 50 hour experiments once, but we have performed similar experiments of 4-5 hours more than 10 times which are consistent with the data in Figure 5. 3. Since nitrogen is assumed to be electronically passive on CuPc and F_{16}CuPc, the change in the current in N_2 is ascribed to the desorption of surface dopants. The drain currents of n- and p-channel devices can be restored reversibly by storing the devices in dry air over a week. The results show that oxygen is a primary dopant for the MPc thin-films in both n- and p-channel ChemFETs.

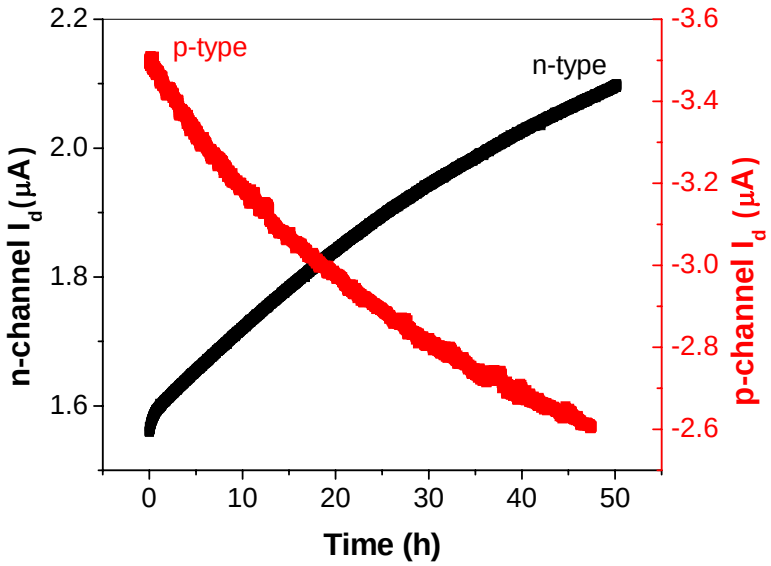

Figure 5.3. The time evolution of the n- and p-channel drain currents in dry N_2 measured in saturated region. The bias conditions: n-channel (V_{ds} = +6 V, V_{gs} = +10 V), p-channel (V_{ds} = -6 V, V_{gs} = -10 V). The chamber temperature was kept at 25 ^{o}C.

The role of oxygen doping in the electrical conductivity of MPc materials has been extensively discussed in literature.[48] For CuPc sandwiched devices, the electrical conductivity in vacuum is below pA.[48] However, after the oxygen doping, the electrical conductivity increased by three orders of magnitude.[119] The effect is reversible after prolonged vacuum pumping at elevated temperature or in H_2 reducing gas flow.

The multistep process of oxygen adsorption in MPc surface is proposed in Eq. (1)[120]:

$$MPc + O_2 \xleftrightarrow{K_1} MPc\text{-}O_2 \xleftrightarrow{K_2} MPc^{\delta+}\text{-}O_2^{\delta-} \xleftrightarrow{K_3} MPc\text{-}O_2^{-} + h^{+} \qquad (1)$$

The first process is the oxygen adsorption on the MPc surface, the second process is the charge transfer between MPc and O_2, and the third process is the charge delocalization; K_1, K_2, and K_3 are the equilibrium constants for these three processes. For solid state

chemical sensors, the gas adsorption only induces chemical responses after charge delocalization. The gas physisorption typically has very low activation energy ($\leq$ 0.3 eV).[121] For the MPc based sensors, step 2 and 3 were found to be the rate limiting steps in MPc chemiresistors.[122] It is likely that the slow current response due to O_2 desorption (0.7%/h) is due to slow charge transfer or delocalization processes (steps 2 and 3 in Eq. (1))

For organic films over 10 MLs, the gas adsorption primarily occurs at organic/air interface.[119] We hypothesized that the electronic process of gas adsorption in ChemFETs is a surface doping process. For an operating n-channel ChemFET (see schematic diagram at Figure 5. 4), there are two charge sheets present in the organic film, located at the organic/SiO_2 interface (Q_c) and the organic/air interface (Q_s). For a thick ChemFET (> 10 MLs), the gas surface doping layer and charge transport layer of the transistor are distinct. At high gate voltage, the charge density accumulates primarily in the first two layers (> 95%) above the oxide.[123]

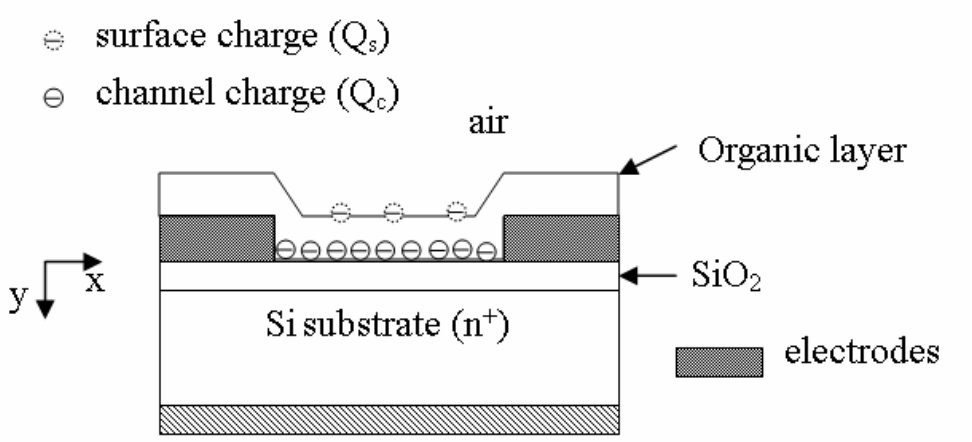

Figure 5.4. Device structure of an n-channel ChemFET in accumulation mode (not drawn to scale). There are two charge sheets: a thin layer of surface charge (Q_s) at the organic/air interface and channel charge (Q_c) at the organic/SiO_2 interface.

5.3.2. The Role of Oxygen Surface Doping in Chemical Response

Since oxygen has significant effect in the channel conductivity of MPc ChemFETs, the role of pre-adsorbed oxygen in the chemical response is investigated in the following section. We varied the surface oxygen concentration and compared the chemical responses in air and N_2. The samples were stored in N_2 till the baseline current changed over 25% in both devices. DMMP and MeOH were studied as model analytes. The chemical responses to DMMP (a tight binding analyte) for the two ChemFETs are compared in air and in N_2 carrier gas (see Figure 5. 5). MeOH is studied as a model weak binding analyte to MPc molecules. The chemical responses to MeOH for the two ChemFETs are also compared in air and in N_2 carrier gas (see Figure 5. 6).

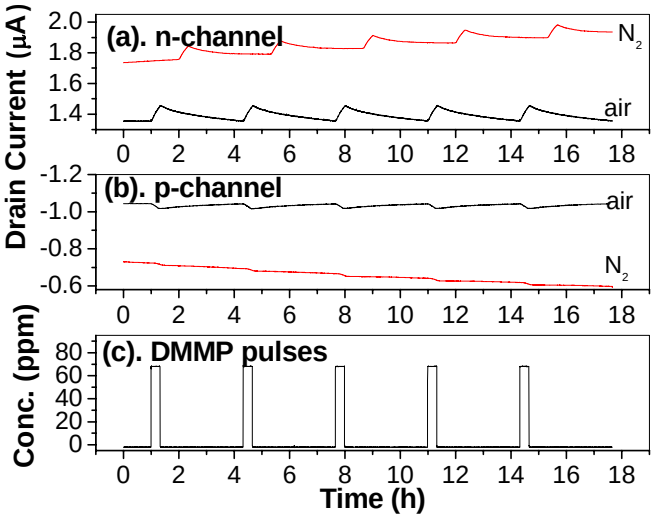

Figure 5.5. The chemical responses of n- channel $F_{16}CuPc$ (a) and p- channel CuPc (b) ChemFETs to DMMP in air and N_2 at 25 ^oC. (c). Each DMMP dose is 68 ppm.

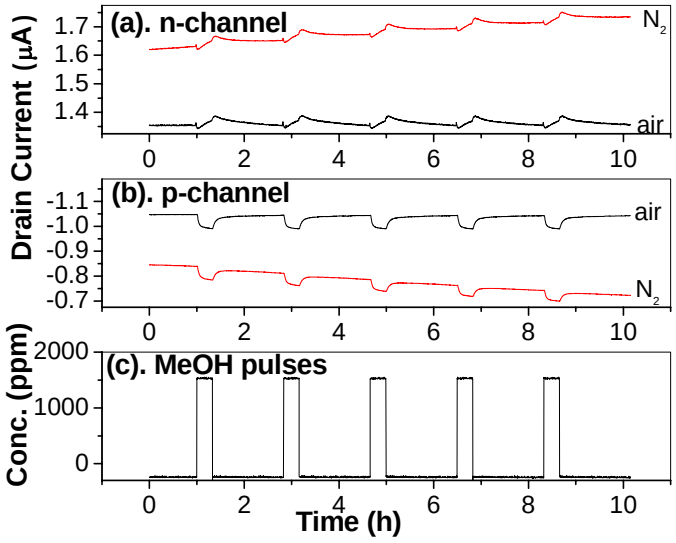

Figure 5.6. The chemical responses of n- channel $F_{16}CuPc$ (a) and p- channel CuPc (b) ChemFETs to MeOH in air and N_2 at 25 ^oC. (c). Each MeOH dose is 1520 ppm.

We note that the baseline is recoverable for analyte dosing in N_2 as well as in air. The result rules out the possibility of DMMP or MeOH causing a change in output current by irreversibly displacing surface bound O_2. Instead, DMMP and MeOH must be

acting as counter dopants to O_2. Possible counter doping mechanisms would include the "co-absorption" or "remote absorption". (a) Co-absorption: Analytes could be co-absorbing on the same MPc molecule as the O_2 and acting as an electron donor to O_2 so O_2 no longer withdraws charge from the film; (b) remote absorption: Analytes could be co-absorbing on a remote site and acting as electronic dopants. In both cases, the analyte may change the surface carrier concentration and trap energy of the binding sites. We note that in the standard model of organic semiconductors there is no distinction between changing the carrier concentration and perturbing the trap energies.

The above mechanisms can be distinguished by how the analyte response varies as the surface oxygen concentration decreases in dry N_2. For co-absorption, the percentage change $(\Delta I / I)$ in current is predicted to be invariant to time in N_2 carrier gas because the ratio of O_2 sites without analyte to O_2 site with co-absorbed analyte is independent of the absolute concentration of O_2 sites. For remote absorption, ΔI is predicted to be invariant to time in N_2 carrier gas since the O_2 and analyte act independently. The ΔI and $\Delta I / I$ values for the n- and p-channel ChemFETs were extracted from Figure 5.5 & 5.6 and shown in Table 5.1. ΔI was extracted from the current difference between the beginning and the end of each dose using a Matlab program. The $\Delta I / I$ values were calculated by dividing ΔI by the current before each dose. The ratios between air and N_2 for ΔI and $\Delta I / I$ were shown for comparison.

Table 5.1. The comparison of $\Delta I / I$ and ΔI in dry air and N_2 carrier gas for n- and p-channel ChemFETs. The data were extracted from Figure 5.5 & 5.6. The standard deviations for each quantity were shown in parenthesis.The ratio between quantities in air over quantities in N_2 were also shown.

carrier gas	n-channel ChemFET				p-channel ChemFET			
	ΔI (nA)		$\Delta I / I$ (%)		ΔI (nA)		$\Delta I / I$ (%)	
	DMMP	MeOH	DMMP	MeOH	DMMP	MeOH	DMMP	MeOH
air	100.4 (1.82)	32.6 (0.97)	7.4 (0.14)	2.41 (0.07)	25.6 (0.89)	54.2 (1.30)	-2.4 (0.08)	-5.2 (0.13)
N_2	81.6 (1.52)	36.8 (0.85)	4.46 (0.20)	2.2 (0.04)	10.0 (1.22)	48.0 (5.0)	-1.5 (0.21)	-6.1 (0.32)
ratio	1.23 (0.01)	0.89 (0.01)	1.66 (0.07)	1.10 (0.02)	2.56 (0.30)	1.13 (0.11)	1.60 (0.22)	0.86 (0.04)

The only number which strongly deviates from unity is the ΔI ratio for DMMP on p-channel ChemFETs. It indicates that co-absorption is a better model for DMMP on p-channel. For DMMP on the n-channel ChemFET, the ratio is closer to unity for $\Delta I / I$, more consistent to remote adsorption model than co-adsorption model. It could be due to larger electronic donating effect of DMMP to F_{16}CuPc than to CuPc, thereby, trumps the electron withdrawing effect of oxygen. For MeOH, since all the ratios are close to 1 for both $\Delta I / I$ and ΔI, the results indicate that some mixing of remote absorption and co-absorption probably occurs.

5.3.3. Comparison of Chemical Responses Between n- and p- Channel ChemFETs

The responses for the n- and p-channel ChemFETs have been measured with analytes such as DMMP, DIMP, nitrobenzene (NB), MeOH and H_2O. The chemical responses were measured in the saturated regime at 25 ^oC. A survey of the chemical responses to DIMP, NB, MeOH and H_2O is shown in Figure 5.7 for qualitative

comparison. We haven't tried to optimize the baseline drift for these analytes. More detailed study of responses to DMMP and MeOH pulses are shown in Figure 5.9. For all analytes tested, the responses were of opposite sign between n-type and p-type ChemFETs, which is consistent with the primary mechanism by which the analytes change the output current is counter doping of the surface pre-adsorbed oxygen.

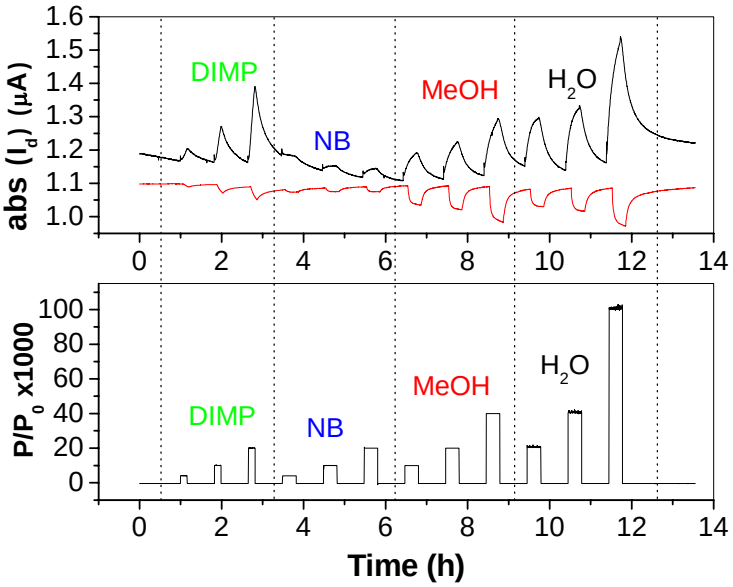

Figure 5.7. The typical chemical responses of the n- and p- channel ChemFETs to DIMP, NB, MeOH and H_2O. P and P_0 are the partial and saturated pressures of the analytes. The saturated vapor pressures of the analytes at 25 ^oC are: DIMP (0.7 mmHg), MeOH (127.1 mmHg), H_2O (23.7 mmHg) and NB (0.24 mmHg).

The chemical responses to five analytes were tested over 8 months. The average chemical sensitivity and standard error values were extracted from 6 runs and show in Figure 5.8. The analyte doses (P/P_0) were between 0.005 and 0.1, where P and P_0 are the partial and saturated pressures of the analytes. Each analyte dose was 20 min long followed by a recovery time of 45 – 180 min. The chemical sensitivity is calculated by dividing the percentage current change over the concentration. We found the difference

in sensitivity between the analytes is much greater than the differences in sensitivity between n-type and p-type ChemFETs. There are differences up to a factor of 3.5 between the sensitivity on the n-type and p-type ChemFETs consists with the analytes having a different perturbation of electron vs hole trap in n-type and p-type MPc ChemFETs.

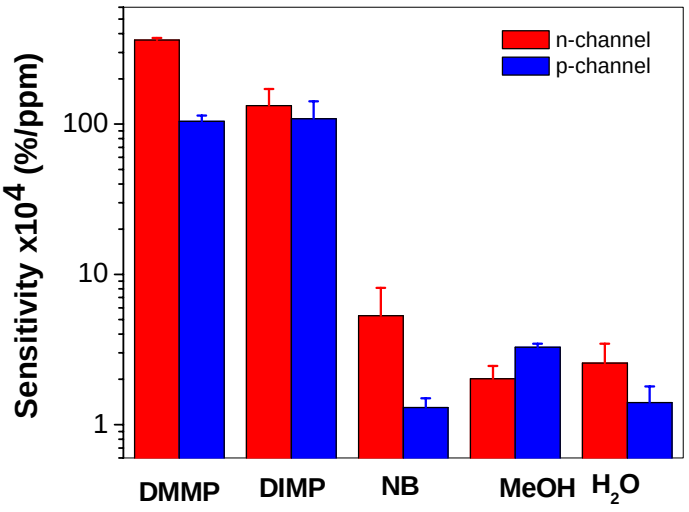

Figure 5.8. The sensitivity of n- and p- channel ChemFETs to nerve agent simulants (DMMP and DIMP) and other analytes: MeOH, H_2O and nitrobenzene (NB) at 25 ^oC. The sensitivity is in logarithmic scale. The error bars represent standard errors.

We compare the chemical responses of n- and p-channel ChemFETs to DMMP and MeOH in air in detail. The time-dependent current plots for sensor response to five constant dosage pulses of each analyte are shown in Figure 5.9. The DMMP doses in the experiment were 68 ppm and 20 min long, followed by a 180 min recovery period. The MeOH doses in the experiment were 1520 ppm and 20 min long, followed by a 90 min recovery period. The long recovery times were chosen to insure identical and fully reversible analyte responses.

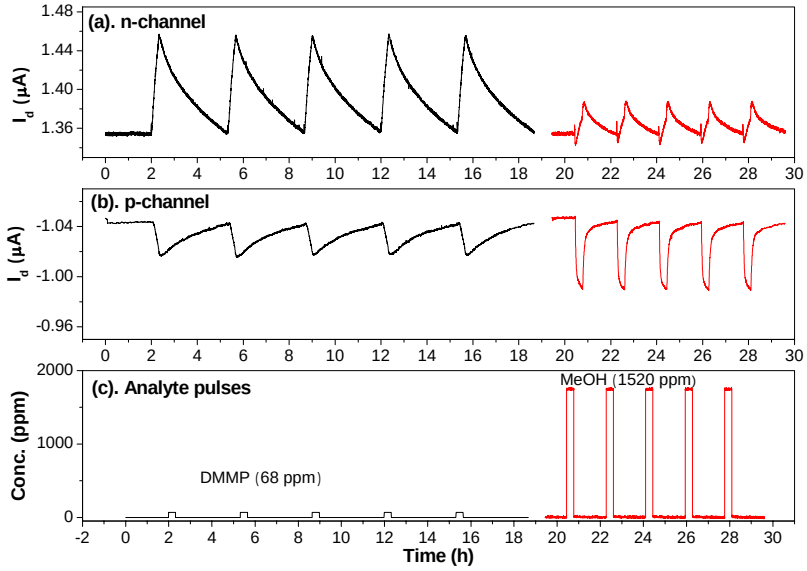

Figure 5.9. The time-dependent current plot of n- and p channel ChemFETs responses to DMMP and MeOH doses in dry air at 25 ^{o}C.

It is found that DMMP increases the current of n-type F_{16}CuPc device but decreases the current of p-channel CuPc ChemFET. This is consistent with the study of DMMP detection using carbon nanotube thin-film transistors, which indicates that DMMP is a strong electron donor.[124] The chemical responses in the form of $\Delta I / I$ are shown in Figure 5. 10 for side-by-side comparison. The percentage current change refers to the current at t = 0 s. At the same dosage, the n-channel ChemFET has larger response to DMMP in comparison to the p-channel ChemFET. MeOH analyte pulses also induce opposite chemical responses in n- and p- channel ChemFETs. At the same MeOH dosage, the p-channel ChemFET has larger response in comparison to the n-channel ChemFET, which is opposite to the relative responses to DMMP on p-channel and n-channel devices. We note that there was about 1% current overshoot at the beginning and end of each MeOH pulse in n-channel ChemFET (see the inset of Figure 5.10). The time

scales of the overshoots were 130 s and 190 s for downward and upward shifts. Therefore, it is unlikely caused by the open and close of solenoid valves during the vapor delivery. We infer that there are two processes occur during MeOH adsorption/desorption to MPc molecules.

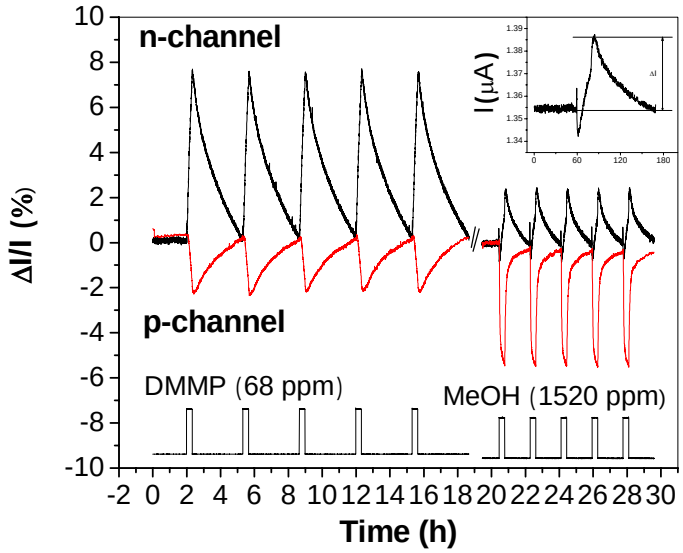

Figure 5.10. The percentage current change in response to DMMP and MeOH pulses converted from Figure 5. 9. The DMMP and MeOH analyte pulses are not drawn to scale. The inset shows the time-dependent current plot of a methanol pulse.

The desorption processes of DMMP and MeOH in CuPc and F_{16}CuPc ChemFETs can be fitted with exponential decay functions. For the DMMP responses, the time evolution of current during analyte desorption was fitted with a first order exponential decay as

$$I_d(t) = I_0 - A_1 \exp\left(\frac{-t}{\tau_1}\right) \qquad (2)$$

where I_0 is the baseline current, A_1 is the pre-exponential coefficient and τ_1 is the desorption time constant. For MeOH responses in p-channel ChemFET, the desorption process has to be fitted with a double-exponential process,

$$I_d(t) = I_0 - A_1 \exp\left(\frac{-t}{\tau_1}\right) - A_2 \exp\left(\frac{-t}{\tau_2}\right) \qquad (3)$$

where A_2 and τ_2 are the pre-exponential coefficient and desorption time constant for the second (fast) exponential decay process. We have fit the desorption of MeOH in n-channel ChemFET with a double exponential, but of opposite sign of pre-exponential coefficient. The exponential fits of the desorption process for DMMP and MeOH in n- and p- channel ChemFETs are shown in Figure 5. 11.

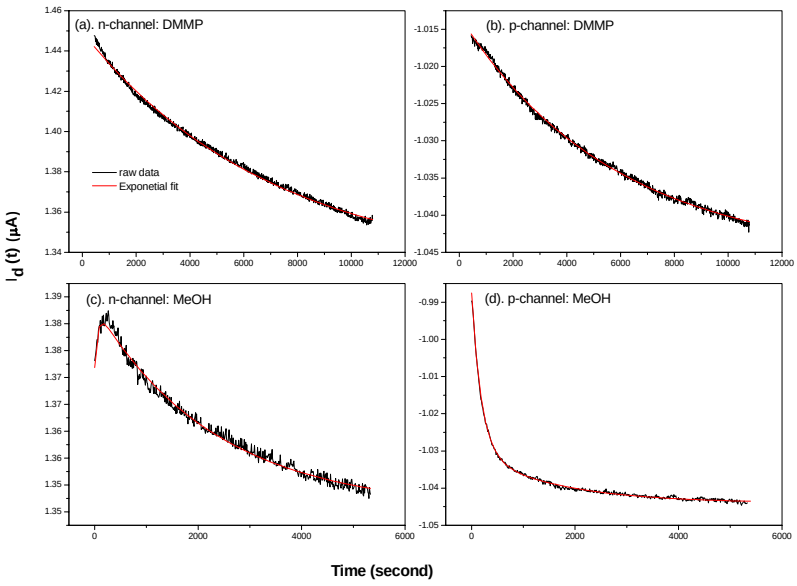

Figure 5.11. The exponential fit of the desorption of DMMP and MeOH from n- and p-channel ChemFETs. The correlation coefficients for the fitting are above 0.99.

To quantify the sensing properties of CuPc and F_{16}CuPc ChemFETs to DMMP and MeOH, the chemical responses and desorption time constants were tabulated in

Table 5.2. The chemical response (R) was calculated as of the percentage current change to chemical pulses using the current just prior to each pulse as the reference current. We note the current continued to change even after the analyte was turned off for some analytes, i.e., MeOH response of n-channel ChemFET. The peak values were extracted from Figure 5. 10 as shown in the inset. We note that these chemical responses were calculated at a single concentration of analyte, which has not taken the non-linear response into account; chemical responses a function of concentration are shown later, but this simple estimate is employed to show the relative response of n-channel and p-channel ChemFETs is reversed for DMMP and MeOH.

Table 5.2. The chemical response (R), desorption constants of n- and p-channel ChemFETs extracted from Figure 5. 10. The doses were 68 ppm and 1520 ppm for DMMP and MeOH pulses. The pre-exponential and desorption time constants were fitted according to Eq. (1) & (2). R is in unit of %, τ_1 and τ_2 are in unit of minute, A_1 and A_2 have been multiplied by 10^3. The standard deviations for each quantity are shown in parenthesis.

Device	DMMP			MeOH				
	R (%)	τ_1 (min)	A_1	R (%)	τ_1 (min)	A_1	τ_2 (min)	A_2
n	7.64 (0.068)	106.0 (3.88)	117.3 (2.30)	2.41 (0.022)	37.1 (0.58)	37.8 (0.12)	0.89 (0.04)	-11.6 (0.04)
p	-2.23 (0.075)	100.9 (10.35)	32.4 (1.68)	-5.49 (0.026)	39.1 (10.86)	13.4 (0.36)	3.3 (0.14)	42.6 (0.67)

The desorption time constants for DMMP are nearly identical on n- and p-channel ChemFETs, consistent with DMMP having similar binding strength to CuPc and F_{16}CuPc. We infer that DMMP binds to similar sites in both n- and p- channel films. Therefore, the 3.4 times difference in the DMMP chemical response between n- channel and p-channel is ascribed to the difference in the changes induced in the electronic structure of the n- and p-channel MPc films by DMMP

There is co-existence of a fast and a slow process during the adsorption and desorption of MeOH to MPc molecules. The fast component during the adsorption is observed as a current overshoot in the n-channel ChemFET and a fast decay in the p-channel ChemFET. The slow component acts as an electron donor (or hole acceptor) on both the n-and p-channel devices, causing a decrease in the magnitude of the current on p-channel devices and an increase in current on n-channel devices. Conversely, the fast component acts as an electron acceptor on n-channel devices and a hole acceptor on p-channel devices thereby decreasing the magnitude of the current on both n-channel and p-channel devices. The time constants for recovery show that the slow component is nearly identical on n-channel and p-channel devices and the fast component is similar on n-channel and p-channel devices. One possible type of chemisorption which would be consistent with the fast response is charge trapping by MeOH. MeOH is a polar molecule; therefore, it can stabilize holes in p-channel devices and electrons in n-channel devices. Trapping of free charges in both n- and p-channel devices causes a decrease in output current magnitude in both types of devices consistent with the observed behaviour of the fast process.

Note that there is about 20 times difference in the DMMP vs MeOH dosages so that the chemical response magnitudes for DMMP and MeOH appear to be similar in Figure 5.10. The actual chemical sensitivity is one order of magnitude higher for DMMP. The greater sensitivity to DMMP compared to MeOH is consistent with stronger binding of DMMP to MPc as observed by the 3x slower desorption time for DMMP compared to MeOH. The 3x difference in desorption time for DMMP vs MeOH on n-channel

ChemFETs corresponds to a log(3) difference in binding energy and a 3x difference in surface concentration at identical partial pressure. Therefore, some of the 10x difference in sensitivity between DMMP and MeOH is due to DMMP strongly perturbing the electronic structure of the MPc/air interface at equivalent surface concentration to MeOH.

We further investigate relative sensitivity of the n- and p- channel ChemFETs to DMMP and MeOH as a function of concentration. The chemical responses were measured as a function of DMMP concentration in dry air (see Figure 5. 12). Each dose was 20 min long followed by 180 min recovery in dry air. All DMMP doses caused a current increase in n-channel ChemFETs and a current decrease in p-channel ChemFETs. The desorption time constants fitted according to Eq. (2) are 71 +/-22 min and 83 +/- 21 min for n- and p- channel ChemFETs where the error reflects the variation in desorption times with concentration. Within the error margin of the time constants, the DMMP desorption time constants between n- and p- ChemFETs are comparable.

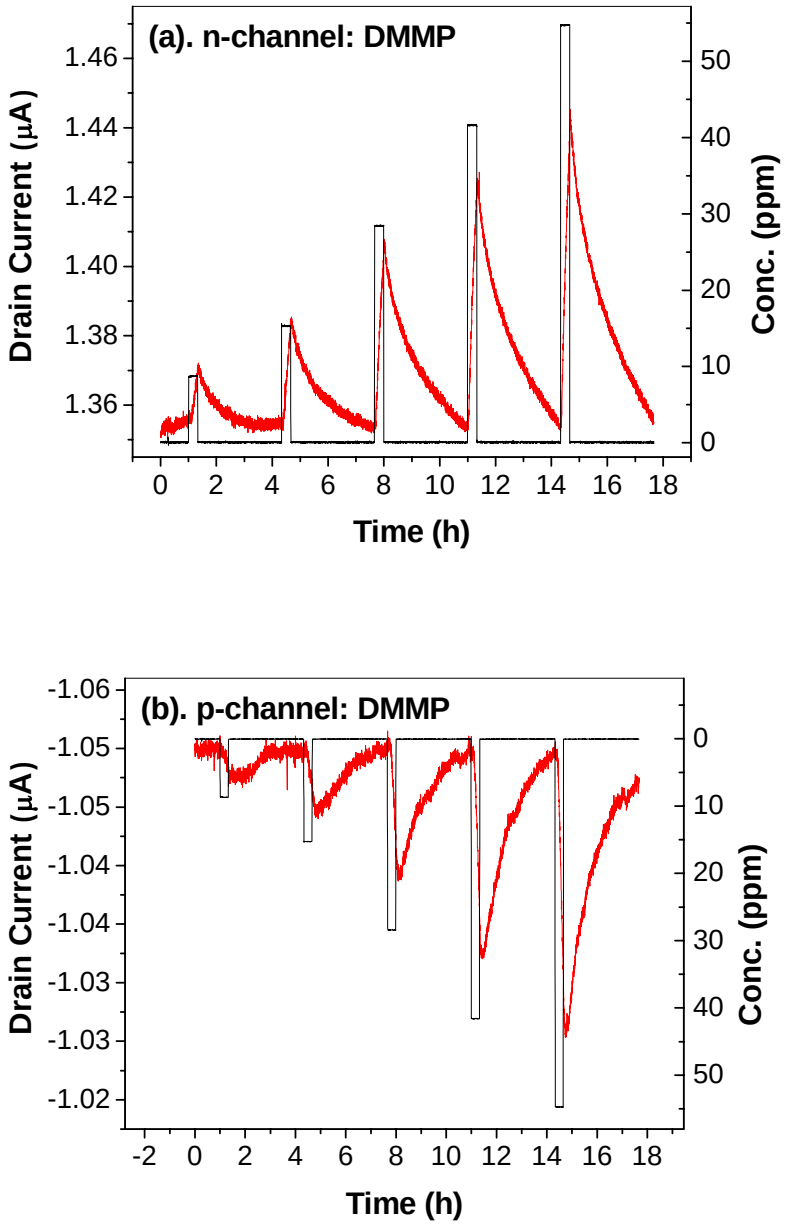

Figure 5.12. The chemical responses of n-channel F_{16}CuPc (a) and p-channel CuPc (b) as a function of DMMP concentration at 25°C.

The chemical response as a function of concentration is extracted from Figure 5. 12 and shown in Figure 5. 13. The $\Delta I / I$ has a linear dependence on the DMMP concentration in both devices. It is confirmed that both the p-type and n-type ChemFETs

are operated in the kinetically controlled region[125] and have excellent linear dependence on the analyte concentration. We note that the linear fits of $\Delta I / I$ as a function of DMMP concentration have non-zero interceptions at zero concentration (0.18% and 0.95% for p- and n- channel ChemFETs). The non-zero interceptions are due to the non-linear chemical response at very low DMMP concentration, which might be due to strong analyte binding to defect sites.

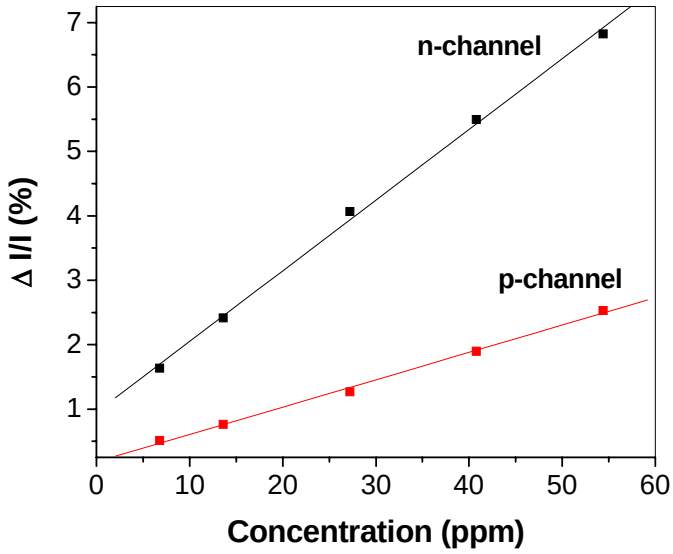

Figure 5.13. The current change ($\Delta I / I$) as a function of DMMP concentration at 25°C in dry air for n- and p- channel ChemFETs.

We note that there is a significant difference between the chemical sensitivity of F_{16}CuPc and CuPc to DMMP. The slope of $\Delta I / I$ vs concentration is 2.5 times larger for the n-channel ChemFET. The greater sensitivity to DMMP on n-type F_{16}CuPc ChemFETs can be attributed to either stronger binding to the surface of F_{16}CuPc or to a greater change in electronic structure induced by DMMP in comparison to CuPc. Since the desorption time constants of DMMP to CuPc and F_{16}CuPc are similar, we ascribed

the chemical sensitivity difference solely to differences in DMMP perturbation of the electrons trap energies vs hole trap energies in the n-channel and p-channel devices.

Similarly, the concentration dependent chemical responses to MeOH are shown in Figure 5.14. $\Delta I / I$ was extracted to the same procedure shown in the inset of Figure 5.10. We found there is non-linear dependent of chemical responses on the concentration. The nonlinear response is consistent with there being at least two distinct chemisorption mechanisms (slow and fast) for MeOH on the n- and p-channel devices.

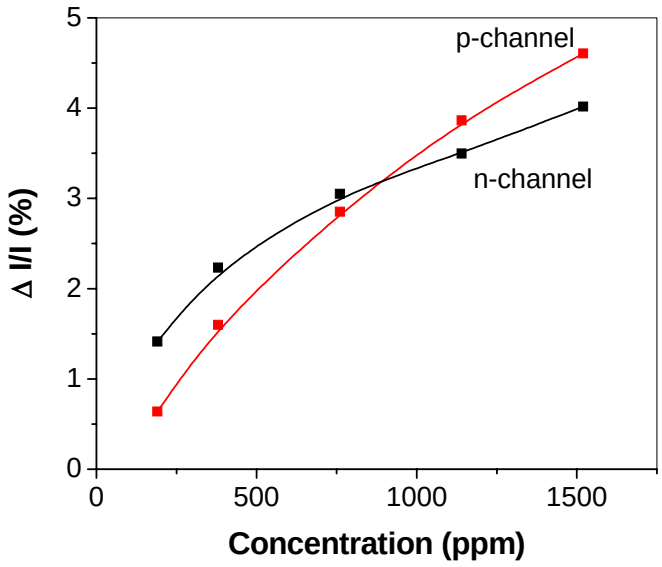

Figure 5.14. The current change ($\Delta I / I$) as a function of DMMP concentration at 25°C in dry air for n- and p- channel ChemFETs. The time-dependent plots of chemical response to MeOH pulses at different concentrations are shown in the AIP achieve.

5.4. CONCLUSIONS

N-type and p-type ChemFETs have been fabricated with F_{16}CuPc and CuPc materials. It is identified that oxygen act primarily as surface dopant (electron acceptor) for the n- and p- channel ChemFETs. Removing oxygen increases the n-channel current

while decreasing the p-channel current. The chemical responses to DMMP and methanol in air and N_2 for both devices have been compared. For all analytes tested, the responses are of opposite sign on n-type and p-type ChemFETs which is consistent with the primary mechanism by which the analytes change the output current is counter doping of the surface oxygen. We note a factor of 3 times difference between the chemical sensitivity of CuPc and F_{16}CuPc to DMMP even though it has the simliar binding strength to both MPc molecules. The effect is attributed to the difference in the analyte induced trap energy in n- and p- type MPc materials.

6. ULTRATHIN ORGANIC TRANSISTORS FOR CHEMICAL SENSING

6.1.Introduction

Organic thin-film transistors (OTFTs) are candidates for chemical vapor sensing due to a strong charge transport dependence on the chemical environments.[9,21,22,85,86,93] OTFT sensors combine the advantages of organic materials, such as low processing cost and high chemical selectivity, with the advantages of the field-effect device structure, such as multiparameter readout. Herein, OTFTs employed for chemical sensing using small organic materials are denoted as chemically sensitive field-effect transistors (ChemFETs). In this chapter, we will discuss the application of ultrathin organic transistors for chemical sensing.

Previous studies on ChemFETs used relatively thick films (> 10 MLs).[9,21,22,85,86,93,106] In this work, cobalt phthalocyanine (CoPc) films as thin as 4 MLs have been deposited by organic molecular beam epitaxy (OMBE). In the absence of analytes, these devices show mobilities comparable (within a factor of 3) with films as thick as 50 MLs. However, we have demonstrated significant improvements in the chemical response, baseline stability, and sensing kinetics using the ultrathin ChemFETs. The differences in chemical response and kinetics between the ultrathin and thick ChemFETs provide insights into the sensing physics of the ChemFETs.

Fundamental studies of the charge transport process in OTFTs show carriers conduct primarily through the first 1-5 MLs above the gate dielectric.[123] The free carrier

concentration in thermal equilibrium depends on both the molecular doping level and trap activation energies. Due to the presence of a large trap density, trap states dominate the carrier transport properties of organic films.[11] We hypothesize that analytes adsorbed on the surface of the CoPc films change both the doping level and the trap energy of the air/CoPc interface layer. The change in doping level affects the output current in both thin and thick channel devices. However, the changes in surface trap energy affect the charge transport more strongly in thin devices because the charge transport layers are closer to the air/CoPc interface as compared to the thick devices. The observed improvements in baseline stability and dynamic response to gas sensing confirm the active participation of the surface traps in charge transport in the ultrathin transistors.

6.2.Measurement Setup

CoPc was purchased from Sigma-Aldrich and purified by zone sublimation below 10^{-5} Torr. CoPc thin-films have shown large responses to chemical analytes using chemiresistors[126] and have been employed for analyte identification using impedance spectroscopy.[127] Bottom-contact devices were fabricated on n^+ silicon wafers with 100 nm of thermally grown SiO_2. The channel length and width of the devices were 10 μm and 2 mm respectively. CoPc thin films of 4 ML and 50 ML were deposited by OMBE at pressure of 2 x 10^{-9} Torr at 80 ^oC. Chemical sensing experiments were performed inside a custom built computer controlled flow system. Ultrathin OTFTs have been fabricated using high mobility but chemically nonspecific materials such as sexithiophene[128] and pentacene[129], but ChemFETs with thickness of a few monolayers have not been reported previously. Chemically selective materials, such as CoPc generally have several orders of

magnitude lower mobility than materials typically employed in the ultrathin OTFTs. Therefore, very careful control of the taper of the gold electrodes to avoid undercutting of the electrodes and three cycles of ultrasonication in trichloroethylene/ acetone/ isopropyl alcohol cleaning are required to ensure excellent contact between the CoPc channels film along the gold electrodes.

The devices were characterized in an optically isolated chamber at 25 ^{o}C to minimize photocurrent. Each device was stabilized in a dry air flow for three days prior to chemical response measurements to equilibrate doping from atmospheric oxygen and humidity. For each film thickness, six devices were deposited simultaneously, and the mobility variation was less than 5% with the same operating voltages. Typical transfer curves for a 4 ML and 50 ML device are shown in Figure 6.1a. The mobility values extrapolated from the linear region are 1.0 x 10^{-4} cm^2/Vs and 2.6 x 10^{-4} cm^2/Vs for the 4 ML and 50 ML device, respectively. The lower mobility of the 4 ML device may be due to incomplete film coverage above the third layer or differences in film texture. Similarly, the mobility in pentacene films is reported to reach the bulk value only above 5 MLs.[129] The threshold voltages are +0.38 V and -0.38 V for the thin and thick device, respectively. We note that the current noise is larger in the ultrathin ChemFET as compared to the thick ChemFET in aged devices. However, the noise level in the ultrathin devices was the same as the thick devices when they were less than one month old. Therefore, the noise could come from degradation in electrical contacts of the solder bumps or degradation of CoPc/Au contacts. The noise issue in ChemFET is under investigation and will be reported in the future.

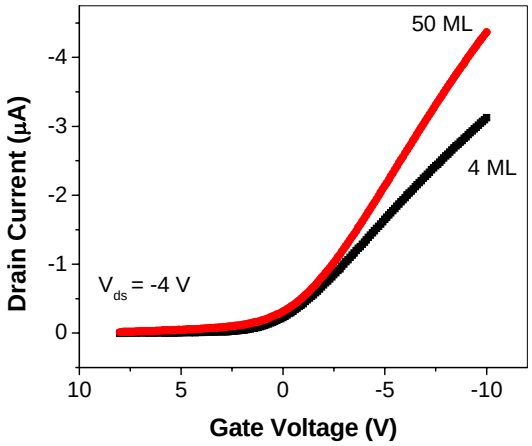

Figure 6.1.Transfer characteristics of the 4 ML and 50 ML CoPc thin-film devices measured at V_{ds} = -4 V, V_g sweeps at 0.1 V/step at rate of 10 V/s.

6.3.Results and Discussion

6.3.1. AFM and X-ray Diffraction Analysis

The nominal film thickness determined by X-ray diffraction (XRD) is 3.8 MLs (51 Å), see Figure 6.2a. The d-spacing is 13.3 Å in accordance with previous measurements that show the molecular planes of CoPc are oriented perpendicular to the substrate surface. The surface morphology measured by atomic force microscopy (AFM) is shown in Figure 6.2b. The CoPc thin-films grown at 80 ^{o}C have an average grain size of 36 nm and the surface RMS roughness from AFM is 6.6 Å (for the bare substrate it is 0.9 Å). By combining the average height from the AFM (2.3 nm) with the average thickness from the XRD data, we infer that there are two complete MLs of CoPc in these ultrathin ChemFETs.

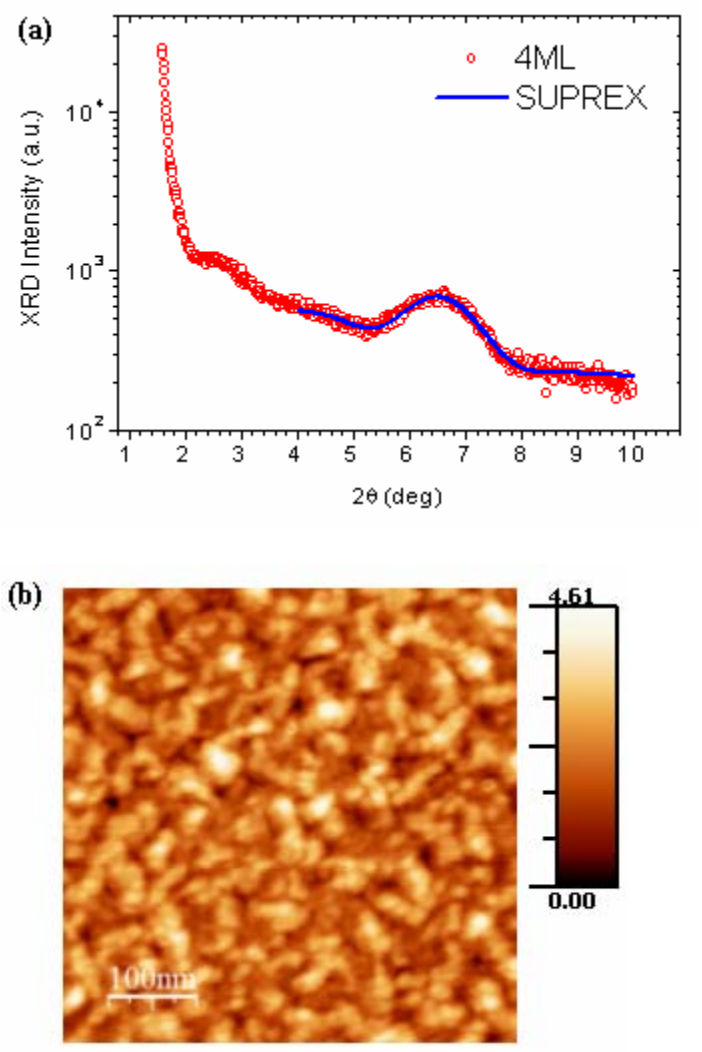

Figure 6.2. (a). X-ray diffraction for a 4 ML CoPc thin film grown on a SiO_2/Si substrate. The line is a fit using a quantitative refinement program. (b) The AFM image with a color scale range over 4.6 nm.

6.3.2. Chemical Sensitivity Enhancement

For determination of the chemical response and dynamic response properties of ChemFETs, the devices were exposed to 25 chemical pulses, each exposure was 20 minutes long and followed by a 40 minutes recovery in a dry air flow. To minimize bias stress effect in devices by static gate bias[101], a 0.5 Hz pulsed, 1% duty cycle gate bias was used for both devices. The chemical responses of chemical pulses in dry air are shown in

Figure 6.3. Three analytes were chosen to represent stimulants for nerve gases (DIMP), explosives (nitrobenzene) and volatile organic vapors (methanol). Two other volatile organics, ethyl acetate and toluene, were also tested in the same manner for comparison of chemical responses between thin and thick devices. The chemical response is defined as $R \equiv \frac{I_{analyte} - I_0}{I_0} * 100\%$, where I_0 is referred to the initial drain current.

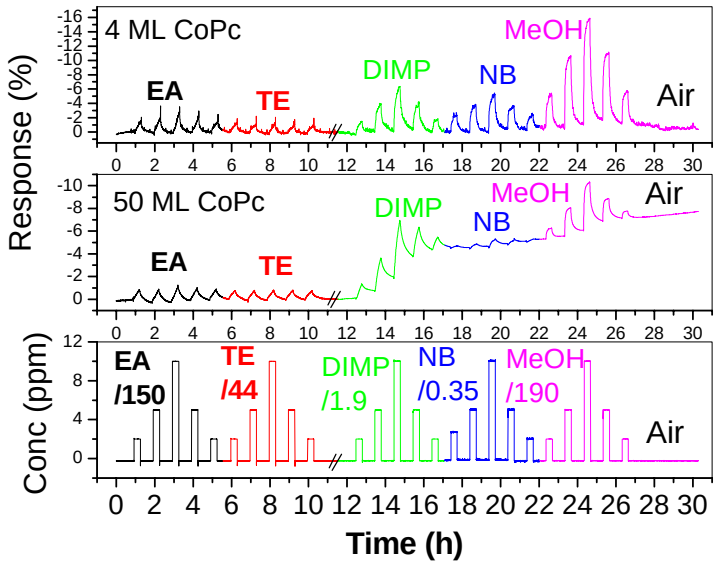

Figure 6.3. Chemical response to ethyl acetate (EA), toluene (TE), diisopropyl methylphosphonate (DIMP), nitrobenzene (NB) and methanol (MeOH) for a 4 ML and 50 ML device measured at V_{ds} = -4 V, V_g = -8V. The break lines represent two separate runs.

The 4 ML device shows enhanced chemical response to all the analytes compared to the 50 ML device. The average enhancement factors (R_{4ML} / R_{50ML}) for toluene, DIMP, ethyl acetate, MeOH, and NB are between 1.5 - 20. The chemical responses here are calculated with a linearly extrapolated baseline to account for the baseline drift in each pulse. Any linear correlation between the enhanced chemical response and a molecular

property, such as dipole moment or vapor pressure, is not readily apparent. We infer that the analyte interaction with the surface sites is a complex function of analyte dipole, polarizability and molecular structure.

The chemical sensitivities of the thick and thin ChemFETs have been calculated by normalizing the chemical response by the analyte concentration. Average values and standard errors of five chemical pulses for each analyte are shown in Table 6.1. The standard errors for analytes other than toluene and ethyl acetate are less than 15%. Since there are three different levels of analyte concentration, non-linear chemical response and baseline drift will contribute to the standard error in statistics. It is found that CoPc ChemFETs are over 200 more sensitive to NB as compared to the three organic volatile vapors (EA, toluene and MeOH). The results imply that CoPc ultrathin ChemFETs are good sensors for detecting nitroaromatic compounds even in the presence of low concentration hydrocarbon vapor interference. Diluted NB concentrations as low as 75 ppb were detected using the ultrathin device. The test is limited by the accuracy of our smallest mass flow controller (2% of 10 sccm). The 75 ppb dose of nitrobenzene gave a relative response of 0.1 % of the 2.70 μA output current in the 4 ML transistor. This chemical sensitivity is among the best reported in the literature for nonredox active reducing analytes on ChemFETs, but we note that far higher sensitivities have been obtained for highly oxidizing analytes (e.g. ozone) on NiPc ChemFETs.[88]

All five analytes reduce the drain current in both thin and thick films. The output current decrease is a result of the lower concentration of free carriers. This loss of free carriers can be ascribed to a reduced “surface doping” concentration, an increased trap

energy, or both. It is known that the conductivity of CoPc films is very small in vacuum due to its low bulk doping.[130] Upon exposure to air, CoPc films conduct due to O_2 chemisorption at CoPc surface sites.[119] The conductivity gain through O_2 chemisorption at the air/CoPc interface is effectively equivalent to "surface doping". For both thin and thick films, exposure to analytes changes the surface doping concentration. Given the difference in electron affinities or polarizabilities of analytes compared to O_2, we hypothesize that the analytes can also change the trap energies at the air/CoPc surface layer as compared to oxygen, but this is much more important for thin ChemFET than for thick ChemFETs. The supporting evidence of the role of O_2 in device conductivity and chemical response is shown in Figure 6.4 by comparing the sensor responses in air and N_2 carrier gases. The drain current was found to decrease by 8% after 4 hours flow in dry N2. Using the same procedure described previously, the chemical response is reduced by 20% in dry N_2 as compared to in air flow.

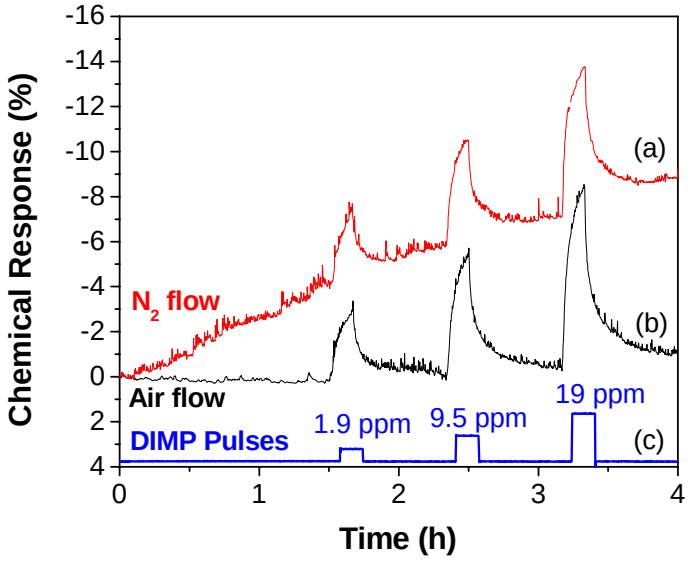

Figure 6.4. A comparison of chemical responses in dry N_2 and air flow (4 ML CoPc ChemFET). (a). Response to DIMP in dry N_2. (b). Response to DIMP in dry air. (c). DIMP pulses.

The relationship between trap energy and analyte response was quantified using the most straightforward approach. Analyte exposure changes the mobility and threshold voltage simultaneously. To simplify the quantification of the analyte induced changes in mobility, we operate the device at a gate voltage (-8 V) that is 20 times larger than V_t (-0.38 V and 0.38 V) in the linear region. Therefore, the chemical response is mainly determined by the change in mobility at a fixed V_g, $R = \frac{\Delta I}{I_{base}} = \frac{\Delta \mu}{\mu_{base}}$, where $\Delta \mu = \mu_{analyte} - \mu_{base}$. The effective mobility is related to trap energy E_a as

$$\mu = \mu_0 \exp\left(\frac{-E_a}{kT}\right) \qquad (6.1)$$

where μ_0 is the mobility related to the dopant concentration. We note that OTFT conductivities are modeled as a trap mediated conductivity so the carrier density does not appear explicitly in the equation and instead is incorporated into the mobility term.[123] In OTFTs, the charge carriers are transported in a few MLs adjacent to the gate oxide;[123] therefore, the relevant trap energy E_a comes from the CoPc/SiO_2 interface. Consequently, in thick films, the effect of the analyte on the relevant E_a is minimal, because the analytes affect only the trap energies far from the CoPc/SiO_2 interface. Conversely, in ultrathin films, the air/CoPc surface is near the CoPc/SiO_2 interface so that the surface trap states affect the charge transport even at very high gate voltage. We note that the greatest enhancement for the response was observed for nitrobenzene, which should be a good hole trap since it has the largest dipole moment of the five analytes and probably the largest polarizability.

6.3.3. Baseline Stability Improvements

As shown in Figure 6.3, the sensor baseline drift over 20 h in the second run was reduced by a factor of 12 in the 4 ML device compared to the 50 ML device with pulsed gating. Baseline drift has plagued OTFTs made from a wide range of materials.[101] With a static gate bias, the output current can diminish by 40% in 20 h. We found that a pulsed gate bias (0.5 Hz, 1% duty cycle) reduces the electrical drift in the absence of analytes in both 4 ML and 50 ML ChemFETs to 0.05%/h. The mean baseline drift value is calculated for each analyte by measuring the accumulated drift each of the 5 pulses using the same starting point. For the analytes with significant drift (MeOH and DIMP), the baseline drift is 3-4 times less in the ultrathin vs the thick ChemFETs. The overall drift difference over 20 h is larger because it takes account the cumulative drift of each chemical pulse. The reduced baseline drift in the presence of analytes in ultrathin films may be attributed to the close location of the surface trap states to the gate dielectric. In ultrathin devices, the potential gradient from the gate is sufficiently strong and close to the oxide/CoPc interface that it tends to remove positive charges from the surface trap states, thereby, reduces irreversible trapping that produces baseline drift.

Table 6.1. The average chemical sensitivity (S) in 10^{-3} %/ppm, drift (D) in %/h and response time t_{50} in second of 4 ML and 50 ML devices to the vapor doses are extracted from Figure 5.3. Note the analytes are presented in order of sensitivity. Standard errors estimated from five pulses for each analyte are shown in the parenthesis. Drift below 0.05%/h is listed as non-significant (NS).

Analyte/Device		S(%)	D(%h)	$t_{50}(s)$
NB	4 ML	2372(345)	NS	134(14)
	50 ML	116(13)	0.07(0.04)	552(40)
DIMP	4 ML	400 (30)	0.26(0.05)	265 (30)
	50 ML	260 (10)	1.0 (0.1)	568 (42)
MeOH	4 ML	11 (1)	0.15 (0.15)	61 (14)
	50 ML	2.0 (0.2)	0.42 (0.05)	73 (16)
TE	4 ML	7.7 (2.2)	NS	420 (56)
	50 ML	5.4 (1.4)	NS	467 (17)
EA	4 ML	3.5 (0.7)	NS	558 (45)
	50 ML	2.0 (0.5)	NS	579 (15)

We have also observed faster dynamic response in ultrathin sensors as shown in Table 6.1. The turn-on response t_{50} is quantified by the time it takes to reach 50% of the maximum chemical response. While the response times for ethyl acetate, toluene and MeOH decrease by only 10%, for the other two analytes, the response time t_{50} is reduced by a factor of 2 in the 4 ML devices compared to the 50 ML devices. Generally, we found that the t_{50} response time depends on the dose used. The larger dose results in a faster response time for adsorption. For NB, the faster response time could be due to the increased sensitivity for ultrathin compared to thick ChemFETs. However, for DIMP, the improvement in response time is much greater than the improvement in sensitivity for thin vs thick ChemFETs; therefore, the improvement in dynamic response is not just due to increased sensitivity in the ultrathin devices. As explained below, this result is consistent with the electronic theory of gas adsorption on semiconductor surfaces

proposed by Wolkenstein, which correlates gas adsorption rates with the film's Fermi levels.[131]

To explain the effect of film thickness on ChemFET sensing, a qualitative electronic band diagram model illustrating the difference between the 4 ML and 50 ML devices is shown in Figure 6.5. Positive holes are accumulated at the CoPc/SiO_2 interface by the gate capacitor and at the air/CoPc interface by oxygen surface doping. The hole accumulation at the CoPc/SiO_2 interface bends the valence band towards the Fermi level. For ultrathin ChemFETs the hole accumulation extends to the air/CoPc interface, therefore, the surface traps participate in carrier transport and the perturbation of the surface trap energies by the analytes renders the ultrathin ChemFETs more sensitive than the thick ChemFETs. The extension of the hole accumulation to the surface of the ultrathin ChemFETs is also responsible for the surface traps being depleted by the gate thereby reducing bias stress and changing the analyte absorption energy/kinetics.[131]

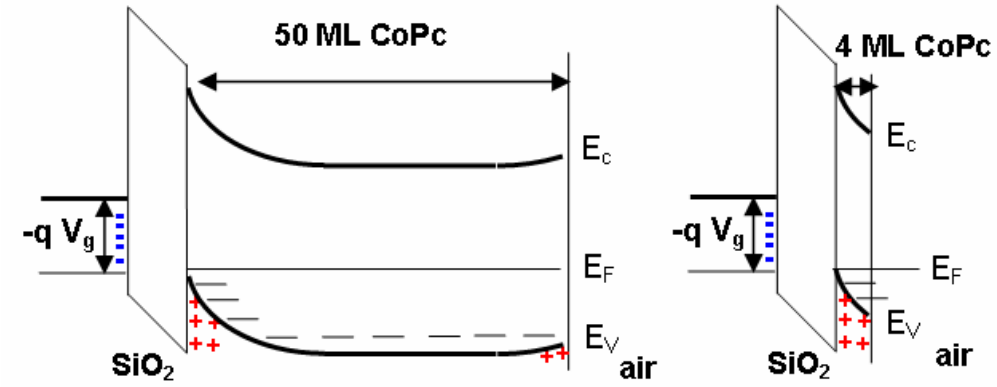

Figure 6.5. Electronic band models of thick and thin ChemFETs with a negative gate bias. Holes accumulate at the CoPc/SiO_2 interface by gate biasing and at the air/CoPc interface by oxygen doping. The broken lines represent trap states in the organic film.

6.4.Conclusion

In conclusion, ultrathin ChemFETs have been reproducibly prepared by OMBE deposition. Due to the proximity of the air/CoPc interface to the charge transport layer in ultrathin ChemFETs, chemical response enhancements by a factor up to 20 compared to thick ChemFETs have been observed. The effect can be ascribed to the analyte influencing not just the surface doping but also the trap energy for carrier transport in ultrathin devices. Further evidence of the role of surface traps in the chemical sensing physics of ChemFETs is provided by the greatly reduced baseline drift in the presence of analytes and the more rapid analyte response rates in the ultrathin ChemFETs.

This chapter in full has been accepted by *Appl. Phys. Lett.* for publication. The authors are **R. D. Yang**, T. Gredig, J. Park, C. N. Colesniuc, I. K. Schuller, W. C. Trogler, and A. C. Kummel.

REFERENCE

[1]J. M. Shaw and P. F. Seidler, IBM J. Res. Dev. **45**, 3 (2001).

[2]T. W. Kelley, P. F. Baude, C. Gerlach, D. E. Ender, D. Muyres, M. A. Haase, D. E. Vogel, and S. D. Theiss, Chem. Mater. **16**, 4413 (2004).

[3]G. Yu, J. Gao, J. C. Hummelen, F. Wudl, and A. J. Heeger, Science **270**, 1789 (1995).

[4]P. Peumans, S. Uchida, and S. R. Forrest, Nature **425**, 158 (2003).

[5]B. Crone, A. Dodabalapur, Y. Y. Lin, R. W. Filas, Z. Bao, A. LaDuca, R. Sarpeshkar, H. E. Katz, and W. Li, Nature **403**, 521 (2000).

[6]C. D. Dimitrakopoulos and P. R. L. Malenfant, Adv. Mater. **14**, 99 (2002).

[7]H. Klauk, *Organic Electronics: Materials, Manufacturing and Applications*. (Wiley-VCH, Weinheim, 2006).

[8]M. Pope and C. E. Swenberg, *Electronic Processes in Organic Crystals and Polymers*, 2nd ed. (Oxford University Press, New York, 1999).

[9]J. B. Chang, V. Liu, V. Subramanian, K. Sivula, C. Luscombe, A. Murphy, J. S. Liu, and J. M. J. Frechet, J. Appl. Phys. **100**, 014506 (2006).

[10]M. J. Madou and S. R. Morrison, *Chemical Sensing with Solid State Devices*. (Academic Press, San Diego, 1989).

[11]R. Schmechel and H. von Seggern, Phys. Status Solidi A **201**, 1215 (2004).

[12]K. C. Kao and W. Hwang, *Electrical Transport in Solids*. (Pergamon, Oxford, 1981).

[13]M. A. Lampert and P. Mark, *Current Injection in Solids*. (Academic Press, New York, 1970).

[14]A. Dodabalapur, L. Torsi, and H. E. Katz, Science **268**, 270 (1995).

[15]H. C. Yang, T. J. Shin, M. M. Ling, K. Cho, C. Y. Ryu, and Z. N. Bao, J. Am. Chem. Soc. **127**, 11542 (2005).

[16]S. Kobayashi, T. Nishikawa, T. Takenobu, S. Mori, T. Shimoda, T. Mitani, H. Shimotani, N. Yoshimoto, S. Ogawa, and Y. Iwasa, Nat. Mater. **3**, 317 (2004).

[17]M. C. J. M. Vissenberg and M. Matters, Phys. Rev. B **57**, 12964 (1998).

[18]G. Horowitz, M. E. Hajlaoui, and R. Hajlaoui, J. Appl. Phys. **87**, 4456 (2000).

[19]A. R. Brown, C. P. Jarrett, D. M. deLeeuw, and M. Matters, Synth. Met. **88**, 37 (1997).

[20]J. Janata and M. Josowicz, Nat. Mater. **2**, 19 (2003).

[21]T. Someya, H. E. Katz, A. Gelperin, A. J. Lovinger, and A. Dodabalapur, Appl. Phys. Lett. **81**, 3079 (2002).

[22]Z. T. Zhu, J. T. Mason, R. Dieckmann, and G. G. Malliaras, Appl. Phys. Lett. **81**, 4643 (2002).

[23]L. Wang, D. Fine, and A. Dodabalapur, Appl. Phys. Lett. **85**, 6386 (2004).

[24]A. W. Snow and W. R. Barger, in *Phthalocyanines Properties and Applications*, edited by A. B. P. Lever (John Wiley & Sons, Inc, New York, 1989), Vol. 1, pp. 341.

[25]S. V. Patel, T. E. Mlsna, B. Fruhberger, E. Klaassen, S. Cemalovic, and D. R. Baselt, Sens. Actuators, B **96**, 541 (2003).

[26]R. G. Kepler, P. M. Beeson, S. J. Jacobs, R. A. Anderson, M. B. Sinclair, V. S. Valencia, and P. A. Cahill, Appl. Phys. Lett. **66**, 3618 (1995).

[27]B. J. Chen, W. Y. Lai, Z. Q. Gao, C. S. Lee, S. T. Lee, and W. A. Gambling, Appl. Phys. Lett. **75**, 4010 (1999).

[28]G. G. Malliaras, Y. L. Shen, D. H. Dunlap, H. Murata, and Z. H. Kafafi, Appl. Phys. Lett. **79**, 2582 (2001).

[29]J. R. Macdonald, *Impedance Spectroscopy*. (John Wiley and Sons, New York, 1987), p.2.

[30]H. C. F. Martens, H. B. Brom, and P. W. M. Blom, Phys. Rev. B **60**, R8489 (1999).

[31]S. Berleb and W. Brutting, Phys. Rev. Lett. **89**, 286601 (2002).

[32]N. D. Nguyen, M. Schmeits, and H. P. Loebl, Phys. Rev. B **75**, 075307 (2007).

[33]J. Gutierrez, L. Ares, M. C. Horillo, I. Sayago, J. Agapito, and L. Lopez, Sens. Actuators, B **4**, 359 (1991).

[34]F. Josse, R. Lukas, R. N. Zhou, S. Schneider, and D. Everhart, Sens. Actuators, B **36**, 363 (1996).

[35]R. C. Hughes, W. G. Yelton, K. B. Pfeifer, and S. V. Patel, J. Electrochem. Soc. **148**, H37 (2001).

[36]H. C. F. Martens, J. N. Huiberts, and P. W. M. Blom, Appl. Phys. Lett. **77**, 1852 (2000).

[37]G. Blatter and F. Greuter, Phys. Rev. B **33**, 3952 (1986).

[38]C. Tanase, P. W. M. Blom, D. M. de Leeuw, and E. J. Meijer, Phys. Status Solidi A **201**, 1236 (2004).

[39]F. Iwatsu, T. Kobayashi, and N. Uyeda, J. Phys. Chem. **84**, 3223 (1980).

[40]M. E. H. Amrani, K. C. Persaud, and P. A. Payne, Meas. Sci. Technol. **6**, 1500 (1995).

[41]C. C. Leznoff and A. B. P. Lever, (John Wiley & Sons, Inc, New York, 1989), Vol. 1.

[42]A. Schmidt, L. K. Chau, A. Back, and N. R. Armstrong, Phthalocyanines **4**, 307 (1996).

[43]N. R. Armstrong, J. Porphyrins Phthalocyanines **4**, 414 (2000).

[44]L. S. Hung and C. W. Tang, Appl. Phys. Lett. **74**, 3209 (1999).

[45]Z. Bao, A. J. Lovinger, and A. Dodabalapur, Appl. Phys. Lett. **69**, 3066 (1996).

[46]T. G. Abdel Malik and R. M. Abdel-Latif, Thin Solid Films **305**, 336 (1997).

[47]R. D. Gould, J. Appl. Phys. **53**, 3353 (1982).

[48]R. D. Gould, J. Phys. D: Appl. Phys., 1785 (1986).

[49]R. D. Gould, Coord. Chem. Rev. **156**, 237 (1996).

[50]R. D. Gould and N. A. Ibrahim, Thin Solid Films **398-399**, 432 (2001).

[51]R. D. Gould and T. S. Shafai, Thin Solid Films **373**, 89 (2000).

[52]A. K. Hassan and R. D. Gould, Int. J. Electronics **73**, 1047 (1992).

[53]A. M. Saleh, A. K. Hassan, and R. D. Gould, J. Phys. Chem. Solids **64**, 1297 (2003).

[54]S. Hiller, D. Schlettwein, N. R. Armstrong, and D. Wohrle, J. Mater. Chem. **8**, 945 (1998).

[55]J. W. Pankow, C. Arbour, J. P. Dodelet, G. E. Collins, and N. R. Armstrong, J. Phys. Chem. **97**, 8485 (1993).

[56]J. Blochwitz, T. Fritz, M. Pfeiffer, K. Leo, D. M. Alloway, P. A. Lee, and N. R. Armstrong, Org. Electron. **2**, 97 (2001).

[57]A. K. Hassan and R. D. Gould, J. Phys.: Condensed Matter **1**, 6679 (1989).

[58]T. Inabe and H. Tajima, Chem. Rev. **104**, 5503 (2004).

[59]T. Inabe, J. Porphyrins Phthalocyanines **5**, 3 (2001).

[60]O. El Beqqali, M. Al Sadoun, G. Guillaud, M. Gamoudi, M. Benkaddour, A. S. Skal, and M. Maitrot, J. Appl. Phys. **69**, 3670 (1991).

[61]Q. Zhou and R. D. Gould, Thin Solid Films **317**, 432 (1998).

[62]B. Bott and T. A. Jones, Sens. Actuators **5**, 43 (1984).

[63]M. Bouvet, G. Guillaud, A. Leroy, A. Maillard, S. Spirkovitch, and F.-G. Tournilhac, Sens. Actuators, B **73**, 63 (2001).

[64]G. Guillaud, J. Simon, and J. P. Germain, Coord. Chem. Rev. **178-180**, 1433 (1998).

[65]J. C. Hsieh, C. J. Liu, and Y. H. Ju, Thin Solid Films **322**, 98 (1998).

[66]E. S. Kolesar Jr and J. Wiseman, M., Anal. Chem. **61**, 2355 (1989).

[67]A. B. P. Lever, J. Porphyrins Phthalocyanines **3**, 488 (1999).

[68]J. D. Wright, Prog. Surf. Sci. **31**, 1 (1989).

[69]W. R. Barger, H. Wohltjen, A. W. Snow, J. Lint, and N. L. Jarvis, ACS Symp. Ser. **309**, 155 (1986).

[70]R. Zhou, F. Josse, W. Gopel, Z. Z. Ozturk, and O. Bekaroglu, Appl. Organomet. Chem. **10**, 557 (1996).

[71]J. W. Grate, M. Klusty, W. R. Barger, and A. W. Snow, Anal. Chem. **62**, 1927 (1990).

[72]L. Burgi, H. Sirringhaus, and R. H. Friend, Appl. Phys. Lett. **80**, 2913 (2002).

[73]K. P. Puntambekar, P. V. Pesavento, and C. D. Frisbie, Appl. Phys. Lett. **83**, 5539 (2003).

[74]P. W. M. Blom, C. Tanase, D. M. de Leeuw, and R. Coehoorn, Appl. Phys. Lett. **86** (2005).

[75]Sworakow.J and K. Pigon, J. Phys. Chem. Solids **30**, 491 (1969).

[76]W. R. Silveira and J. A. Marohn, Phys. Rev. Lett. **93**, 116104 (2004).

[77]G. Beernink, T. Strunskus, G. Witte, and C. Woll, Appl. Phys. Lett. **85**, 398 (2004).

[78]D. Eder and R. Kramer, J. Phys. Chem. B **108**, 14823 (2004).

[79]J. R. MacDonald, *Impedance Spectroscopy*. (John Wiley and Sons, New York, 1987).

[80]E. Endres, S. Drost, and F. Hutter, Sens. Actuators, B **22**, 7 (1994).

[81]J. Hogan, A. W. Brinkman, and T. Hashemi, Appl. Phys. Lett. **202**, 3077 (1998).

[82]P. Kurzweil, W. Maunz, and C. Plog, Sens. Actuators, B **25**, 653 (1995).

[83]J. Gutierrez, L. Ares, M. C. Horillo, I. Sayago, J. Agapito, and L. Lopez, Sens. Actuators, B **4**, 359 (1991).

[84]M. Knupfer and H. Peisert, Phys. Status Solidi A **201**, 1055 (2004).

[85]L. Torsi, A. Dodabalapur, L. Sabbatini, and P. G. Zambonin, Sens. Actuators, B **67**, 312 (2000).

[86]B. Crone, A. Dodabalapur, A. Gelperin, L. Torsi, H. E. Katz, A. J. Lovinger, and Z. Bao, Appl. Phys. Lett. **78**, 2229 (2001).

[87]F. Liao, C. Chen, and V. Subramanian, Sens. Actuators, B **107**, 849 (2005).

[88]M. Bouvet, G. Guillaud, A. Leroy, A. Maillard, S. Spirkovitch, and F. G. Tournilhac, Sens. Actuators, B **73**, 63 (2001).

[89]R. D. Yang, T. Gredig, J. Park, C. Colesniuc, I. K. Schuller, W. C. Trogler, and A. C. Kummel, Appl. Phys. Lett. (Submitted).

[90]T. C. Pearce, S. S. Schiffman, H. T. Nagle, and J. W. Gardner, *Handbook of Machine Olfaction*. (Wiley-VCH, Weinheim, 2003).

[91]S. V. Patel, T. E. Mlsna, B. Fruhberger, E. Klaassen, S. Cemalovic, and D. R. Baselt, Sens. Actuators, B **96**, 541 (2003).

[92]H. E. Katz, Electroanal. **16**, 1837 (2004).

[93]L. Torsi and A. Dodabalapur, Anal. Chem. **77**, 380A (2005).

[94]S. J. Zilker, C. Detcheverry, E. Cantatore, and D. M. de Leeuw, Appl. Phys. Lett. **79**, 1124 (2001).

[95]H. L. Gomes, P. Stallinga, F. Dinelli, M. Murgia, F. Biscarini, D. M. de Leeuw, T. Muck, J. Geurts, L. W. Molenkamp, and V. Wagner, Appl. Phys. Lett. **84**, 3184 (2004).

[96]R. J. Chesterfield, J. C. McKeen, C. R. Newman, C. D. Frisbie, P. C. Ewbank, K. R. Mann, and L. L. Miller, J. Appl. Phys. **95**, 6396 (2004).

[97]T. Minari, T. Nemoto, and S. Isoda, J. Appl. Phys. **99** (2006).

[98]R. D. Yang, T. Gredig, J. Park, C. Colesniuc, I. K. Schuller, W. C. Trogler, and A. C. Kummel, Appl. Phys. Lett. (2007).

[99]S. Jung, T. Ji, and V. K. Varadan, Appl. Phys. Lett., 062105 (2007).

[100]A. Salleo and R. A. Street, J. Appl. Phys. **94**, 471 (2003).

[101]J. B. Chang and V. Subramanian, Appl. Phys. Lett. **88**, 233513 (2006).

[102]C. Goldmann, C. Krellner, K. P. Pernstich, S. Haas, D. J. Gundlach, and B. Batlogg, J. Appl. Phys. **99**, 034507 (2006).

[103]C. W. Miller, A. Sharoni, G. Liu, C. N. Colesniuc, B. Fruhberger, and I. K. Schuller, Physical Review B **72** (2005).

[104]M. J. Powell, C. Vanberkel, and J. R. Hughes, Appl. Phys. Lett. **54**, 1323 (1989).

[105]D. K. Schroder, *Semiconductor Material and Device Characterization*. (John Wiley & Sons, Inc, New York, 1998).

[106]M. Bouvet, Anal. Bioanal. Chem. **384**, 366 (2006).

[107]R. D. Yang, T. Gredig, J. Park, C. Colesniuc, I. K. Schuller, W. C. Trogler, and A. C. Kummel, Appl. Phys. Lett. (In Press).

[108]L. Torsi, A. J. Lovinger, B. Crone, T. Someya, A. Dodabalapur, H. E. Katz, and A. Gelperin, J. Phys. Chem. B **106**, 12563 (2002).

[109]M. Bora, D. Schut, and M. A. Baldo, Anal. Chem. **79**, 3298 (2007).

[110]A. R. Hopkins and N. S. Lewis, Anal. Chem. **73**, 884 (2001).

[111]D.-S. Private communication with Dr. Barrena from Max Planck Inst Met Res, Germany.

[112]D. G. de Oteyza, E. Barrena, J. O. Osso, S. Sellner, and H. Dosch, J. Am. Chem. Soc. **128**, 15052 (2006).

[113]D. G. de Oteyza, E. Barrena, S. Sellner, J. O. Osso, and H. Dosch, J. Phys. Chem. B **110**, 16618 (2006).

[114]D. G. de Oteyza, E. Barrena, J. O. Osso, H. Dosch, S. Meyer, and J. Pflaum, Appl. Phys. Lett. **87**, 183504 (2005).

[115]Z. A. Bao, A. J. Lovinger, and J. Brown, J. Am. Chem. Soc. **120**, 207 (1998).

[116]M. M. Ling and Z. N. Bao, Org. Electron. **7**, 568 (2006).

[117]R. D. Yang, J. Park, C. Colesniuc, I. K. Schuller, W. C. Trogler, and A. C. Kummel, J. Appl. Phys. (Accepted).

[118]H. Peisert, M. Knupfer, T. Schwieger, G. G. Fuentes, D. Olligs, J. Fink, and T. Schmidt, J. Appl. Phys. **93**, 9683 (2003).

[119]J. D. Wright, Prog. Surf. Sci. **31**, 1 (1989).

[120]M. Passard, C. Maleysson, A. Pauly, S. Dogo, J. P. Germain, and J. P. Blanc, Sens. Actuators, B **19**, 489 (1994).

[121]K. W. Kolasinski, *Surface Science*. (John Wiley & Sons, West Sussex, England, 2002).

[122]R. Tongpool and S. Yoriya, Thin Solid Films **477**, 148 (2005).

[123]G. Horowitz, J. Mater. Res. **19**, 1946 (2004).

[124]J. P. Novak, E. S. Snow, E. J. Houser, D. Park, J. L. Stepnowski, and R. A. McGill, Appl. Phys. Lett. **83**, 4026 (2003).

[125]F. I. Bohrer, A. Sharoni, C. Colesniuc, J. Park, I. K. Schuller, A. C. Kummel, and W. C. Trogler, J. Am. Chem. Soc., 5640 (2007).

[126]K. A. Miller, R. D. Yang, M. J. Hale, J. Park, B. Fruhberger, C. N. Colesniuc, I. K. Schuller, A. C. Kummel, and W. C. Trogler, J. Phys. Chem. B **110**, 361 (2006).

[127]R. D. Yang, B. Fruhberger, J. Park, and A. C. Kummel, Appl. Phys. Lett. **88**, 074104 (2006).

[128]F. Dinelli, M. Murgia, P. Levy, M. Cavallini, F. Biscarini, and D. M. de Leeuw, Phys. Rev. Lett. **92** (2004).

[129]R. Ruiz, A. Papadimitratos, A. C. Mayer, and G. G. Malliaras, Adv. Mater. **17**, 1795 (2005).

[130]A. W. Snow and W. R. Barger, *Phthalocyanines Properties and Applications*. (John Wiley & Sons, New York, 1989).

[131]T. Wolkenstein, *Electronic Processes on Semiconductor Surfaces During Chemisorption*. (Plenum, New York, 1991).